Study on River Dyke Breach Characteristics by Overtopping Flow

A dissertation submitted in partial fulfillment for the requirement

Doctoral Degree in Civil and Earth Resources Engineering

by

BHATTARAI Pawan Kumar

Supervised by Prof. NAKAGAWA Hajime

Laboratory of Hydro-Science and Hydraulic Engineering

Department of Civil and Earth Resources Engineering

Graduate School of Engineering

Kyoto University

Japan

2015

Abstract

A large number of dykes (levees or banks or river embankments) have been built by humans or formed naturally along the rivers throughout the world. River dykes, considered as defense structure, are constructed to prevent flooding of valleys and their inhabitants and confine the flow of the river for higher and faster flow.

In this context of work, we refer to dykes as to man- made earthen embankments built along a river parallel to the river flow and flow strikes the dyke length not perpendicularly. River Dykes is an important and effective measure to prevent floods. The main consequences on the flood risk due to construction of river embankments or dykes are that, firstly, it increases the flood hazard reducing the lateral flow storage area and hence the flow capacity of peak discharges attenuation and, secondly, the amount of potential damages induced by flooding is dramatically increased, being the surrounding areas often urbanized. Therefore, although the existence of dyke lowers the probability of flooding but the consequences to personal safety and property are much higher should a dyke overtop or fail.

In the context of study, Dyke failure is considered to be the situation where erosion or structural failure of the earthen embankment cause flood water to pass over or through the embankment in an increasingly uncontrolled manner (Morris et. al. 2009), leading to a hole or breach in the dyke. The problem of embankment failures has always been of great importance because of their disastrous effects. Most of the embankments are not designed to be overtopped hence are vulnerable and sensitive to overtopping flow. The failure of river embankment due to overtopping flow may cause widespread inundation and catastrophic damages of properties, even if a failure occurred at one spot. Recent climate change will lead to an increase in heavy rainfall events. The occurrence of river water level rise, which exceeds the design, is increasing.

Dyke may fail by erosion due to overtopping, abrupt collapse of the dam body or progressive failure. However, in-depth knowledge of the mechanism of the dyke failures and measured data are still lacking. Dyke failure has been frequently studied as an earthen dam failure despite of their differences in geometry, dimensions and material properties. Very few models are developed for dyke failure that can treat the flow as both sediment flow and debris flow. In this context, an attempt is made to integrate separate models (i.e. seepage flow model, dam surface

erosion and flow model) to predict the lateral widening pattern and outflow hydrograph resulted from failure of dyke by overtopping. The seepage flow model calculates pore water pressure and moisture content inside the dam body. The model of the dam surface erosion and flow calculates dam surface erosion due to overflowing water. Infiltration process and role of suction are incorporated in the integrated model although this process is neglected in almost all available models. The model can predict both total discharge and sediment discharge hydrographs. The model is capable of treating all types of flows according to sediment concentration.

Preliminary experimental studies are carried out to determine the initial understanding of the lateral widening and breach hydrograph using the dyke as the side using four types of sediments (sediment numbers 5, 6, 7 and 8). Within the range of test parameters, the dyke breach process is accelerated with increasing sediment d_{50}. For coarse sediment, due to quick saturation of the dyke body, the collapse time decreases. The width of the breach increases at the top and toe section than the middle section which acts like a hinge point. At the final stage, the middle section also fails leading to whole dyke collapse. The breach discharge and sediment discharge shows the time lag and peak according to the sediment size. Finally, the time of failure curve is proposed for the pre determination of occurrence of peak breach discharge based on the pre-disaster parameters.

Dyke surface erosion and flow model is developed for simulation of outflow hydrograph due to dyke failure by overtopping. The proposed model is tested for different experimental cases of dyke failure for overtopping over partial pilot channel width. The model is able to reproduce the resulting hydrograph reasonably. The simulated overtopping time and dyke surface erosion at different time steps are also in good agreement with experiments. The incised channel is almost vertical for both simulations and experiments in small inflow discharge. In the case of larger inflow discharge and larger reservoir volume, slumping occurred at irregular time steps. The lateral widening pattern is somehow reproduced well with experimental values. Also, the scour pattern at the foundation of dyke for various scenarios with the variation of different sediment sizes due to overtopping are also analyzed experimentally. The scour pattern is also following a trend with regards to materials forming the dyke and the foundation. The finer the materials,

more vulnerable to the scouring were observed.

The proposed model is tested for experimental case of dyke failure due to overtopping. The model reproduced reasonably similar hydrograph as that of experiment. The numerical simulation and experimental results of lateral widening, sediment hydrograph etc. are also in good agreement.

Acknowledgements

This dissertation would not have been possible without the guidance and the help of several individuals who in one way or another contributed and extended their valuable assistance in the preparation and completion of this study. It is a pleasure to convey my gratitude to them all in my humble acknowledgment.

First and foremost, I offer my utmost gratitude to my supervisor Professor Dr. Hajime Nakagawa, Disaster Prevention Research Institute (DPRI), Kyoto University for his supervision, advice and guidance from the very early stage of this research as well as giving me extraordinary experiences throughout the work. Above all and the most needed, he provided me with unflinching encouragement and support in various ways whilst allowing me the room to work in my own way. Without him this dissertation would not have been completed or written. One simply could not wish for a better or friendlier supervisor. I am indebted to him more than he knows.

I am also grateful to other faculty members, Dr. Kenji Kawaike and Dr. Hao Zhang, for his valuable advice, supervision and crucial contribution to this dissertation. My appreciation also goes to Dr. Hidaeki Mizutani, Dr. Lee Seung Soo, Dr. Kim Yeong Jung, Dr. Masakazu Hashimoto and Dr. Kim Nam Gyun for their support in many aspects. I appreciate Mr. Ueda san for providing me invaluable help for construction, running and every aspect of experimental study. I am also in debt to French students Mr. Laurent Dupont and Mr. Valentin Syre-Congi who worked under me as an intern and helped me in the experimental works.

In my daily work I have been blessed with a cheerful group of fellow students and friends at Ujigawa Open Laboratory. I would like to acknowledge them for being a constant support: Mr. Kim Nam Guen, Mr. Ko Dong Woo, Mr. Rocky Talchabadel, Mr.Osamu Kitaguchi, Mr. Hiratsuka Shunsuke, Mr. Tanaka Nanahiro, Mr. Omoto Taku, Ms. Wang Yu, Mr. Nishio Kei , Mr. Shogo Harigae, Mr. Synnichi Sugihara and Ms. Shoko Fujita. I would like to thank specially Ms. Natsuyo Iguchi and all the staffs in Ujigawa Open Laboratory, Disaster Prevention Research Institute of Kyoto University for their support in routine administrative process and experiment.

I am also greatly indebted to many teachers in the past, Professor Dr. Narendra Man Shakya, Prof. Dr. Durga Pd. Sangroula (Tribhuvan University, Nepal) and Prof. Haakon Stole (NTNU, Norway) for getting me interested in each and every topic of water recourses engineering and coming to Japan. I gratefully acknowledge the financial support of the Monbukagakusho (Ministry of Education, Culture, Sports, Science and Technology, Japan).

Moreover, this dissertation is dedicated to the memory of my late father Mr. Govind Pd. Bhattarai who died during my Ph.D. study but always persuaded me to join Ph.D. and even at dying moment encouraged me to finish the study. I miss him every day and feeling happy that I fulfilled his dream. My deepest gratitude also goes to my mother Radha Bhattarai and all other family members for their encouragement and loving support.

Last but not least, I thank with love to Ashu and Pramshu (Bobo), my wife and son. Understanding me best as a Ph.D. herself, Ashu has been my best friend and great companion, loved, supported, encouraged, entertained, and helped me get through this agonizing period in the most positive way.

Finally, I would like to thank everybody who was important to the successful realization of this dissertation, as well as expressing my apology that I could not mention personally one by one.

Table of Contents

CHAPTER 1

INTRODUCTION

1.1 General

A dyke is a man-made structure (usually an earthen embankment of earth and (or) rock) designed and constructed in accordance with sound engineering practice to contain, control, or divert water flow to provide protection from flooding for flows up to a certain return period. Dykes are mainly used in river engineering to prevent floods or in costal engineering as a protection from high-tide. In contrast, a dam is a barrier that serves the primary purpose of retaining water for various purposes such as energy production. Normally dykes are made up of loosely placed sediments like gravel, sand, silt and clay. As they are only temporarily exposed to high water pressure, they are mostly built without a surface seal or a core. Compared to dams, dykes are small in height but can have lengths of several 1,000 kilometers.

a) Levee protected near Yazoo River (Mississippi)   b) Jubilee River Embankment (England)

Figure 1.1 Examples of dykes outside Japan (Source: www.theatlantic.com)

Further differences compared to a dam are: (1) A dyke may become saturated for only a short time (hours to a few days) beyond the limit of capillary saturation; (2) Dyke construction is dictated primarily by flood protection requirements resulting often in constructions on poor foundation; and (3) Dyke material is often heterogeneous and not ideal as it is generally taken from the vicinity of the watercourse subjected to floods.

    a) Yodo River Embankment (Japan)   b) Yamazaki River (Nagoya, Japan)

Figure 1.2 Examples of dykes in Japan (Source: Mizutani et.al.2012)

A large number of **embankment structures** have been built by humans or formed naturally along rivers, lakes, and coastal lines around the world (Figure 1.1 and Figure 1.2). A **dyke** is defined by geometric properties (e.g. height and width of the crest, slopes etc.) and by material characteristics (density, grain size diameter, cohesive strength, erodability, permeability etc.). River dykes are constructed to prevent flooding of the valley and its population and confine the flow of river for higher and faster flow. Flooding of river valleys is an old concern and still a number of events occur yearly causing both monetary and human losses.

Flooding is a natural hazard which probably has the highest occurrence in time and space across the world, causing every year a considerable amount of damage in terms of loss of life and property. Levees are among the most ancient and widely used defense structures against river flooding in the world. In the context of this work, we refer to levee as to man-made earthen embankments built along a river parallel to the river flow. Several most important European and Italian rivers are embanked; this flood defense structural system is aimed to reduce the natural

flooded area allowing extensive portions of alluvial plains to become available for human activities. However, the construction of embankments has two main consequences on the flood risk: first, it increases the flooding hazard by reducing the lateral flood storage area and hence the flow capacity of peak discharges attenuation; second, being the surrounding areas often urbanized, the amount of potential damages induced by flooding is dramatically increased. Therefore, although the probability of flooding may be lower because a levee exists, the consequences to personal safety and property are much higher should a levee overtop or fail.

1.2 Terminology

The modern word "*Dyke"* is most probably derived from the Dutch word "dijk", by which the construction of dykes in Frisia (now part of the Netherlands and Germany) is well attested as early as the 12th century. In the Netherlands as well as England, the origin of the word lies in digging a trench and forming the excavated soil into a bank alongside it. Levee or Embankment Dam is similar terms used in the literature.

1.3 World historical perspective

The first settlements next to rivers or the sea were mostly built on small hills to protect the people from floods and high tide. When people started using the fertile soil next to rivers and the sea, they required additional protection for the harvest and the cattle. Therefore simple earth walls were built which can be regarded as the first dykes. The poor construction technique and an absence of knowledge of hydrology, hydraulics and geotechnics resulted in numerous dyke failures. Often the design flood was estimated on the basis of the highest known flood or the last flood that occurred. With ongoing time and industrialization, river engineering gained more and more in significance. Both technical and economic developments would not have been possible without river works as dykes, ensuring secure navigation routes as well as bridge crossings and protecting both settlements and agricultural land from flooding (Figure 1.3).

The First dyke constructions in Europe date from the early Middle Ages. Mostly ring shaped dykes to protect individual buildings were built in the 9th century at the Rhine River and in the 12th century at the Elbe River (Schmidt 2000). The first dykes of the Netherlands date from the 13th century. In the first decades, different large dyke constructions were mainly built in

Figure 1.3 Early dyke constructions (ca. 1928) along Mississippi River (Courtesy U.S. Army Corps of Engineers)

Germany and the Netherlands.The quality and building techniques were rather inferior as there were no general guidelines available. The first dykes were setup of two walls made of simple fences then backfilled with loose soil. As the soil mostly came from local borrow areas, dykes from the Middle Ages consists of varied materials. The technical dyke development was mainly a consequence of the various dyke failures and the resulting restorations.

1.4 Japanese perspective

Japan is located on the eastern edge of monsoonal Asia and its climate varies according to the seasonal and regional conditions. Typically, heavy rains hit various parts of the country both during rainy season in June and July and during the typhoon season from August to October. This precipitation is predominantly in the form of locally specific temporary downpours. In winter, the northern part of the country usually receives heavy snowfall, which causes prolonged snowmelt floods in spring. The average annual precipitation in Japan is rather high, around 1500-1600 mm. Precipitation in Tokyo is twice as much as other large cities in western countries. Some 50-60 % of the annual precipitation in the Pacific coast of Japan is concentrated in the months from June to October.

Location of Satsuma Levee(bank)

The surviving part of the Satsuma Levee(bank)

Figure 1.4 Traditional satsuma levee of 17th century at Abe River, Japan (Source: MLIT, Japan)

Thus, typhoon, typhoon induced rainfall and rainfall induced landslides and sediment disasters are rather common in Japan. Japan's modern engineering application started in 1868 during Meiji period, when the country incorporated river improvement works, first for navigation and then flood control. The first River Law was enacted in 1896 reflecting the occurrence of a series of tragic floods in 1880s. It declared the public ownership of rivers and river water and assigned to the central government. The flood control responsibility for works that demand large funds, high technology and nationwide planning while the local governments assumed the principal responsibility of ordinary flood management. The basic strategy for flood control was to lead water to the sea as soon as possible. The means of the control were continuous levee system, divergent canals and sediment control by Sabo works (Takeuchi and Shaw 2009b).

In Japan, The first dyke or levee construction date during the reign of Emperor Nintoku mentioned in Nihon-Shoki (first official history of Japan). The levee namely Manda-no-Tsutsumi (Manda Levee) was constructed in Yodo river (Neyagawa city, Osaka Prefecture, Owada). Similarly, The Satsuma Levee (figure 1.4) is said to have been built by the order of Tokugawa Ieyasu to protect the town of Sunpu from floods. The levee was constructed

at Abe River (Shizuoka City, Shizuoka Prefecture).

1.5 Improvement in Dyke Construction

Dyke construction has been improved continuously through the years up to the detailed current set of guidelines (e.g. TAW 1991, USACE 2000a). All these present basic principles used in the design and construction of dykes. However, the general dyke cross-section has not significantly changed over the years. Figure 1.5 shows typical dyke cross-sections of (a) Kreuter (1921) and (b) DWA (2011). The general components like the dyke body, the dyke crest and the berms on both the water and the landside are noted in both plots. As old guidelines mainly specify information on the dyke cross-section or material types, modern dyke guidelines include a detailed design procedure. This mainly starts with the definition of the design water level and the determination of the freeboard and consequently the required dyke crest elevation. Then, the dyke cross-section is defined depending on the crest width, the dyke slope and possible berms and maintenance tracks. One main aspect is the control of seepage.

(a)

(b)

Figure 1.5 Typical dike cross-section of (a) Kreuter (1921) and (b) DWA (2011) (adapted)

Figure 1.6 Major cities spread below the dyke (Tokyo and New York; Source: MLIT,Japan)

Either the dyke body itself exhibits the sealing or additional elements as a surface sealing, a core or foot drainage are applied. Once the dyke cross-section and the design parameters are determined, field investigations are conducted to provide geotechni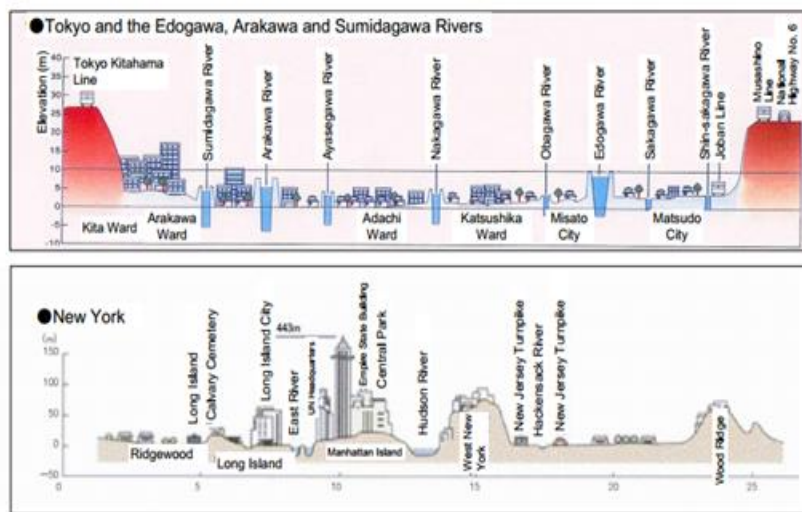cal information on the foundation and the soil characteristics in the construction area. Then the entire analysis regarding dyke stability, hydraulic safety, structural safety and usability has to be conducted. Once construction starts, strict guidelines control the material specification, the construction procedure, material compaction and quality control. Finally, detailed guidelines are available regarding dyke inspection, maintenance, repair and defense.

In Japan, 1977, the river commission of the Ministry of Construction recommended the "Comprehensive Flood Control Measures" in rapidly urbanizing basins. It suggested that not only retardation by dams upstream and river channel improvement downstream be undertaken, but also that the residential area should be developed so that no new extra discharge was generated. In 1987, the River commission recommended the high standard Levee policy and the construction of super levees started such as in the downstream of the Sumida River, Tokyo. A super levee is usually a land elevation behind the original narrow laser-like levee. The base length of a levee is typically 100-150 m long. The super levee protects the urban areas where extensive urban facilities stand and absolutely no levee breakage allowed. The River commission of the Ministry of Construction, Japan issued a new policy "Effective Flood

Management, including Basin Response" in December 2000 and passed the implementation role to the reorganized new Ministry of Land, Infrastructure and Transport. The new policy accepts flood inundation in habited areas through open dykes and secondary dykes. In the present era, the construction of large dykes and dams with concrete is adopted as major technological solutions (figure 1.6).

1.6 Literature review

1.6.1 Introduction

This chapter summarizes the relevant scientific research on dyke breach modelling. Only the theories that are essential for this work are discussed in detail and alternatively the relevant literature is indicated. The main topics discussed are: (1.6.2) Experimental analysis in the past; (1.6.3) Dyke failure modes; (1.6.4) Overtopping erosion; (1.6.5) Breach process; (1.6.6) Measuring devices; and (1.6.7) Numerical Simulations of dyke breaching. The research gaps and the resulting purpose of the present study are summarized in 1.6.8. No literature review on the historical analyses of dyke breaches and guidelines to dyke construction are presented.

1.6.2 Experimental analysis in the past

Table 3.1a and b give an overview on past hydraulic dyke breach modelling due to Overtopping, whereas model investigations involving e.g. cohesive materials, piping failure, seepage or surface protection measures are not considered herein. The parameters are H = dyke height, C_L = crest length, L = dyke width, Su = upstream (subscript u) dyke slope, S_d = downstream (subscript d) dyke slope and dm = mean grain diameter. The listed investigations differ particularly regarding the erosion process (2D or 3D), constant or falling reservoir levels and the presence or absence of a surface or core layer. The dyke dimensions and the sediment diameters are comparable with the present research. All investigations mainly determined the breach process, the breach profiles and the breach discharge.

Research on dyke erosion started once the basics of sediment transport were available. Tinney and Hsu (1961) conducted laboratory and field experiments on the washout of an erodible fuse plug and described the side erosion characteristics. They explained the washout mechanisms

based on the laws of sediment transport. Hydraulic model tests on the protection of rock and earth fill dams with armoring against overtopping flow erosion were investigated by Sarkaria and Dworsky (1968). Martins (1981) analyzed the stability of small overflow rockfill dams, thereby concentrating on downstream slope failure. Fujita and Tamura (1987) investigated enlargement of breaches in the flood levee on alluvial plains and find out the hydraulic characteristics and the mechanism that operate during enlargement of a breach. Fujita et al., (1987) conducted on the inflow of river water and sediment due to levee breach; they investigated breach expansion process using different sizes of levee.

A large study on the mechanism of overflow erosion on embankments was conducted by Powledge et al. (1989 a, b). Part I presents model and research activities on dams and levees subjected by overtopping flow, discussing the effectiveness of various protection systems, whereas Part II focuses on the hydraulics of water flowing over a dyke levee including distinctive erosion zones. Islam et al., (1994a) examined embankment failure and sedimentation over the floodplain in Bangladesh: field investigation and basic experiment; they carried on field investigation and conducted a physical model study, to find out the process of floodplain sedimentation due to river embankment failure.

Coleman et al. (2002) conducted flume experiments on overtopping breaching of non-cohesive homogenous embankments. Their results include information on the breach erosion process, the breach geometry and the breach discharge, allowing for flood prediction due to dyke failure. Chinnarasri et al. (2003) investigated flow patterns and the progressive damage of dyke overtopping, distinguishing various stages of dyke damage and accounting for the degradation rate of the dyke crest. Aureli and Mignosa (2003) described the comparisons between experimental and numerical results of 2D flows due to levee-breaching; mainly, they focus on flow phenomena on the breaching section. Rozov (2003) conducted laboratory experiments to investigate the process of dam breach erosion. He described the physical mechanism of dam washout and developed a mathematical model for simulating the dam breach process.

A unique series of field tests to study the stability of embankment dams of various materials was presented by Höeg et al. (2004). Their tests included failures due to overtopping and piping of

up to 6 m high dykes and the corresponding laboratory scale tests. Cao et al. (2004) presented one of the first computational models on breach hydraulics of erodible dykes, based on sediment transport and the morphological breach evolution. Tsujimoto et al., (2006) studied levee breach process of a river by overflow erosion; they conducted numerical approach for the evolution process of levee using unlike relative height of floodplain to river bed. In Hokkaido, Japan also, Full Scale overflow breakage tests were first performed using the Chiyoda Test Channel (completed in 2007) to examine the dyke breakage/widening mechanism. Shimada et al., (2010) observed levee breach experiment by overflow at the Chiyoda experimental channel; they observed the process of levee widening with time using different sizes of levee materials.

1.6.3 Dyke failure modes

A dyke failure can be either natural or man-made. Natural failures occur due to extreme flood events, earthquakes, soil settlements, piping, seepage, overtopping, or animal burrowing. Man-made causes include e.g. poor construction, incorrect design, improper location, or sabotage. In many cases, a combination of several failure modes leads to the actual dyke failure. In the particular case of earth dykes, the most common failure causes and modes are (Singh 1996):

(1) Overtopping caused by extreme floods

(2) Structural failure due to internal erosion (piping)

(3) Structural failure due to shear slide

(4) Structural failure due to foundation problems

(5) Failure due to natural or induced seismicity

Causes (1) and (2) are related to hydraulic failure, whereas causes (3) to (5) are mainly dominated by geotechnical processes and therefore correspond to 'geotechnical failures'. All failure mechanisms are discussed below. The governing mechanisms of dyke failures were also described by the University of California in 2006. The majority of dykes and earthen embankments breach due to overtopping or a combination of overtopping and internal erosion (Singh 1996). Therefore, this work focuses exclusively on the overtopping failure mode. Most earth dykes are not designed to resist overtopping and their resistance to surface erosion is limited.
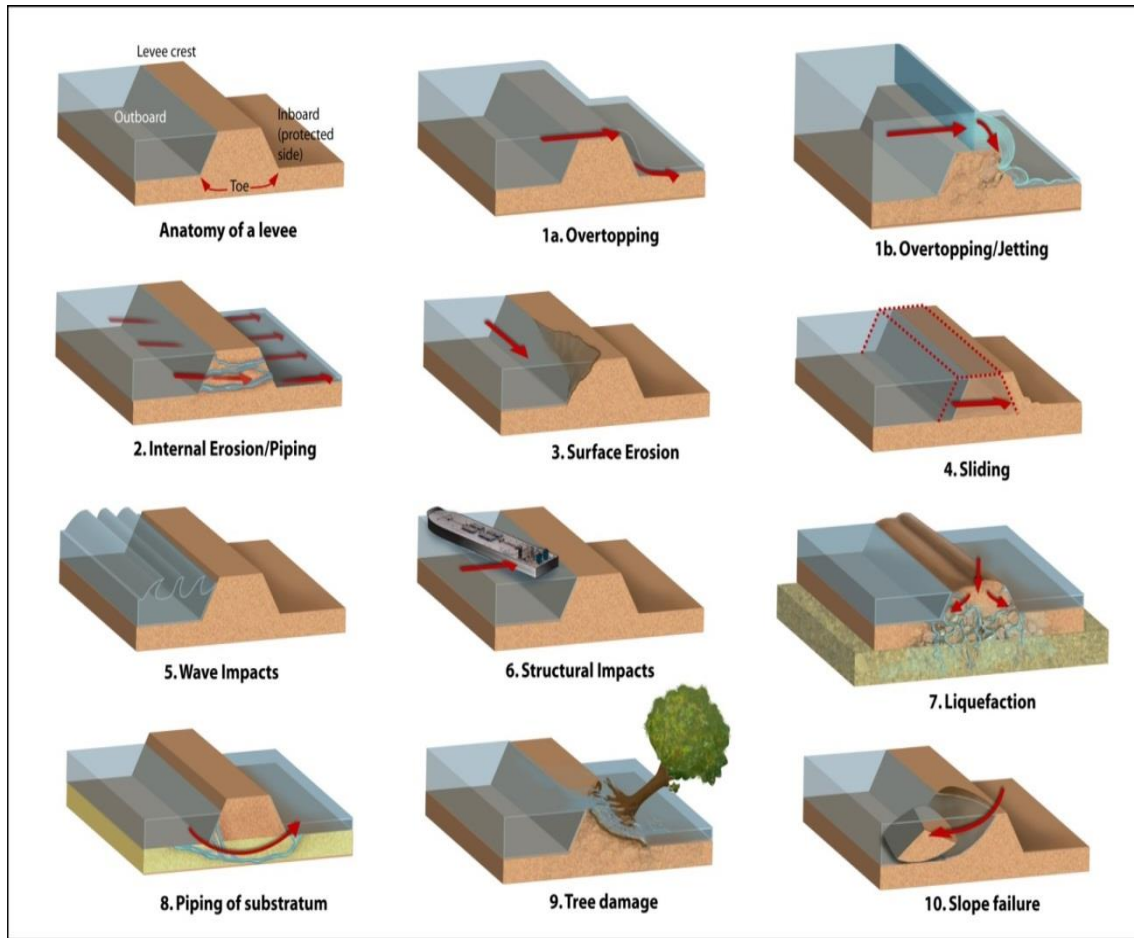
Figure 1.6   Dyke failure mechanism (Source: National Science Foundation)

1.6.3.1 Overtopping caused by extreme floods

Dyke overtopping starts normally at the lowest crest elevation or at a local dyke discontinuity, e.g. at a bridge abutment. The shear stresses induced by the water flow over the downstream dyke slope initiate the erosion process. Erosion starts if the induced shear stress exceeds the critical sheer stress of the dyke material. The soil particles are then entrained and transported downstream. Any initial small breach or a local soil settlement represent a crest weakness and may develop into a larger breach resulting in dyke failure. During the 2005 Hurricane Katrina in New Orleans (LA), fifty dyke breaches occurred, of which forty breaches were due to overtopping (Daniel 2007). Figure 1.8 and 1.9 shows dyke breaches due to overtopping.
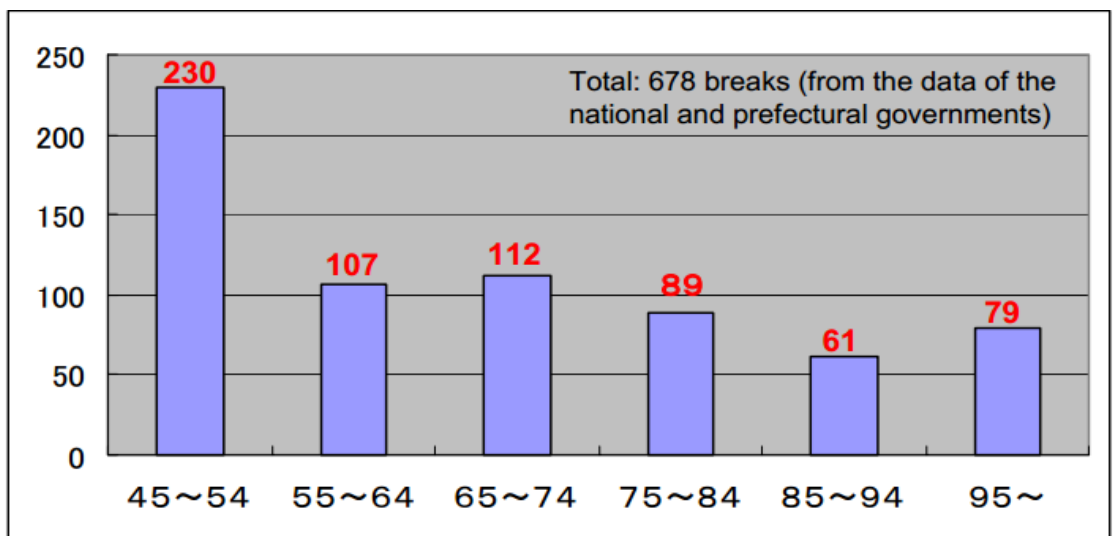
Reference: Actual states of breaking of dykes WWII (2002, River Improvement and Management Division)

Figure 1.7 No. of breaks in Japan per year for each decade after 1945

Figure 1.8 Example of a burst in dyke caused by seepage and overtopping combined
(Maruyama River, October 2004; Source: MLIT, Japan)

a) Yabe River (Japan) Dyke breach   b) Embarrass River Dyke breach

Figure 1.9 River dyke breach due to overtopping examples (Source: Mizutani et.al.2012)

1.6.3.2 Structural failure due to internal erosion (piping)

Internal erosion occurs if particles of the dyke are entrained downstream by seepage or groundwater. It only develops if two conditions are met: particles must be entrained and then be transported by the flow. Various processes are distinguished (Hagerty, 1991a): entrainment, backward erosion, blowout, buoyancy, dissolution, suffusion (washout of small soil particles from an inhomogeneous soil) and piping. Internal erosion initiated by seepage that removes solid particles and builds tubular cavities is called piping. The water seeping through a dyke creates an open path for flow, carrying particles with it and washes them out, resulting in a loss of material essential for dam safety. The instability of the undercut layer located above the zone of soil loss may result in a collapse of the dyke.

The necessary conditions for piping include an open exfiltration face, a source of water, concentration of flow, removal of failed and displaced soils and a sufficient hydraulic gradient at the exfiltration face. Unlike overtopping, piping is often detected in its early stage and remedied before it becomes a serious issue. For new dykes, the potential for internal erosion and piping can be controlled by a good geotechnical design and construction of a dyke core and additional

Table 3.1 a: Experimental Study on Dyke breaching due to overtopping

| Author	Breach Process	Dyke Dimension	Dyke material	Core/drainage	Results
Bhattarai et al. 2015 (Present Study)	3D, rectangular pilot channel, dyke not perpendicular to flow direction, constant inflow discharge	$H=0.15m$, $C_L=0.075m$, $L=1m$, $S_u=S_d=1:2$	Sand, $dm=0.314,0.166$ and $0.089mm$	None	Breach process, Breach and sediment discharge, lateral widening, scour
Mizutani et.al. 2012	2D, falling reservoir level	$H=0.15m$, $C_L=0.1m$, $L=0.3m$, $S_u=S_d=1:2$	Sand, $dm=0.314,0.166$ and $0.089mm$	None	Breach profiles, breach discharge, seepage movement
Schmocker 2011	2D,3D, triangular pilot channel, falling reservoir level	$H=0.1-0.4m$, $C_L=0.05-0.1m$, $L=0.2-1m$, $S_u=S_d=1:2-1:3$	Sand, $dm=1-2mm$ Gravel,$dm=2-58mm$	Bottom Drainage	Breach Process, breach profiles, breach discharge
Pickert et al. 2011	3D, rectangular pilot channel, constant reservoir level	$H=0.3m$,$C_L=0.1m$, $L=1m$, $S_u=S_d=1:3$	Sand $d=0.185,0.50,0.64mm$	Toe drain	Breach process, breach profiles, breach discharge
Gregoretti et al.2010	3D, constant inflow discharge, sloping bed 0-10%	$H=0.2-0.4m$, $C_L=0.4m$ $L=0.5m$, various S_u and S_d.	Uniform gravels $d=3.9, 6.8,10.3mm$	None	Breach process, head cutting failure
Jandora and Jaromir 2008	3D, rectangular pilot channel, falling reservoir level	$H=0.86m$,$C_L=0.2m$, $L=3.75m$, $S_u=S_d=1:2$	Sand $d=1.7mm$	None	Breach process, lateral erosion
Dupont et al. 2007	2D, falling reservoir level	$H=0.25m,0.35m$, $C_L=0.2,0.28m$, $S_u=1:1.75,1:2$ $S_d=1:2$	Gravels $d=2-4mm$ and $2-7mm$	Clay surface layer	Breach process, breach discharge

Table 3.1 b: Experimental Study on Dyke breaching due to overtopping

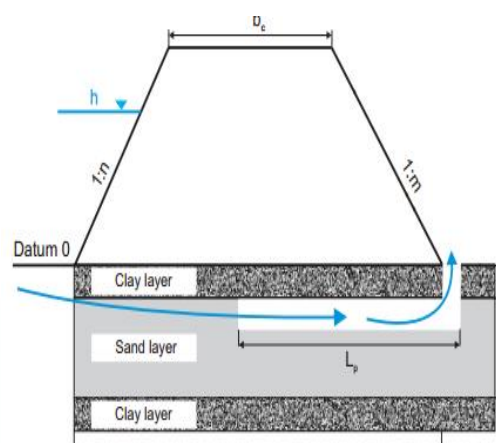| Author	Breach Process	Dyke Dimensions	Dyke materials	Core/drainage	Results
Hager and Unger 2006	2D, falling reservoir	H=0.05-0.3m, C_L=0.1m, Su=Sd =1:3	Uniform coarse sand dm=1.15,2.3,5 mm	None	Breach process, breach profiles
Spinewine et al. 2004	3D, trapezoidal pilot channel, falling reservoir level	H=0.47m, C_L=0.2m, Su=1:2, Sd =1:3	Uniform coarse sand D=1-2 mm	None	Breach discharge, surface velocities, water and bed level profiles, 3D breach profile
Chinnarasri et al. 2003	2D, falling reservoir level	H=0.80m, C_L=0.3m, Su=1:3, Sd =1:2,1:2.5,1:3	Sand d =0.36 and 0.86mm	Bentonite surface layer	Flow patterns, breach process, degradation rate of dyke crest
Rozov 2003	3D, rectangular pilot channel, constant reservoir level	H=0.20m, C_L=0.2m,Su=Sd =1:3	Sand d =0.34 mm	None	Breach process, breach profiles, breach discharge
Coleman et al. 2002	3D, triangular pilot channel, constant reservoir level	H=0.30m, C_L=0.065m,Su=Sd =1:2.7	Homogenous sediments dm=0.5, 0.9, 1.6, 2.4mm	Toe drain	Breach process, breach profiles, breach discharge
Pugh 1985	3D, triangular pilot channel, constant reservoir level	H=0.15-0.38, C_L=0m ,Su=Sd =1:2	Sand dm= 0.5-8mm Gravel dm= 3-15mm	Clay core and sand filter	Breach process, breach discharge
Tinney and Hsu 1961	3D, rectangular pilot channel, falling reservoir level	H=0.20-0.40, ,Su=1:1.25 Sd =1:1.5	Coarse sand d = 4mm Pea gravel d = 6mm Crushed rock d =10mm	Clay core and sand filter	Breach process, washout rate and scaling issues.

provision of filters to intercept seepage. A discussion of piping/seeping erosion in stream banks is presented by Hagerty (1991a, b).

A catastrophe caused by piping was the failure of the St. Francis Dam in California in 1928. The dam failed suddenly after a highly-erodible sediment rock formation was washed out, undermining portions of the concrete dam. Different piping events occurred during the flood events in Switzerland 2005 along the dykes of the Linth River channel, fortunately not resulting in any dyke breach. Further, uncontrolled seepage through dykes can led to severe dyke damage. Detailed descriptions of seepage and drains are found e.g. in Cedergren (1989). Before the twentieth century, the engineering works made of earth material had no theoretical background. The resulting designs were often uneconomical offering no safety against seepage failure. Darcy's fundamental experiments with seepage phenomena furnished a simple explanation for the seepage process trough homogenous soil and drainage systems. Further improvement for scientific and experimental earthwork design was achieved by Terzaghi (1925). The explanation of the seepage theory for practical aspects by Casagrande (1937, 1961) represents a major step forward in the design of earth dams and dykes.

The most common methods to control seepage are sealing and drainage methods. Drainage is the process by which percolating water is removed from soils and rocks by natural or artificial means. Dykes often contain no internal drainage system but foot drainage or a sealing. However, all dykes will experience seepage, even if they are made relatively impermeable by using selected, possibly artificial materials or watertight membranes. Therefore it is necessary to know the flow net to predict the seepage rate. The seepage depends mainly on the dyke geometry, the dyke and foundation materials, and the hydraulic characteristics of the dyke and its foundation. There are different methods available to predict the seepage rate of dykes. For homogenous dykes or central core dykes the seepage can be estimated by the method of Kozeny (1927) or Casagrande (1937).
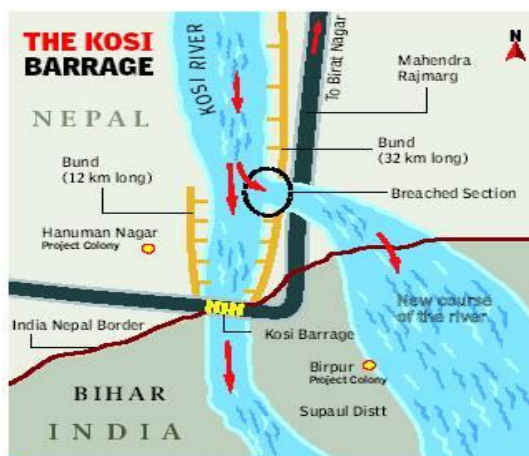
a)   River Dyke Breach in Nepal   b) Schematic representation of piping failure

Figure 1.10 Dyke breach in Nepal and piping failure mechanism

The seepage rate is predicted by either graphical techniques (flow net) or numerical methods. The Casagrande method and most numerical models do not consider unsaturated flow. Chapuis and Aubertin (2001) presented a numerical model to estimate saturated and unsaturated seepage through dykes under steady state conditions. An overview and comparison of different methods to predict steady state or transient seepage through dykes is given by Haselsteiner (2007).

1.6.3.3 Geotechnical failures

All geotechnical failures have in common that the effective driving forces on the dyke or foundation exceed the resistance, so that the original dyke profile cannot be obtained. The effective forces are the dead load and the traffic loads, horizontal forces (water pressure, ice pressure, waves, or wind) and the dynamic forces (seismic, machine and ram works). The effective resistances are conditional characteristics of a dyke and its foundation materials (friction, cohesion, coefficient of elasticity). The failure can affect the dyke itself (sliding) or just part of it (slope failure), as well as the entire foundation (settlements) or part of it (bearing capacity failure, shear failure).

1.6.4 Concept of overtopping erosion

The overtopping flow of a dyke is similar to the flow over a broad-crested weir with low or no tail water. Powledge et al. (1989a, 1989b) presented model and prototype research studies on overtopping flow over embankments, dams, dykes, roadways and stated three flow regimes and three corresponding erosion zones. The three regimes shown in Figure 1.11 are described below.

Erosion Zone 1 – Subcritical flow over dyke crest
A subcritical velocity state dominates the change from the river to the upstream portion of the dyke crest. The flow proceeds from relatively static head in the river to a combination of static and dynamic heads along the upstream dyke slope. Due to the small energy gradient and minute flow velocities (F < 1) the hydraulic forces are small. Even though the flow depth may be quite large, the small energy gradient imposes a small tractive stress. Erosion will occur only if the dyke crest consists of highly erodible material.

Erosion Zone 2 – Supercritical flow over dyke crest
In this zone transitional flow occurs, characterized by critical flow and the critical flow depth. The energy level is about the same as in Zone 1, but the energy gradient can be large resulting in a significant increase of the tractive stress. However the distance over which they occur is limited, depending on the dyke crest geometry, so that erosion is mainly expected at the downstream crest portion. Erosion starts if the critical shear stress of the dyke material is exceeded.

Erosion Zone 3 – Supercritical flow on dyke downstream slope
In erosion Zone 3, the energy head progressively increases as the water flows down the dyke face. The energy gradient is steep resulting in a significant velocity increase until energy loss equilibrium and uniform flow are attained. This will however only occur for high embankments. The tractive stresses are large, leading to a high erosion potential.

Based on observations of embankments slopes during overtopping, the erosion process initiates most commonly at a point of slope discontinuity, such as the toe or base of the dyke. However, depending on the particular condition and configuration of the embankment, the initial erosion may start anywhere. In many cases, after the erosion was initiated, surface discontinuities occur resulting in a cascading flow. The tractive stresses on the downstream dyke surface are therefore not consistent.
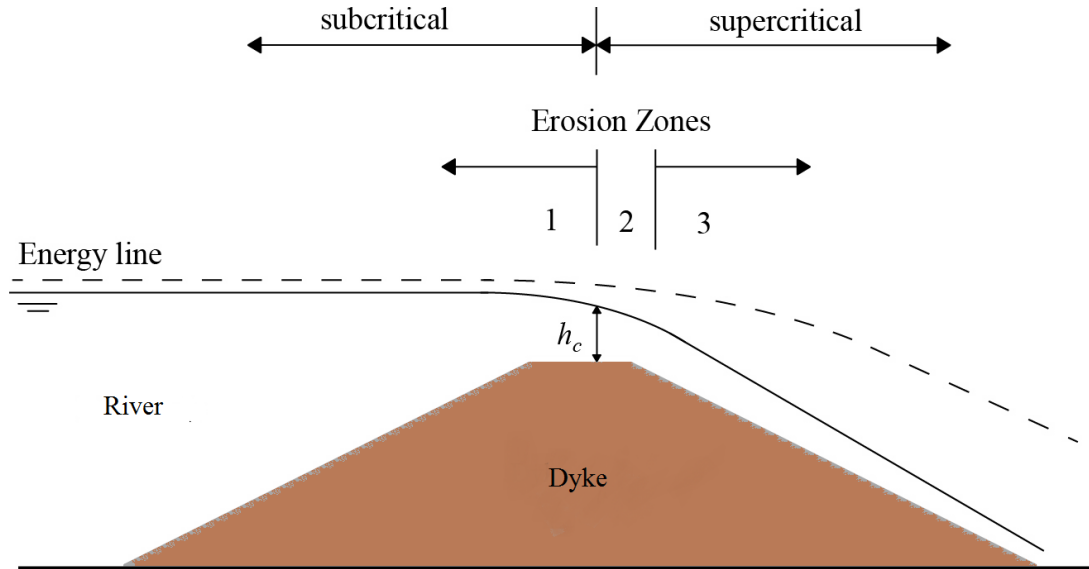

Figure 1.11 Hydraulic flow regime and erosion zones (modified after Powledge et al. 1989b)

For embankment dams, Powledge et al. (1989b) listed the following physical factors having a strong effect on ignition and erosion rate: (1) Embankment configuration, types of material and fill densities; (2) Maximum flow velocity; (3) Discontinuities (berms, roads, outlets, ditches), cracks, or voids in the slope; (4) Presence and height of tail water on downstream slope; (5) Flow concentration at low points along the embankment or at the abutment groins; and (6) Toe drains, or blanket drains. The breach process is discussed in Chapter 1.7.

1.7 Breach Process

1.7.1 Introduction

Dyke breaching represents a complex interaction between hydraulic, geotechnical and structural processes. The breaching process varies with material type and state, hydraulic load and dyke condition. Several distinct stages have been observed and differ especially for cohesive or non-cohesive materials. As the current project is limited to breaches of incohesive dykes due to overtopping, only this process is discussed below. Various model studies in the past investigated both plane (2D) and spatial (3D) breach processes due to overtopping using hydraulic modeling. Further, the evaluation of real case data resulted in additional information on the breach process.

1.7.2 Plane dyke breach process

Plane dyke erosion was investigated among others by Powledge et al. (1989 a, b), Chinnarasri et al. (2003) or Dupont et al. (2007). Powledge et al. (1989b) described the breach development for both granular and cohesive embankments due to overtopping. Especially for granular embankments, seepage can have a significant effect on the erosion process. Once overtopping occurs, the seepage exiting on the downstream dyke face accelerates the erosion. Surface slips and sliding failures result in a fast enlargement of the breach. Cohesive embankments are generally more resistant to overtopping breaching due to the greater erosion resistance and the reduction of seepage. Erosion starts often on the embankment toe and propagates upstream, undercutting the slope, causing large chunks of material to be removed by soil tensile and shear failure on the over steepened slope. Powledge et al. (1989a) listed several factors influencing the overtopping erosion, mainly: (1) Dyke configuration, material types and density for earth fill, (2) Maximum flow velocity, (3) Discontinuities, cracks in the slope and anomalies at the toe, (4) Presence and height of tail water, (5) Flow concentration at low points along the embankment, and (6) Toe drains, or blanket drains.

Chinnarasri et al. (2003) observed four stages in plane dyke erosion (Figure 1.13), namely: (a) Small erosion on dyke crest after initial overtopping, (b) Slope sliding failure with ongoing erosion, (c) Wavelike-shaped dyke profile, and (d) Large sediment wedge deposition with small slope at erosion end. Similar processes were also noted by Dupont et al. (2007). They additionally observed sliding of the lower part of the downstream slope just before actual overtopping. The erosion progresses from the downstream face toward the crest, with the downstream face rotating around a pivot point (Figure 1.12). With ongoing erosion, antidunes are generated on the downstream face.

The observed dyke breach profiles differ mostly due to particular test setups. Pure plane erosion can only be obtained by limiting the dyke length. Otherwise 3D erosion patterns occur and influence the breach process. Further, the existence of a surface layer or a core may affect the erosion process significantly. The volume of the upstream reservoir or increasing inflow discharge mainly determine the breach duration. Despite several extensive hydraulic model tests made in the past, a general plane dyke erosion profile is not yet available. Most of the available data are limited to the test range and were directly used to validate numerical models.

Figure 1.12 Rotation of downstream dyke face around pivot point in the first stage after overtopping (Dupont *et al*. 2007)

1.7.3 Spatial breach process

An overview on spatial breach formation is provided by Singh (1996), Coleman et al.(2002), Rozov (2003), Chinnarasri et al. (2004), Spinewine et al. (2004), Visser et al.(2006), Morris et al. (2008), or Pickert et al. (2011). This erosion process normally occurs in engineering applications and includes both vertical and lateral erosion. Especially the fundamentals of the lateral erosion are currently not fully understood. Colemanet al. (2002) presented embankment breach tests under constant reservoir level and described the breach process in detail. Flow through a pilot channel located at the channel side wall initially erodes a small breach channel on the downstream embankment face from the crest to the toe. The breach then expands primarily vertically to predominantly lateral erosion as the breach channel approaches the embankment foundation.

Embankment material is eroded by the process of tractive shear stress and turbulence. Undermining of the breach channel side slopes causes large volumes of material to collapse into the channel centre and gets transported downstream. The breach channel is of curved (hourglass) shape in plan. This shape increases in curvature with time until the vertical erosion is inhibited by the embankment foundation. Coleman et al. (2002) further accounted for both longitudinal breach profiles and breach cross sections. A similar breach process was observed by Rozov (2003), hence with the pilot channel located in the embankment centre. After the initial vertical breach had occurred, the lateral erosion proceeded to both sides.

Chinnarasri et al. (2004) investigated the breach geometry in homogenous embankments under falling reservoir level. They observed primarily vertical erosion in the initial breach with subsequent lateral erosion after the breach approached the fixed embankment foundation. The lateral erosion was predominated by a combination of tractive shear forces and instabilities of the side slopes, causing the collapse of large volumes of embankment material. The breach shape was rectangular at initial breaching and developed into a trapezoidal shape with ongoing erosion and reservoir drainage.

Visser et al. (2006) distinguished five stages in the process of overtopping breaching, for both sand and clay dykes. The breach started with the flow entering a small initial breach located at the top in the middle of the dyke. During Stages I and II, the breach developed gradually by decreasing the height of the dyke and increasing the width of the initial breach channel. During Stage III the breach growth accelerated until the dyke was completely washed out in its breach section. The breach then expanded mainly laterally during Stage IV and decelerated in Stage V under decreasing backwater and hence decreasing breach discharge.

Schmocker et al. (2011) presented hydraulic model tests of fuse plug embankments. They investigated both the vertical and lateral erosion processes due to overtopping. Figure 1.15shows the temporal erosion process, initiating as the flow enters the pilot channel and in a first step, proceeds vertically. With ongoing vertical erosion, the lateral erosion increases and is mainly dominated by a collapse of large sediment chunks.

Pickert et al. (2011) conducted a series of spatial embankment breach tests due to overtopping. They divided the failure of homogeneous embankments into two breaching phases. The "breach evolution" started with initial embankment overtopping and ended when the erosion reached the upstream embankment shoulder. The second phase "breaching" was dominated by a rapid increase of both erosion and breach outflow due to vertical and lateral breach widening.

Further, the erosion process depended on the sediment diameter and was especially influenced by apparent cohesion. No continuous erosion was observed for fine sand and the classification of the cross-sectional breach profile was difficult. The lateral erosion was a combination of constant erosion and sudden collapse of the breach side slopes.

The laboratory effort for spatial breach tests is comparatively high. Therefore, systematic investigations are not available and most past research was limited to some five individual tests. Further, recording breach profiles and breach cross-sections is complex as the spatial breach process remains mostly invisible and cannot be simply recorded through the channel side wall.

1.8 Dyke breach measurement process and devices

Several laboratory methods were used in the past to determine the breach and free surface profiles during a dyke breach. The plane dyke erosion process is comparatively simple to record, as no 3D flow patterns occur. Both the temporal water and sediment surfaces during an erosion process can be recorded across a glass channel sidewall. Most researches simply recorded the breach process using a standard CCD camera. The profiles can be directly determined from the images using standard graphical programs.

For spatial breach topography, an observation of the breach profiles across the channel sidewall is impossible, given the 3D erosion patterns. If the pilot channel is located at the channel side wall, the dyke breach may be recorded but only the breach profile directly at the channel side wall is visible. Therefore, other measuring techniques have to be applied to the spatial dyke breach problem. Intrusive instrumentation including point gages is not applicable as they disturb the erosion process. Coleman et al. (2002) drained the reservoir at several stages of the erosion process to record the 'dried' 3D surface topography using a surface profile measurement system. However, the effort to determine these profiles is comparatively high, and the degree of disturbance the embankment during discharge turn-off considerable. The embankment had to be entirely rebuilt once the reservoir was drained and the test was repeated to measure the breach profile at an advanced stage. One experiment only resulted in one temporal breach topography.

Spinewine et al. (2004) used a range of measuring systems to determine both discharge parameters and breach geometry during a dyke breach test. They introduced a non-intrusive technique involving a sweeping laser light sheet system combined with digital imaging algorithms. The principle involves a laser light sheet to illuminate a particular breach cross-section capturing the line imprinted on the dyke onto digital images. The technique can be used to obtain full digital terrain models of evolving breach topography. However, as the laser passes through the water surface it undergoes refraction effects and therefore the measured bed
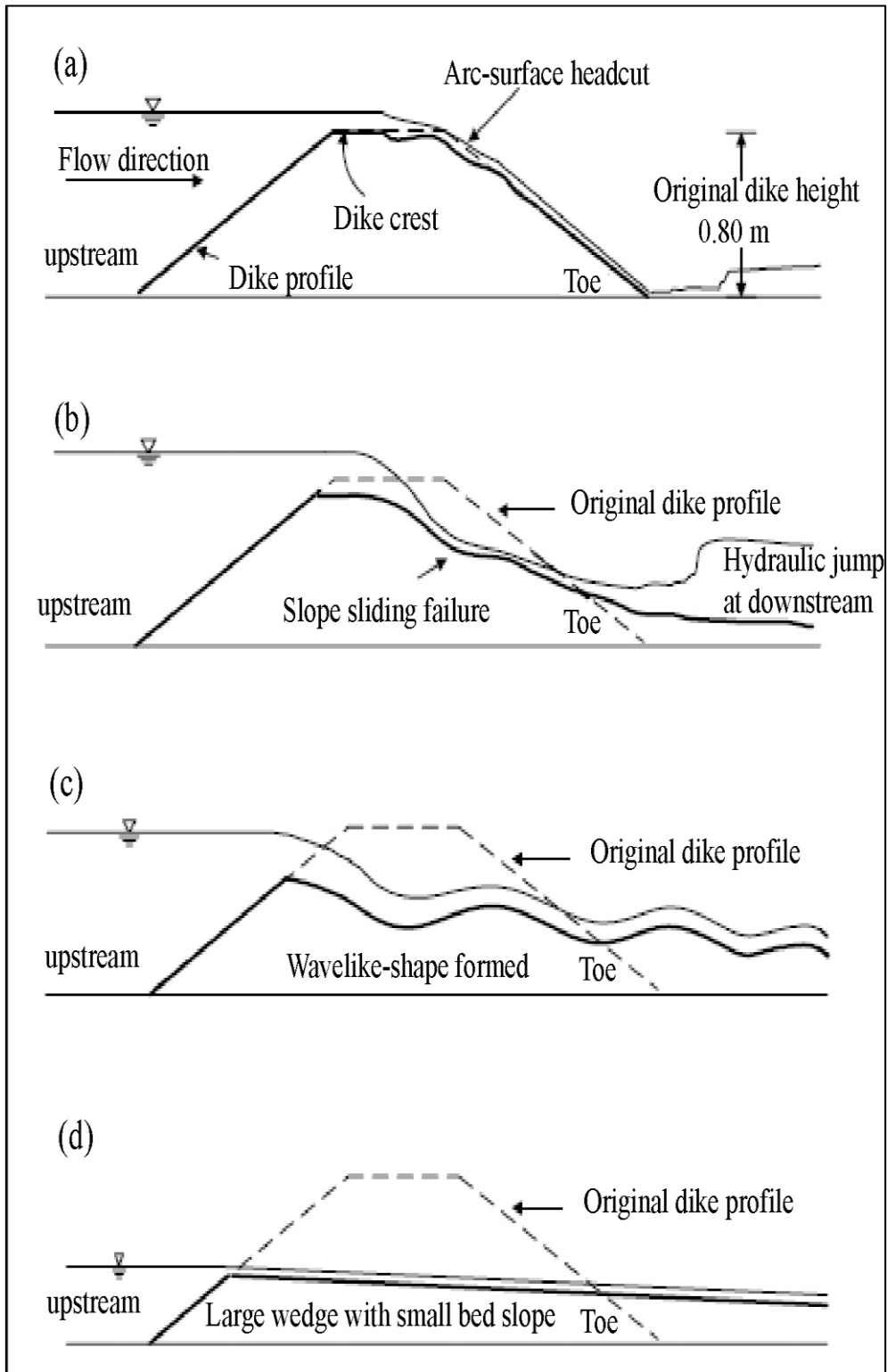
(a)

Arc-surface headcut

Flow direction

Dike crest

Original dike height
0.80 m

upstream

Dike profile

Toe

(b)

Original dike profile

upstream

Slope sliding failure

Toe

Hydraulic jump
at downstream

(c)

Original dike profile

upstream

Wavelike-shape formed

Toe

(d)

Original dike profile

upstream

Large wedge with small bed slope

Toe

Figure 1.13 Process of dyke failure due to overtopping (Chinnarasri *et al.* 2003)

22

level has an error proportional to the water depth and the water surface slope. Pickert et al. (2004, 2011) used a so-called Fringe Projection to continuously measure 3D breach profiles. An alternating black/transparent stripe pattern was produced on the dyke surface using a slide projector and recorded with a video camera through the channel sidewall. The spatial breach profile at various times was determined from the camera images. The breach process could only accurately be observed during the initial phase, however, as the observation through the sidewall failed for large breach widths.
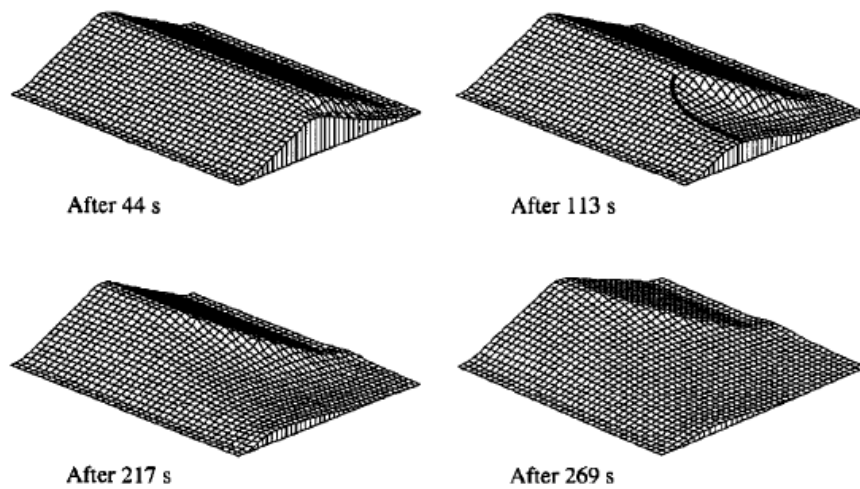
Figure 1.14 Breach developments for coarse-sand embankment (Coleman *et al.* 2002)
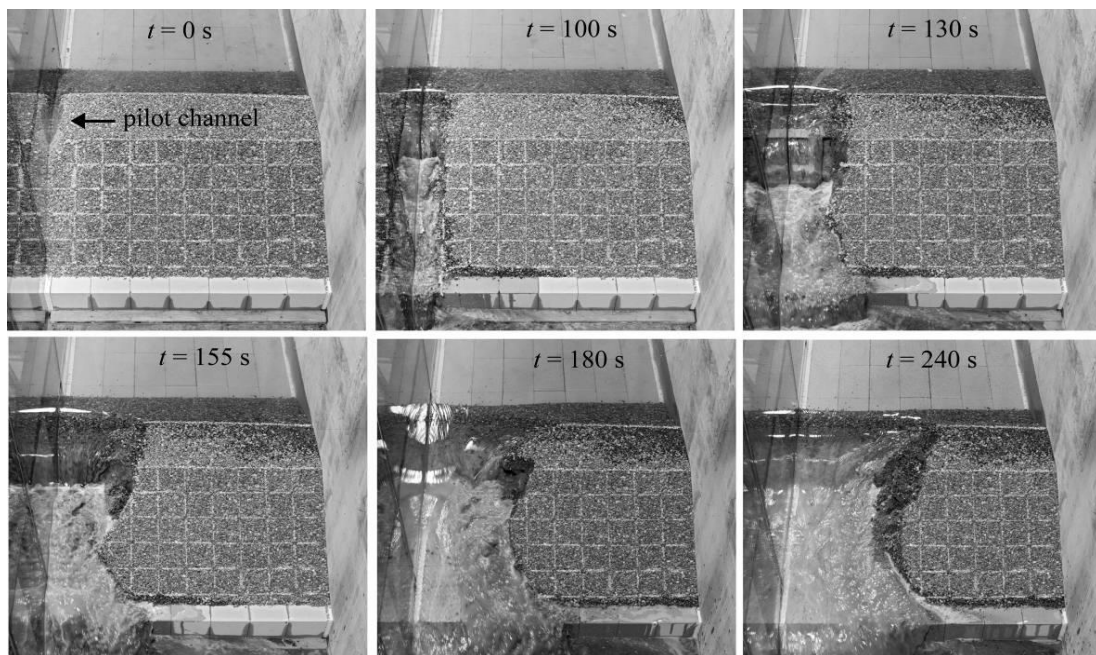
Figure 1.15 Advance of spatial fuse plug erosion at different times *t* (Schmocker *et al.* 2011)

1.9 Numerical simulation of dyke breaching

1.9.1 Seepage flow modelling

Several numerical models have been developed for simulating the movement of water in variably saturated porous media. In most applications, the pressure-based form of the variably saturated flow equation is used (Neuman, 1973; Cooley, 1983; Huyakorn et al., 1984, 1986) since the moisture based formulation cannot be used in saturated regions. However numerical solutions of the pressure-based form of Richard's equation are known to have poor mass-balance properties in unsaturated media (Celia et al., 1990; Kirkand, 1991). In the literature, a variety of numerical schemes including finite-difference, integrated finite difference and finite-element methods have been used to solve variably saturated flow problems (Neuman, 1973; Narasimhan and Witherspoon, 1976; Cooley, 1983; Huyakorn et al., 1984, 1986). Fewer researches have used finite differences to solve variably saturated flow problems (e.g. Rubin, 1968; Cooley, 1971; Freeze, 1971a, b; Kirkland et al., 1992; Clement, 1994). However most of the existing two-dimensional finite differences solutions to variably saturated flow problems have limitations (Clement, 1994). In particular, finite difference algorithms offer three major advantages; ease of coding, ease of data input, and more ready public acceptance in comparison with finite-element models (Clement, 1994)

Seepage analyses are an important tool to assess the susceptibility of seepage failures in dams and to study hydraulic conditions for analyzing the stability of dam slopes. Freeze (1971b) and Neuman (1973) are the foremost researchers who considered the variably saturated soil for transient seepage analysis of dams. 2D transient seepage analysis using saturated-unsaturated seepage theory was conducted to consider initial filling of various reservoirs (Lam et al. 1987; Ng and small 1995; Chen et al., 2005) and water-level fluctuations in front of dams (Aral and Maslia 1983; Lam et al. 1987). For dams built in narrow valleys, three-dimensional effects are likely significant and two dimensional simplifications may not be consistent with field conditions. To consider three dimensional effects in seepage through dams, Gupta et al. (1986), Xie et al. (2001), and other investigators conducted three-dimensional analyses based on saturated seepage theory. Freeze (1971) presented three-dimensional analyses of flow through earth dams that included unsaturated soil domains. Chen and Zhang (2006) studied infiltration into rockfill dam using 3D saturated-unsaturated seepage theory. Their study shows that seepage water flows faster and the hydraulic gradients are greater near the abutment boundary in the dam so the 2D analyses will underestimate the risk of seepage failure, particularly near the abutment boundary.

1.9.2 Embankment breaching

A number of numerical techniques have been developed to predict peak discharge of dam-break flood, time-to-peak, and final breach dimensions. Many empirical formulations have already been developed for predicting dam breach characteristics and peak outflows based on hydraulic and geometric properties of dams and reservoirs. Kirkpatirick (1977), Hagen (1982), MacDonald & Langridge-Monopolis (1984), Costa (1985), Forehilich (1995), Evans (1996),

Walder & O'Conner (1997), Broich (1998) developed regression equations to determine peak discharge. All of these methods, except Walder & O'Connor, are straight forward regression relations that predict peak outflow as a function of various dam with the relations developed from analyses of case study data from real dam failures.

In the last forty years, particularly since the 1980's, many mathematical models have been developed for the simulation of breach growth in embankments. Some models ignore the mechanism of erosion by lumping every possible factor into two principal parameters: final shape and breach formation time (Fread, 1998a; U.S. Army Corps of Engineers, 1981). Other physically based embankment breach models use principles of hydraulics, theory of sediment transport and soil mechanics to simulate the breach growth process and the breach flow hydrograph. The category includes models, e.g. Ponce and Tsivogolu (1981), Fread(1988b), Singh and Scarlatos (1988), Bechteler and Broich (1991), Visser (1988), and Wang and Bowles (2006)

Several previous studies attempted to use numerical simulation to reproduce the phenomenon of embankment erosion and failure due to overtopping flow. For example, Tingsanchali and Chinnarasri (2001) developed a one-dimensional numerical model that considered circular slope stability for embankment failure and compared the simulated results with the experimental results. They indicated the importance of the estimation of the erosion rate calculated using a sediment transport formula. Several sediment transport models were applied to their model, and the coefficients of the sediment transport model were adjusted by trial and error to fit their experimental data and to investigate the effect of coefficients related to the erosion rate. Gotoh et al. (2002; 2008) introduced the moving particle semi-implicit (MPS) method, which is classified in a gridless numerical model, a numerical model of embankment erosion that avoids numerical diffusion in water surface tracking. The pick-up sediments from the embankment surface were calculated using an advanced method—a submodel that considers the effect of the velocity component perpendicular to the slope.

However, this sophisticated numerical model also faced a problem related to disagreement of the erosion rate and used the erosion rate based on data from laboratory experiments to reproduce the phenomenon of the experiments and to focus on other topics in their study. Wang and Bowles (2007) developed an embankment breach model using one-dimensional flow and a three-dimensional slope stability model, and indicated the importance of mechanisms of local sliding during the progressive failure process. Their simulations also adjusted several soil parameters, including cohesion, internal friction angle, and erodibility of the embankment soil, to fit the experimental results.

1.9.3 Parametric models

Parametric models derive discharge hydrographs by assuming a final breach size, geometry, and development time, and calculating instantaneous outflows through the evolving breach using standard hydraulic weir formula. DAMBREAK and OUTFLOW3 are the examples of parametric models which can be used for both landslide dam failure and embankment dam. The

DAMBRK model is a dam break flood routing model developed by Fread in 1977 with the latest version released in 1988. The breach is initiated at the dam crest and grows at a linear rate over the failure duration to the ultimate breach dimensions. The OUTFLOW3 was developed by Manville (2001). Three alternate broad crested weir equations are used to generate different values for the instantaneous peak discharge through a trapezoidal breach that would occur if the breach attained its final size instantaneously when the reservoir was at the dam crest.

1.10 Research gaps and purpose of present study

The literature review reveals that a number of comprehensive hydraulic model studies on dyke breaching due to overtopping are available. These studies cover a wide range of parameters regarding hydraulic conditions, dyke designs and sediment properties. Despite this knowledge, the breach process is still poorly understood because only limited test data are available due to a significant laboratory effort. Systematic model tests are scarce and most research is limited to one specific test setup or one specific failure mode. Most results may therefore only be applied to particular problems, e.g. to special dyke configurations or to a particular grain size. Further, new measuring devices to simultaneously determine water surface and sediment profiles were rarely used and are not yet completely established regarding reliability and measuring errors. Most systems were only applied by one specific research team and the overall experience is therefore limited.

Moreover, a lot of numerical simulations of inundation process following to dyke breach has been conducted to make flood hazard maps for almost all rivers with large to meddle scales basins in Japan. In such simulations, levee breach widths and their widening process are very roughly postulated to be proportional to river channel width and visually gathered empirical data. But, they did not consider so much about subsequent phenomena appearing in the river bed and in the floodplain as well as topographic changes over the floodplain during dyke breach. In this research, the attempted have been taken to recognize the dyke breach phenomena and lateral widening process and scour using a numerical simulation scheme and as well as small-scale laboratory experiments.

The objectives of this thesis can be described as follows:

- To review the river embankment breach cases for Japan and world and find research gaps.
- To analyses with preliminary experiments the breach location, breach morphology and breach initiation process for overtopping failure of river dykes with simple setup.
- To perform flume experiments with elaborate realistic setup to investigate the mechanism of river dykes failure.
- To integrate seepage flow model, erosion/deposition and flow model to predict the outflow hydrograph and lateral widening resulted from the failure of river dykes.
- To analyze experimentally scour developed on the dyke foundation and flood plain.

1.11 Outlines of the dissertation

This research consisting of five chapters is organized as follows.

Chapter 1 presents a brief review of the previous literature, background to the work, and objectives of the study.

Chapter 2 presents outline of preliminary laboratory experimental studies to understand process of lateral widening and breach hydrographs. The time of failure curve is also proposed.

Chapter 3 presents a detailed description of individual numerical simulation model namely, seepage model, flow model and erosion and deposition model in details sand how the integrated model will be developed.

Chapter 4 presents results from the integrated model and its comparison with new experimental results. The lateral widening speed, breach and sediment hydrographs and scour patterns at dyke foundation and flood plain is described in details.

Chapter 5 summarizes the conclusions of the study and recommendations for the future study.

CHAPTER 2

PRELIMINARY EXPERIMENTS ON RIVER DYKE BREACH

2.1 Overview

Given the enormous damage potential regarding dyke breaching, it is necessary to understand the damage process of dyke in detail. As the majority of dyke breaches in the world are due to overtopping, this is investigated in detail in the current research. Systematic breach tests were conducted at the Ujigawa Open Laboratory (UOL), Disaster Prevention Research Institute (DPRI), Kyoto University, Kyoto, Japan. A small-scale laboratory experiments have been carry out using homogenous sand to recognize the phenomena appearing in the dyke and topographic changes in dyke. This section describes the laboratory preparation for the runs with experimental conditions to be maintained for operational procedures to fulfill the aforementioned objectives. The main hydraulic test conditions assumed in the current study include:

1) Trapezoidal shaped dyke kept parallel to the river flow direction,

2) Homogenous sediment,

3) 5 % moisture content by weight was added initially to dyke materials and compacted using similar procedure throughout the all experiments and no core layer added,

4) Steady inflow with downstream gate control,

5) Optical recording by video, high speed and three dimensional cameras.

2.2 Model flume

The breach test were performed in the glass sided flume as a river and the dyke was placed parallel to the river flow and having transparent Poly Vinyl Chloride (PVC) wall at both side of the dyke. The horizontal channel is 0.3 m wide, 0.3 m high and 8 m long and dyke opening at the side of channel is also 0.3 m at a distance of 3.35 m from the upstream. The intake is equipped with a flow straightener to generate undisturbed flow from the underground tank with Pump that circulates water continuously between upstream and downstream. The eroded sediment and the resulting water flow were collected manually with the plastic box at the end point of the dyke. The plan and section of experimental setup is as shown in fig 1 and 2.

The parameters investigated include: Flume discharge $Q = 7.89$ l/s, dyke height $H = 0.15$ m, dyke length $L = 0.3$ m, dyke crest width, $b = 0.075$m $(0.5H)$, sediment size = No. 5, No.6, No. 7 and No. 8 (See fig 3). The upstream dyke slope is $S_u = 1:2.5$(V: H) and downstream slope is $S_d = 1:2$(V: H) resulting in total dyke width of $B = 2.5H+0.5H+2H = 5H$. The pilot channel is made at
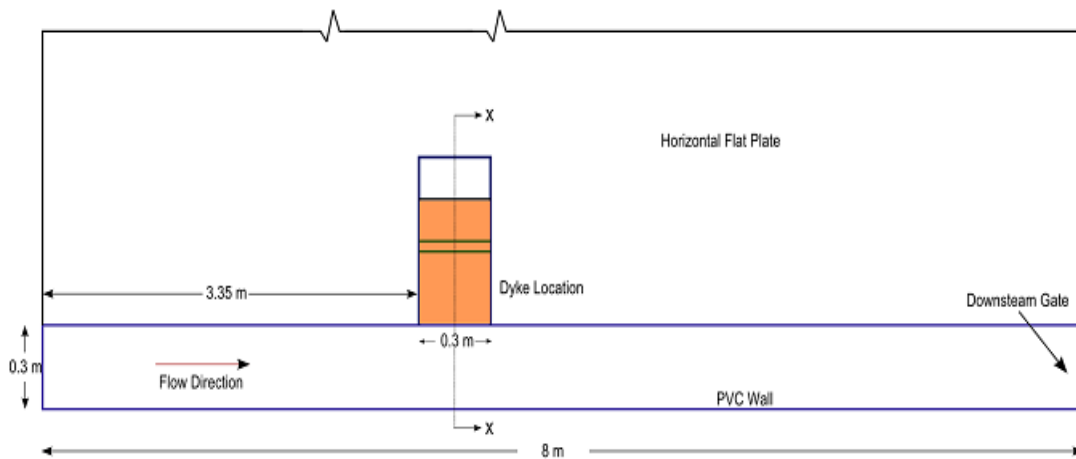
Plan view of Laboratory Set up
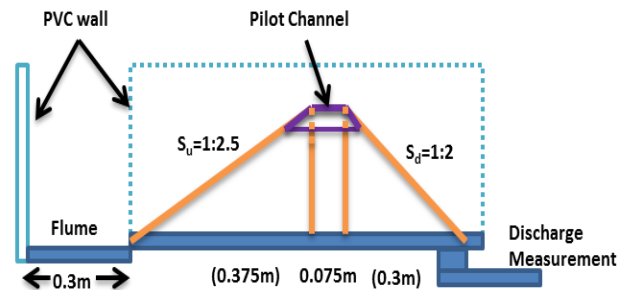
Cross-section along X-X

Figure 2.1 Experimental setup and sediment properties
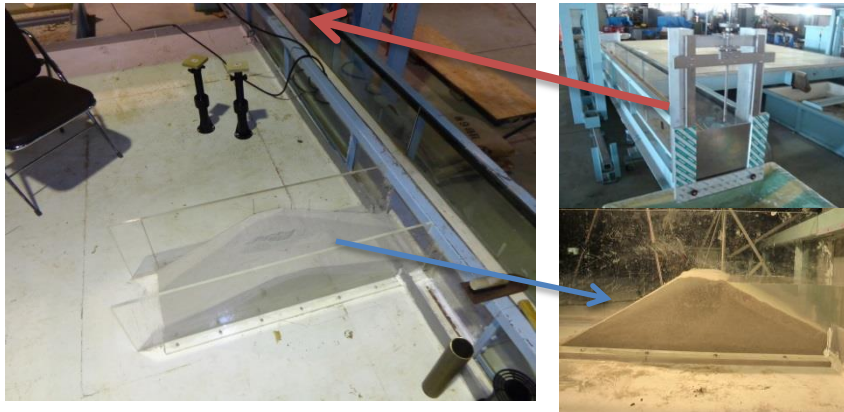
Figure 2.2 Picture of flume, downstream gate and dyke

the center of dyke of size 2.5 cm x 2 cm as a point for the initiation of breach at desired location. To prevent seepage-induced dyke failure prior to overtopping, a temporary wooden plate was used to cover the dyke area until the required depth of water in front of dyke was reached. Then, the wooden plate is slowly removed to generate pure overtopping flow. The discharge was measured at the end of the dyke point with the help of plastic boxes at certain time intervals. The plastic box was then weighed and filtered out wet sediments. The sediment was then put in an oven for 24 hours and weighed. The sediment weight is deducted from the total weight of the box to get actual water volume. Hence, the discharge of the water and sediment is determined by dividing weight by the time interval deduced from the video camera.

2.3 Measurement apparatus

2.3.1 Multi-fold pF meter

The water retentivity of the soil can be expressed by a variety of factors including the volumetric water content and the pF value. The matrix potential (pF value) of a soil sample and its volumetric water content are correlated by a characteristic curve depending on the texture of the soil and this curve is called a "moisture retention curve". DIK-3423 Multi-fold pF meter (Figure 2.3) was used for measuring the moisture retention curve of a soil sample. It can set up to 24 pieces of sampling tubes in the sample chamber. Any optional pF value can be set with the automatic pressure controller. This controller can set an accurate and stable pressure without

taking the influence of atmospheric pressure. A specified pressure is applied to a soil sample and the weight of the soil at equilibrium is measured to determine the volumetric water content corresponding to the matrix potential; this procedure is repeated at various pressures to construct a moisture retention curve for the soil sample.

Fig 2.3 DIK-3421-11 sample chamber, DIK-9221 automatic pressure controller and soil sample inside chamber (Multifold pF meter)

For each magnitude of air pressure applied, the moisture content of the soil sample is determined by calculating the difference between the weight of the measured soil sample and that of the same soil sample in dry state. The determined moisture content corresponds to the applied air pressure, hence, the moisture potential at the time of measurement, thus providing a moisture content corresponding to a given pF value. Four types of sediments, namely, No. 5, No.6, No. 7 and No.8 were used in this study. Typical relationship curve for matric suction - volumetric water content and matric suction-shear strength are shown in figure

Van Genuchten parameters were estimated by non-linear regression analysis of soil moisture retention data obtained by pF meter experiments for different sediment type which are shown in table 2.1.
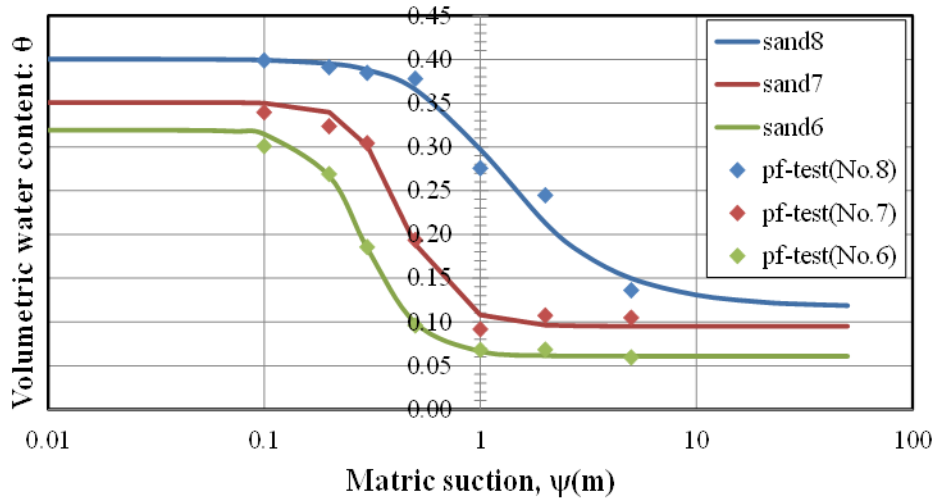
Figure 2.4 Matric suction-volumetric water content curves
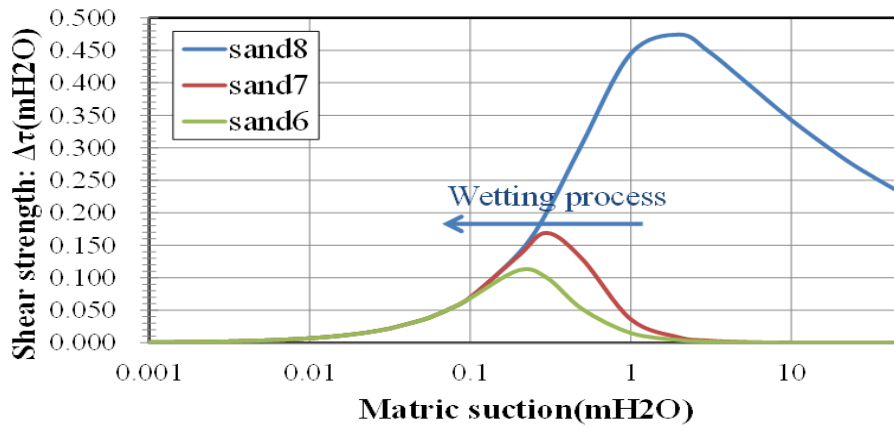
Figure 2.5 Matric suction-shear strength curves

2.3.2 Laser displacement sensor

A Laser Displacement Sensor (LDS) from Keyence (model LK#G502) is used to measure the final dyke surface after the experiment (figure 2.6). The LDS measures distance by emitting a laser beam that reflects off any solid surface within its measurement range. The sampling rate of the LDS is set constant at different samples per second. The LDS is coupled with a linear actuator that moves the device horizontally along the length of the tank.
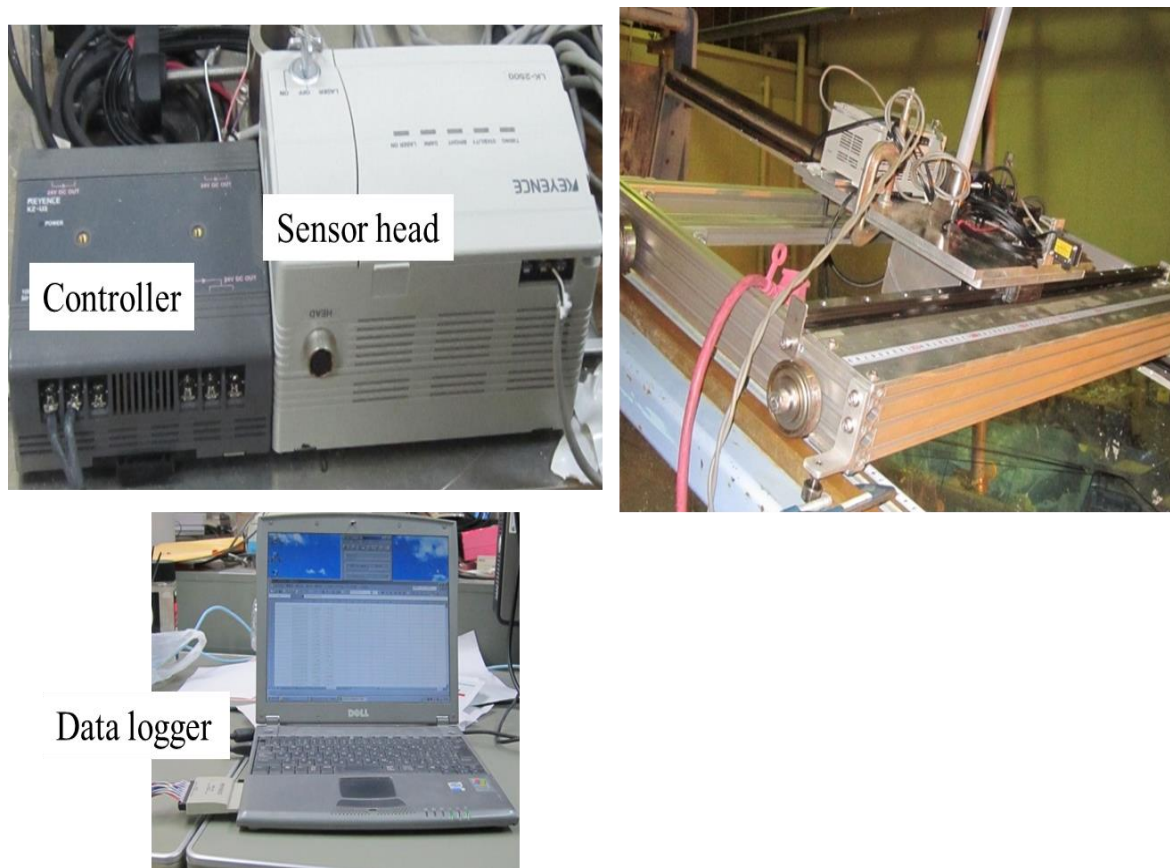
Figure 2.6 Laser displacement sensor and its accessories

2.3.3 Pump arrangement

To supply inflow discharge to the flume, the pump is coupled with frequency controller to increase or /decrease discharge. The available pump system with controller system is as shown in figure 2.8. Calibration curve was produced by the comparision of frequency value and the discharge measured by V-notch installed downstream of the flume.

Figure 2.7 Pump arrangement and frequency controller

2.3.4 Sediment properties

Silica sand No. 5, 6, 7 and 8 are used to make the dyke body. The sediment no. 5 is coarser one and its fineness increases with increase in sediment number. The grain size distributions of relevant sediment particles are shown in figure 2.9.

Table 2.1 Different parameters of the sediment considered

Sediment type	No.6	No.7	No.8
Saturated moisture content, θs	0.319	0.351	0.400
Residual moisture content, θr	0.061	0.095	0.117
α	3.837	2.552	1.107
η	3.852	4.148	2.254
Specific gravity, Gs	2.65	2.65	2.65
Mean grain size, D50 (mm)	0.334	0.174	0.1
Angle of repose, Φ(degree)	34	34	34

Van Genuchten parameters i.e. α and η (including θ_r) were estimated by non-linear regression analysis of soil moisture retention data obtained by pF meter experiment. Some other parameters of sands are listed in Table 2.1.
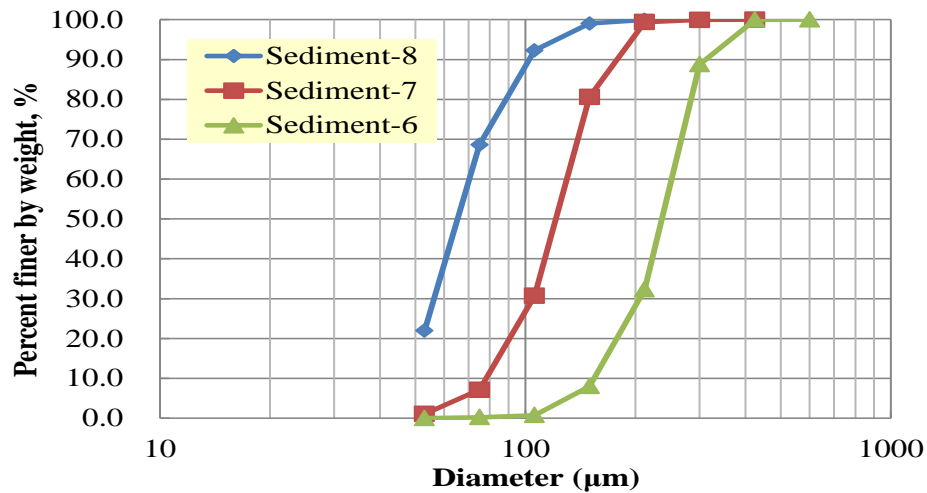
Figure 2.8 Particle size distributions of different sediments.

2.2 Experimental procedure and evaluation

All experiments were conducted using a constant flow discharge in a flume Q, referred to as the inflow, to obtain simple boundary condition. The dyke material is initially provided 5 % moisture content by weight and thoroughly mixed and then compacted with the help of tamping plate and cylindrical roller till the maximum compaction was achieved. The inflow was added fast to attain steady state before overtopping started by adjusting the gate downstream and closing the dyke area by wooden plate. The flow overtopped the dyke from the pilot channel thus resulting the lateral widening of breach from that point.

The total 12 experiments are done for four sediment types. The each experiment was repeated three times to see the effect of repeatability. The repeatability shows very good agreement so the suitable value of result is only presented. There was no tail water effect and the dyke overflow was always free. The test was stopped when the entire dyke material and washed out and the flow from the dyke reaches its equilibrium state. The experiments are therefore limited to dynamic change in lateral widening process. To represent actual dyke breach scenario, the hydraulic model should consists of main channel representing the actual river and a perpendicular side channel where the dyke is placed.

Further, the basic upstream boundary condition is obtained by selecting the constant inflow scenario. In prototypes, a dyke is overtopped once the river water level exceeds the dyke crest elevation. The overtopping flow depends on the breach progress and the river discharge (Schmocker, 2011). The breach and river discharges interact so that there is hardly a constant inflow to the breach section.

As the pilot channel is constructed at the center of the dyke to clearly visualize the lateral widening pattern, the lateral view is representative to analyze the breaching process. The process is recorded with Casio Exlim high speed camera, Go-Pro Black edition high speed Camera, Sony HD camera and Fuji film 3D camera continuously. The 3D camera was used to record the 3D image at the interval of 5 sec and later Fujifilm software was used to generate the spatial coordinates. The lateral widening process at the interval of 5 sec is generated with 3D camera while breach discharge, sediment discharge and seepage movement were analyzed using

recorded image of the optical instrument.

2.3 Results and discussion

2.3.1 Lateral widening process

The effect of sediment particle on the lateral widening process is presented below in the fig 4. For sediment no 5, 6, 7 and 8 with all other parameters constant resulting in different breach shapes but the process of the enlargement seems to be followed similar procedure. For all the processes, initially, as the water overtops through pilot channel, the channel is eroded vertically layer by layer until the water surface touches the fixed bed. The reason for that is the vertical layer is saturated quickly with the flow which creates erosion of the channel surface by shear stress. Interestingly, at the both side of the channel there is the formation of vertical slope of the sediment material.

The vertical slope seems stable enough due to the matric suction of the soil in unsaturated case. When the vertical undermining reaches the fixed bed, then the erosion starts to expand laterally from the toe of the opposite slope of the dyke. In the meantime, the seepage travels through the vertical slope developed at the both side of the channel. If the vertical slope is saturated enough to be overcome the sectional resistance stress, then those slope fell down at the channel flow at the center. The relatively dry sand at test start has a minimal tensile strength. As the degree of saturation of the dyke progressively increases once the overtopping starts, the tensile strength first increases to a maximum depending on the particle size and porosity, followed by a reduction to zero near full saturation (Lu et al. 2009)

Consequently, both falling of vertical slopes as well enlargement of lateral widening from the toe occurs simultaneously and finally the whole dyke collapses. The fig. 5 shows the breach width changing pattern with respect to time. The result shows that the breaching phenomenon was very slow at the beginning at top, middle and toe section. Then as the vertical breaching reaches the fixed bed, the toe section as well as the top section rapidly eroded in comparison with other section causing most of the breaches of the dyke. The middle section acts like a hinge section for both the erosion and finally the middle section collapse suddenly. Thus, finally the collapse of the whole dyke occurs. Similarly, the widening speed curve (Fig 4)also shows that for all the sediment sizes, toe widening velocity increases rapidly in comparison with top and middle point, as the time passes the top and middle widening velocity increases together but at last when the toe widening speed nearly zero, the top widening speed overpass the middle and finally collapse occurs.

From all the results obtained, it can be concluded that sediment no. 8 seems to more resistive to the erosion in the first few seconds than other sediment types due to sediment size and slow saturation rate i.e. the suction pressure acts more in the case of sediment no. 8 and took long time to develop breach and finally collapse. Consequently, the sediment no 7, sediment no.6 and sediment no. 5 follows the sediment no. 8 in the breaching time and collapse process respectively.
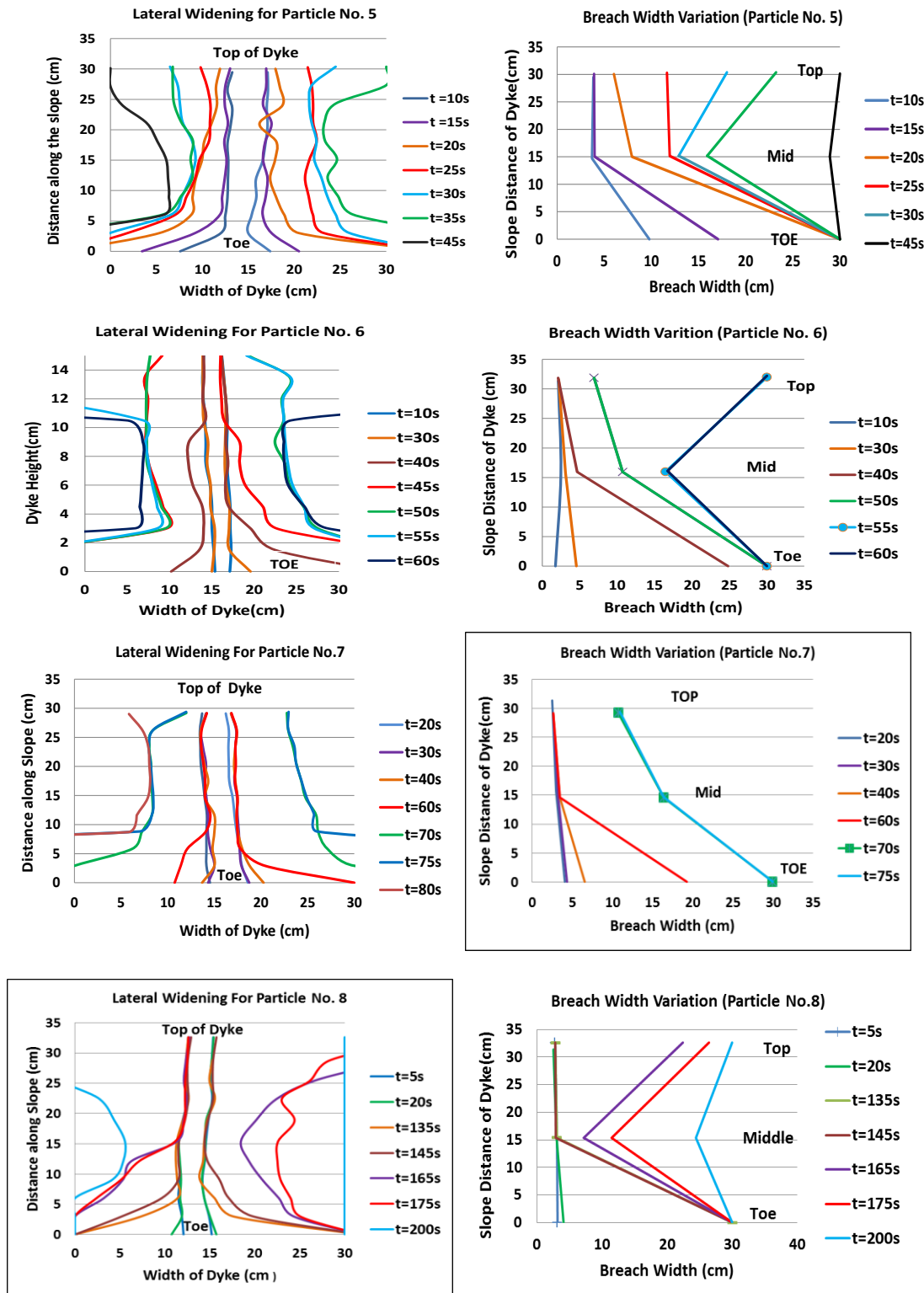
Figure 2.9 Lateral widening and breach width variation for sediment sizes 5, 6, 7, and 8
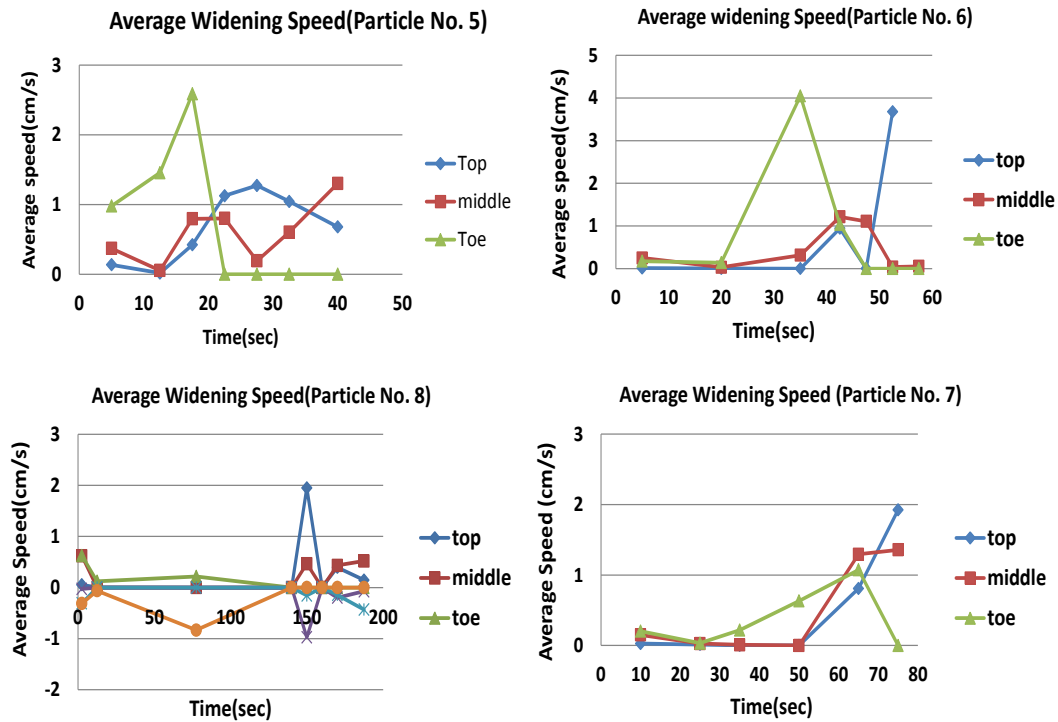
Figure 2.10 Average widening speeds at three section of dyke along height

2.3.2 Water and sediment hydrograph

Given the various factors affecting the dyke breach process, it is necessary to accurately reproduce a certain Test. Test conducted by the same person was repeated three times using identical test parameters. Fig 2.11 and 2.12 shows the flow hydrograph and sediment hydrograph generated due to river dyke breaches due to overtopping for different sediment sizes. The experiment is done three times with same condition to check the repeatability criteria. The curve shows good repeatability and thus, one of the cases is chosen for principle representation of the process.

The final breach hydrograph curve for all the sediment sizes are as shown in figure 2.13. The curve shows that the breach discharge increases fast after initial overtopping until the maximum breach discharge $Q_{max} > Q_{in}$ is attained. After reaching the maximum outflow, the breach discharge decreases slowly to $Q = Q_{in}$ and then remains constant. Given the constant inflow scenario, Q max depends on Qin in contrast to dam break analysis considering reservoir where Q_{max} constantly increase. In fig.6, the dimensionless maximum breach discharge Q_{max}/Q_{in} is discussed for different sediment types The maximum discharge obtained is around 1.6 times the discharge in the flume. The graph clearly shows that the time lag of peak of hydrograph increases with increasing sediment number i.e. decreasing d50.
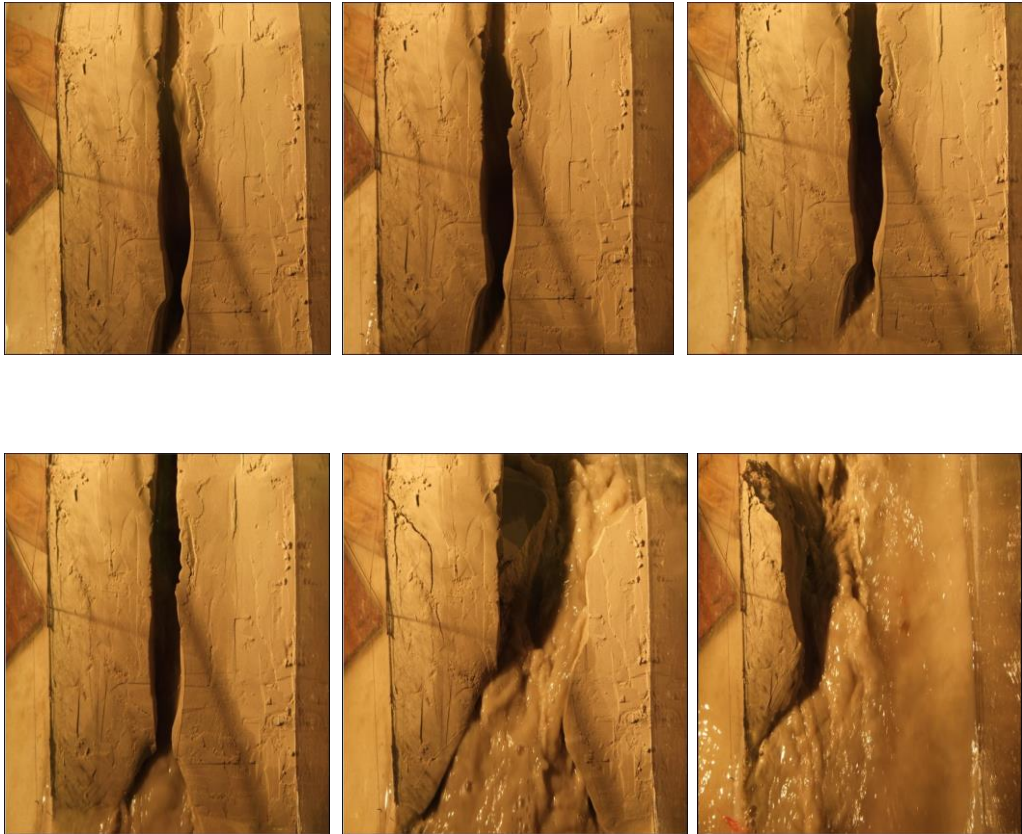
Figure 2.11 Lateral widening processes (sample example for sediment 7)
at t = 10, 20, 30, 70, 80, 90 s

Fig. 2.13 shows the obtained sediment discharge hydrograph. The sediment graphs has more than one peaks which reveals that the vertical stable wall at the side of channel falls into the Centre of breach at different time step. The figure also clearly demonstrates the sediment size effect on the erosion of the sediments that determines the breach width. As previously stated, the sediment no. 8 seems more resistive than other sediment sizes.

For all sediment sizes, the nature of the curve remains same except the rate of erosion i.e. erosion of dyke takes little longer time for finer sediment than coarser one. It shows an important impact of sediment size. Finer the sediment size, higher the development of suction pressures due to unsaturated condition which finally develops resistance against failure so the finer sediments reluctant to faster erosion. Hence the times taken to reach similar final condition for various sediment sizes are different; finer having late. The middle part of the dyke acts like a hinge as top and bottom of dyke already eroded in some extent.
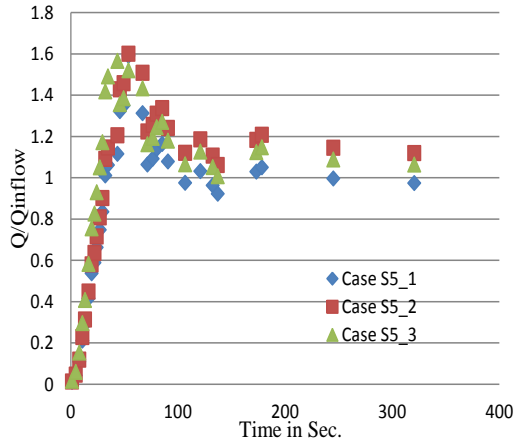
a) Breach Hydrograph
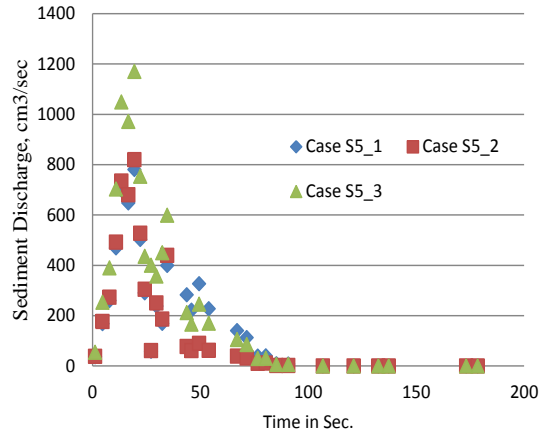
b) Sediment Hydrograph

Figure 2.12 Repeatability tests for breach and sediment discharge (for sediment no.5)
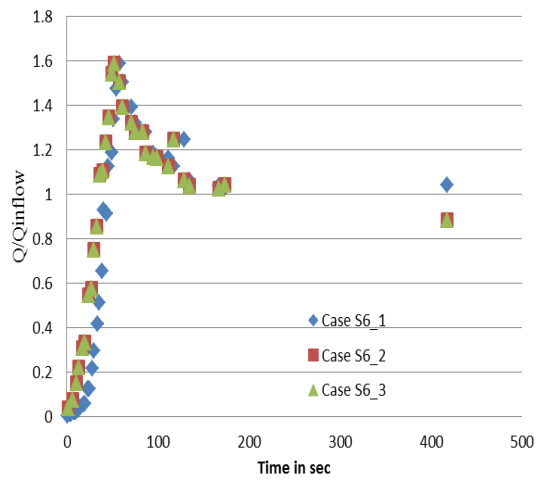
a) Breach Hydrograph
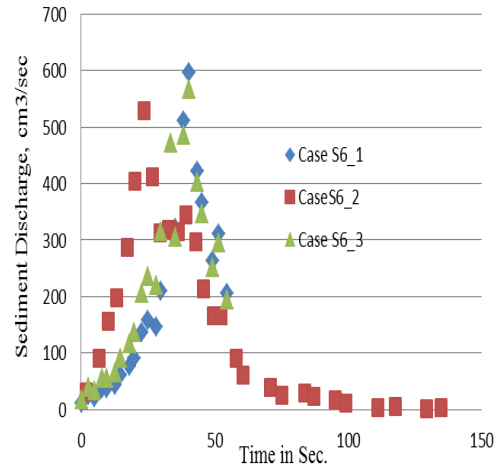
b) Sediment Hydrograph

Figure 2.13 Repeatability tests for breach and sediment discharge (for sediment no.6)
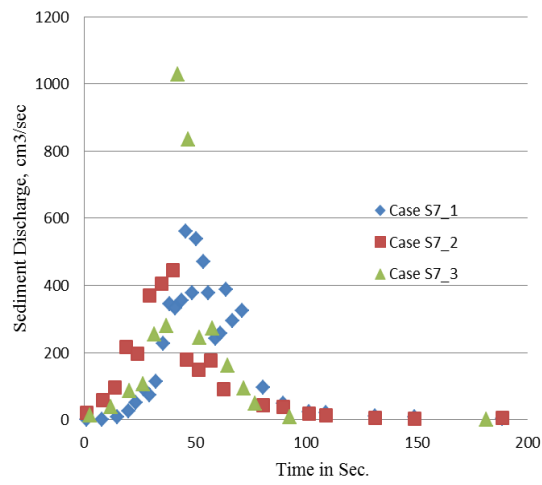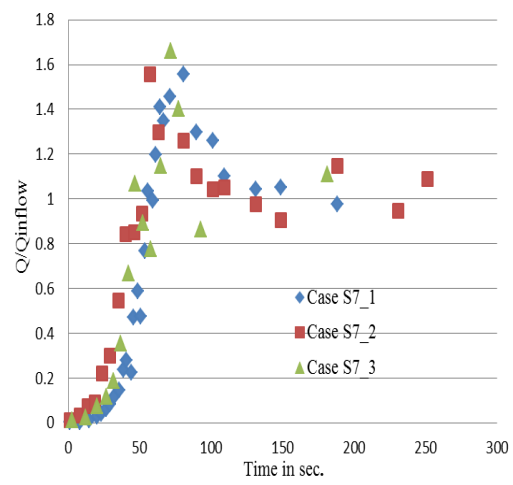
a) Breach Hydrograph   b) Sediment Hydrograph

Figure 2.14 Repeatability tests for breach and sediment discharge (for sediment no.7)
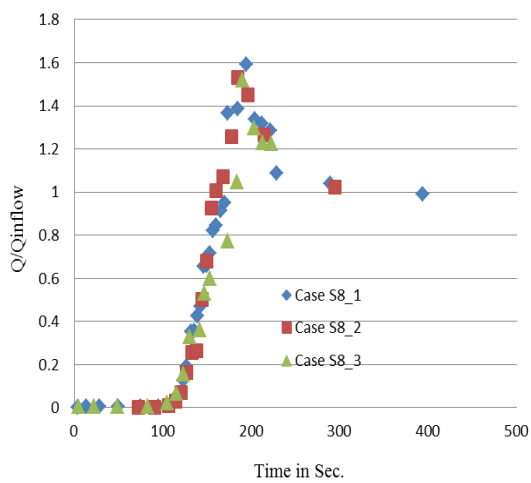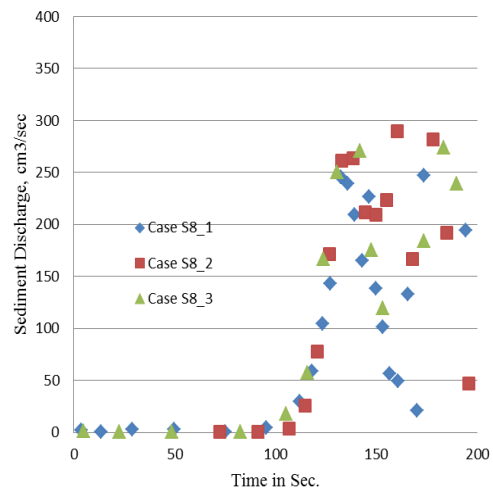
a) Breach Hydrograph   b) Sediment Hydrograph

Figure 2.15 Repeatability tests for breach and sediment discharge (for sediment no.8)
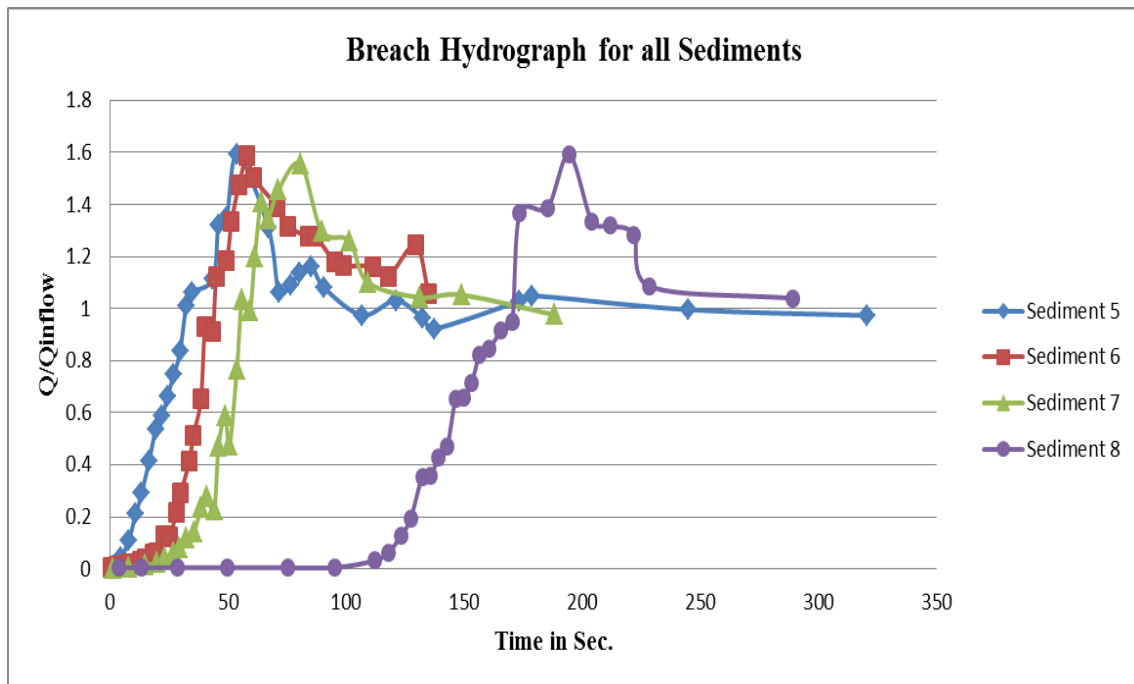
Figure 2.16 Comparison of breach hydrograph for all sediment sizes.
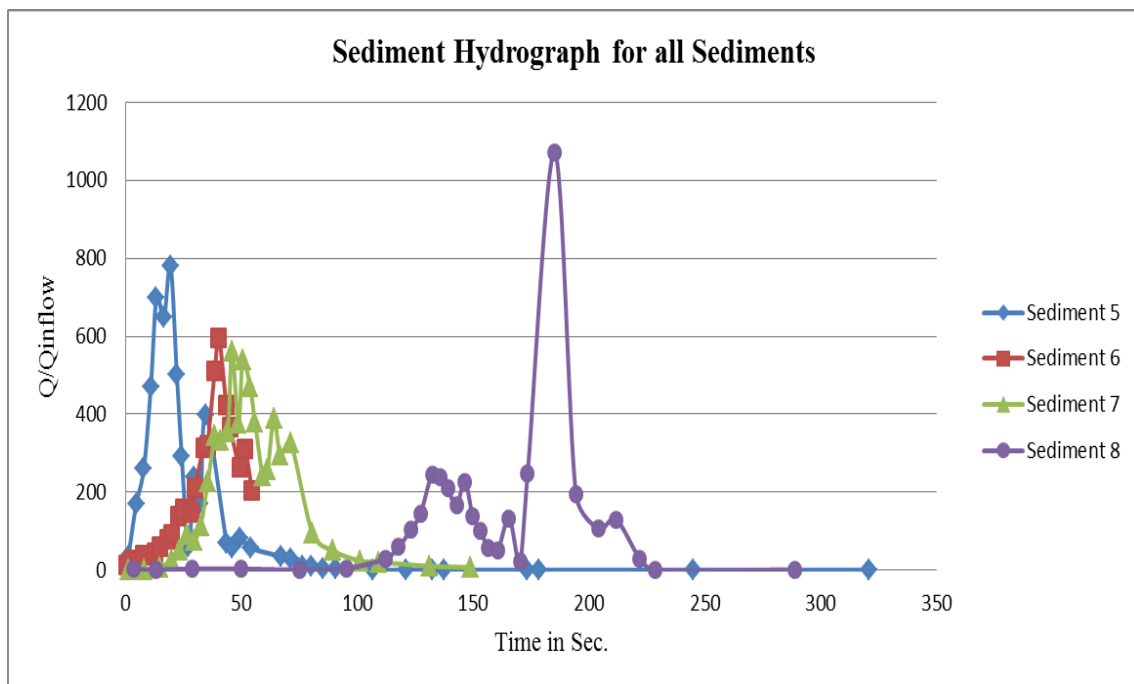
Figure 2.17 Comparison of Sediment hydrograph for all sediment sizes

42

2.3.3 Time of failure

The time of failure, here, is defined as the time taken for the breach discharge to be maximum from the time as overtopping just starts. The time of failure is therefore directly observed from the flow hydrograph from the breach. To generalize the results obtained with the current test, the governing parameters considered are described as a functional relationship i.e.

Time of failure, $T \sim F (q, K_s, y, d_{50}, H, \theta_i, S_u, S_d)$

Here q is discharge per unit width at flume, K_s, hydraulic conductivity of the dyke materials, y is overtopping depth, d_{50} is sediment size 50 % finer, H height of the dyke, S_u is upstream slope, S_d is downstream slope and θ_i initial moisture content of the dyke materials respectively. Parameters like y, θi, S_u and S_d were not systematically varied and are therefore dropped. As only variation with sediment sizes were tested and dyke height and specific discharge is considered as an important parameter also, the dimensional analysis shows the following relations exists:

$$\frac{K_s T}{d_{50}} = F\left[\frac{q}{K_s d_{50}}, \frac{H}{d_{50}}\right] \tag{1.1}$$

Here $\dfrac{K_s T}{d_{50}}$ is named as dimensionless time of failure, $\dfrac{q}{K_s d_{50}}$ is named as dimensionless

specific discharge and $\dfrac{H}{d_{50}}$ is dimensionless height of dyke. The viscosity and surface tension

are assumed to be constant for all tests and therefore not taken account here, given that scale effects are excluded. Fig 2.14 shows the graph showing the relations between different dimensional parameters obtained through the dimensional analysis using experimental results.

The curve is obtained by joining the calculated value from the most suitable experiment out of

all experiment. The curve shows that It has a minimum value at $\dfrac{K_s T}{d_{50}} = 33.5$ which can be

considered as the critical dimensionless failure time. For uniform sediment case as in the current experiment, this value determines the minimum value of time reaching the peak breach discharge. From the sediment 5, 6 to sediment 7, the dimensionless time of failure value decreases at first when both dimensionless specific discharge and dimensionless dyke height increases up to a critical value then increases from the critical value as the other parameters increases.
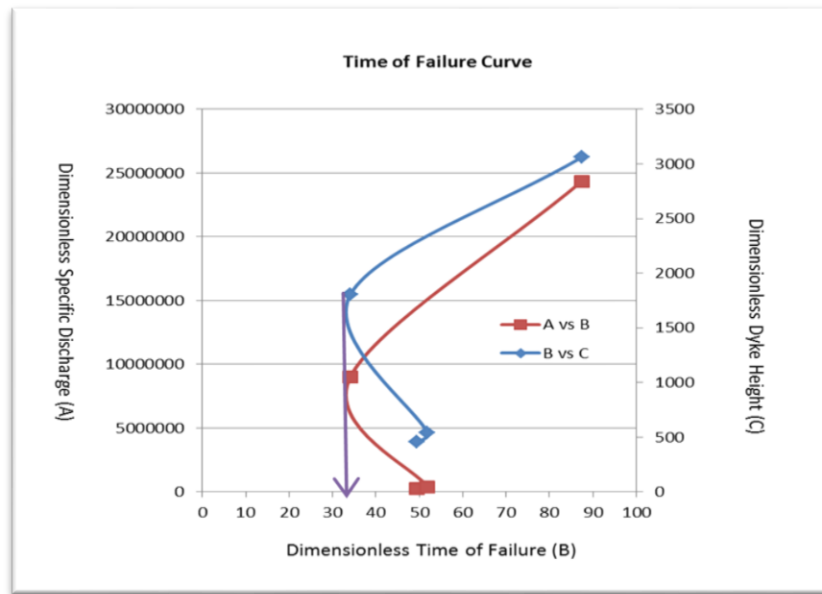
Figure 2.18 Time of failure curve

Validation of the curve is still not complete due to unavailability of such data but this curve can be used later to check the validity of next stage experiment of lateral dyke failure case of our research. But, the result from Civil Engineering Research Institute for cold region, Hokkaido, Japan real scale model study in Chiyoda Experimental Flume shows good validation of the curve.

2.4 Summary

The present experimental work investigates the lateral widening breach characteristics with different sediment sizes due to overtopping. A simple dyke model was used consisting of homogenous, uniform materials of various sand diameters. A steady inflow scenario was tested and the all the breaching process were recorded using high speed camera and 3D camera. In this case, the flow direction to the length of the dyke was perpendicular although the dyke was placed at the side of the river.

Within the range of test parameters, the dyke breach process is accelerated with increasing sediment d_{50}. For coarse sediment, due to quick saturation of the dyke body, the collapse time decreases. The width of the breach increases at the top and toe section than the middle section which acts like a hinge point. At the final stage, the middle section also fails leading to whole dyke collapse. The breach discharge and sediment discharge shows the time lag and peak according to the sediment size. Finally, the time of failure curve is proposed for the pre determination of occurrence of peak breach discharge based on the pre-disaster parameters which, if later, validated will be an important tool for the natural disaster mitigation. The current findings will be expanded with more realistic situation experimental analysis in chapter 4 validated with numerical simulation.

CHAPTER 3

INTEGRATED MODEL TO ANALYSE DYKE BREACH CHARACTERISTICS

3.1 Introduction

Physically based models such as NWS-DAMBRK (Fread 1988) and NWS-BREACH (Fread 1991) are commonly used to predict the outflow hydrograph of moraine dam (Bajracharya et al. 2007b; Wang et al. 2008; Shrestha et al. 2010). Furthermore, HEC-RAS dam breach model (U.S. Corps of Engineers 2002) is also employed by Osti and Egashira (2009) to predict the outflow hydrograph of glacial lake outburst. The actual mechanism of dam surface slope failure and head cut and lateral dam surface erosion are not considered in available breach models. The failure mechanism and erosion process of moraine dam are still not thoroughly understood. In addition, the downstream flooding or impact of some GLOF events is investigated by using flood routing models, which do not consider the erosion and deposition processes of sediment particles in the river bed (Bajracharya et al. 2007b; Wang et al. 2008; Shrestha et al. 2010).

A numerical model for predicting erosion due to overtopping flow at a river embankment was developed by combining four modules: surface flow, seepage flow, sediment transport, and slope failure. The novelty of this study is in the combination of these modules to reproduce the complicated embankment failure process. There are many interactions among the modules, and the highlight of the present model is its estimation of the erosion rate by considering that the effect of resisting shear stress due to suction depends on saturation conditions on the embankment surface, which is calculated using the result from the seepage flow module. In order to focus on the improvement in the treatment of the surface erosion process, the developed model was reduced to vertical two-dimensional calculations in seepage and erosion modules; however, the horizontal 2D flow model was introduced to consider the extensibility for our future work.

3.2 Two-dimensional seepage flow modeling

3.2.1 Governing equations

The seepage flow in the dyke body is caused by the blocked water stage behind the dyke. The transient flow in the dyke body after breaching start in the dyke can be analyzed by Richards' equation (1931). To evaluate the change in pore water pressure in variably saturated soil, pressure based Richards' equation is used (Sharma et al., 2005; Awal et al, 2007).

$$C \frac{\partial h}{\partial t} = \frac{\partial}{\partial x} \left(K_x(h) \frac{\partial h}{\partial x} \right) + \frac{\partial}{\partial z} \left(K_z(h) \left(\frac{\partial h}{\partial z} + 1 \right) \right) \tag{3.1}$$

where h is the water pressure head, $K_x(h)$ and $K_z(h)$ are the hydraulic conductivity in x and z direction, C is the specific moisture capacity ($\partial \theta / \partial h$), θ is the soil volumetric water content, t is the time, x is the horizontal spatial coordinate and z is the vertical spatial coordinate taken as positive upwards. Equation represents flow in both the unsaturated domain as well as in the saturated domain. The unsaturated flow involves a two-phase flow of air and water, however only the flow of the water has been considered, where the air phase is continuous and is at atmospheric pressure, and it does not affect the dynamics of the water phase. Richards' equation is a non-linear parabolic partial differential equation in the unsaturated zone and elliptic in the saturated zone. Line successive over-relaxation (LSOR) is often a very effective method of treating cross-sectional problem grids. LSOR scheme is used in this study for the numerical solution of Richards' equation.

3.2.2 Soil constitutive relationships (*K-h-* θ)

Richards' equation is nonlinear in nature, since the flow and storage properties are functions of the dependent variable. In order to solve Richards' equation, the constitutive equations, which relate the pressure head to the moisture content and the relative hydraulic conductivity, are required. Many empirical relationships have been developed in the past based on field experiments for soil moisture constitutive relationships and are reported in the literature. The most popular being Brookes and Corey (1964), Campbell (1974), Haverkamp (1977), van Genuchten (1980), Kosugi (1994) and Assouline et al. (1998) relationships. In this study, following constitutive relationships proposed by van Genuchten (1980) are used for establishing relationship of $\theta - h$ and $K - \theta$, with m =1 − (1/ η).

3.2.3 $\theta - h$ relationship

The water retention characteristic ($\theta - h$ relationship) of the soil describes the soil ability to store and release water. This relationship is called soil moisture characteristic curve. The shape of the curve depends upon the pore size distribution of the soil.

$$S_e = \frac{\theta - \theta_r}{\theta_s - \theta_r} \tag{3.2}$$

$$S_e = \begin{cases} \frac{1}{(1 + |\alpha h|^n)^m} & for \ h < 0 \\ 1 & for \ h \geq 0 \end{cases} \tag{3.3}$$

where, α and η are parameters related with matric potential of soil and are measure of capillary fringe thickness and pore size distribution of soil respectively, S_e is the effective saturation, θ_s and θ_r are saturated and residual moisture content respectively.

3.2.4 $K - \theta$ Relationship

The unsaturated hydraulic conductivity, K is a nonlinear function of the moisture content, the unsaturated hydraulic conductivity, K is a nonlinear function of the moisture content, θ and it can be expressed as a power function of the effective saturation. And it can be expressed as a power function of the effective saturation.

$$K = \begin{cases} K_s S_e^{0.5} \left[1 - \left(1 - S_e^{1/m} \right)^m \right]^2 & for\ h < 0 \\ K_s & for\ h \geq 0 \end{cases} \tag{3.4}$$

where, K_s is the saturated hydraulic conductivity.

3.2.5 Initial and boundary conditions

Governing Equation needs initial and boundary conditions to get a solution. The values of pressure head or moisture content throughout the domain are specified as initial conditions. To get a unique solution for a given initial condition, two dimensional model (in a vertical cross section) needs boundary values on four sides (Figure). As a boundary condition two different types of conditions can be defined, (i) Drichlet condition, value of the dependent variable is specified, (ii) Neuman condition, flux at the bottom boundary is specified. The process such as infiltration due to rainfall or river flow, evaporation which occur at the dam body constitute the upper, left and right boundary conditions for unsaturated flow. However, rainfall and evaporation effect are not included in the present model. Bottom boundary condition is used as no-flow boundary. Upper, left and right boundary may be no flow boundaries or head boundary based on water level in the upstream reservoir. A seepage face is an external boundary of the saturated zone, where water leaves the soil and pressure head is uniformly zero (atmospheric pressure). The height of the seepage face is not known a priori and is determined iteratively.

3.2.6 Solution methods

There are many available methods of numerical solution, however in this study; line-successive over-relaxation (LSOR) scheme used by Freeze (1971, 1976) is used. Equation is solved by the implicit iterative finite difference scheme, using the over-relaxation technique.
The numerical grid is block centered nodal grid in the x-z plan as shown in Figure 3.1 with a block size (Δ x, Δ z). In the x-direction the nodes are labeled i = 1, 2,…N and in the z-direction

They are labeled j = 1, 2,…M. The value of pressure head at (x_i, y_i) and t is denoted by h_{ij}^t . The finite difference form of Equation 3.1 used in the mode1 is

$$\frac{1}{\Delta x}\left[K(h_I)\left(\frac{h_{i+1,j}^t+h_{i+1,j}^{t-1}-h_{i,j}^t-h_{i,j}^{t-1}}{2\Delta x}\right)-K(h_{II})\left(\frac{h_{i,j}^t+h_{i,j}^{t-1}-h_{i-1,j}^t-h_{i-1,j}^{t-1}}{2\Delta x}\right)\right]+$$

$$\frac{1}{\Delta z}\left[K(h_{III})\left(\frac{h_{i,j+1}^t+h_{i,j+1}^{t-1}-h_{i,j}^t-h_{i,j}^{t-1}}{2\Delta x}\right)-K(h_{IV})\left(\frac{h_{i,j}^t+h_{i,j}^{t-1}-h_{i,j-1}^t-h_{i,j-1}^{t-1}}{2\Delta x}\right)\right]=C(h_V)\left(\frac{h_{i,j}^t-h_{i,j}^{t-1}}{\Delta t}\right) \quad (3.5)$$

For vertical LSOR, the term can be grouped as

$$-A_j\, h_{i,j+1}^t + B_j\, h_{i,j}^t - A_j\, h_{i,j-1}^t = D_j \tag{3.6}$$

Where, A_j, B_j, C_j and D_j are developed from the groupings of the coefficients of Equation as below:

$$A_j = \frac{K(h_{III})}{2\Delta z^2} \tag{3.7}$$

$$B_j = \frac{C(h_V)}{\Delta t} + \frac{K(h_I)}{2\Delta x^2} + \frac{K(h_{II})}{2\Delta x^2} + \frac{K(h_{III})}{2\Delta z^2} + \frac{K(h_{IV})}{2\Delta z^2} \tag{3.8}$$

$$C_j = \frac{K(h_{IV})}{2\Delta z^2} \tag{3.9}$$

$$D_j = \frac{C(h_V)}{\Delta t} h_{i,j}^{t-1} + K(h_I)\left(\frac{h_{i+1,j}^t+h_{i+1,j}^{t-1}-h_{i,j}^{t-1}}{2\Delta x^2}\right) - K(h_{II})\left(\frac{h_{i,j}^{t-1}-h_{i-1,j}^t-h_{i-1,j}^{t-1}}{2\Delta x^2}\right) + K(h_{III})\left(\frac{h_{i,j+1}^{t-1}+h_{i,j}^{t-1}}{2\Delta z^2}\right)+$$

$$\frac{1}{\Delta z}\right) - K(h_{IV})\left(\frac{h_{i,j}^{t-1}-h_{i,j-1}^{t-1}}{2\Delta z^2}+\frac{1}{\Delta z}\right) \tag{3.10}$$
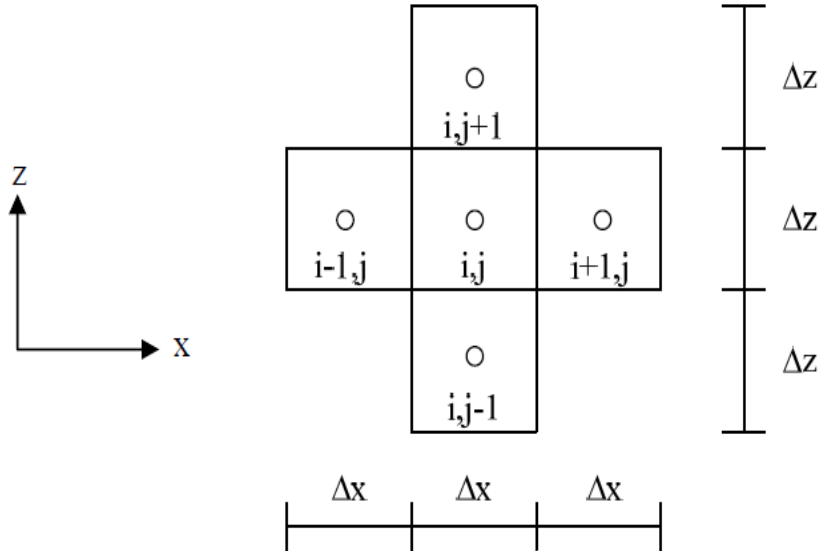
Figure 3.1 Grid scheme

The set of Equations 3.6 for a line scan, form a tri-diagonal matrix equation that can be solved by the well-known triangularization scheme embodied in the following recurrence relation.

$$
\begin{aligned}
h_{i,j}^t &= E_j h_{i,j+1}^t + F_j && for\ j<M \\
h_{i,j}^t &= F_j && for\ j=M
\end{aligned}
\Bigg\}
\tag{3.11}
$$

Where,

$$
E_j = \frac{A_j}{B_j - C_j E_{j-1}} \quad for\ j > 1\ ; \quad E_1 = \frac{A_1}{B_1}
\tag{3.12}
$$

$$
F_j = \frac{D_j + C_j E_{j-1}}{B_j - C_j E_{j-1}} \quad for\ j > 1\ ; \quad F_1 = \frac{D_1}{B_1}
\tag{3.13}
$$

The E and F coefficients are calculated from $j = 1$ to $j = M$ using Equations 3.12 and 3.13 and the $h_{i,j}^t$ s are back calculated from $j = M$ to $j = 1$ using Equation 3.11. The flowchart of seepage flow model is shown in Figure 3.2. At each iteration, it is necessary to predict a pressure head value $h_{(pred)ij}$ at each node from which the current estimates of K and C can be calculated. For the first iteration of the first time step:

$$
h_{(pred)i,j}^t = h_{i,j}^{t-1}
\tag{3.14}
$$

For the first iteration of later time step:

$$
h_{(pred)i,j}^t = (T^t + 1)h_{i,j}^{t-1} - T^t h_{i,j}^{t-2}
\tag{3.15}
$$

where,

$$
T^t = \Delta t^t / 2\Delta t^{t-1}, \ T^t = \tfrac{1}{2}\ for\ \Delta t^t = \Delta t^{t-1}
\tag{3.16}
$$

For later iterations of all time steps:

$$
h_{(pred)i,j}^t = h_{(pred)i,j}^{t,it-1} + \lambda\left(h_{i,j}^{t,it-1} - h_{(pred)i,j}^{t,it-1}\right), \qquad 0 \le \lambda \le 1
\tag{3.17}
$$

The value of h_I in Equation 3.5 is the predicted value of h at the boundary between two nodal blocks and h_I is determined by

$$
h_i = \tfrac{1}{2}\left(h_{(pred)i,j} + h_{(pred)i+1,j}\right)
\tag{3.18}
$$

The value of h_{II}, h_{III} and h_{IV} are determined analogously and h_V is equal to $h_{(pred)ij}$.

The iterations are repeated until the given tolerance is achieved. Although the implicit scheme is unconditionally stable, some difficulties due to the strong nonlinearity of the Richards' equation may occur. Which can be overcome by the adaptable time step, however in this model very small time step is used. At the boundary node, Equation 3.5 is modified to reflect time dependent boundary conditions. Water level in the upstream reservoir in each time step is determined by water-volume balance equation considering inflow discharge, rate of infiltration inside the dam body and flume geometry (width and slope).
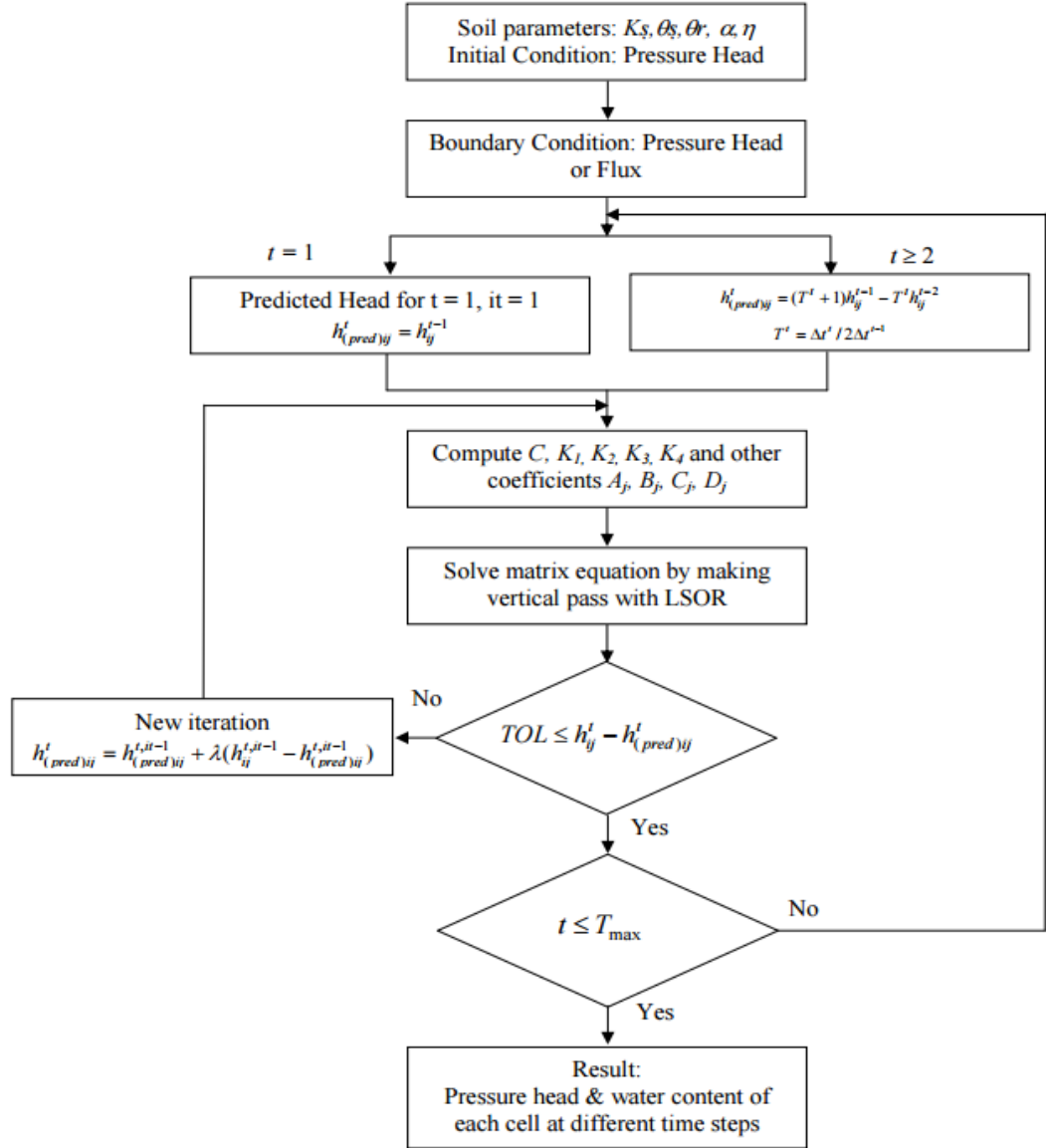
Figure 3.2 Flow chart of seepage flow model

3.2 Two-dimensional depth-averaged flow model

3.2.1 Governing equations

The governing equations of the flow module are the depth-averaged two-dimensional equations and the continuity equation of the flow, which are described as follows:

$$\frac{\partial u}{\partial t} + u\frac{\partial u}{\partial x} + v\frac{\partial u}{\partial y} = -g\frac{\partial H}{\partial x} - \frac{\tau_{bx}}{\rho h} + \frac{\partial}{\partial x}\left(\frac{\tau_{xx}}{\rho}\right) + \frac{\partial}{\partial y}\left(\frac{\tau_{xy}}{\rho}\right) \tag{3.19}$$

$$\frac{\partial v}{\partial t} + u\frac{\partial v}{\partial x} + v\frac{\partial v}{\partial y} = -g\frac{\partial H}{\partial x} - \frac{\tau_{by}}{\rho h} + \frac{\partial}{\partial x}\left(\frac{\tau_{xy}}{\rho}\right) + \frac{\partial}{\partial y}\left(\frac{\tau_{yy}}{\rho}\right) \tag{3.20}$$

$$\frac{\partial h}{\partial t} + \frac{\partial(uh)}{\partial x} + \frac{\partial(vh)}{\partial y} = 0 \tag{3.21}$$

where u and v are flow velocity components in x and y directions, g is the acceleration due to gravity, H is the water level, h is the flow depth, and ρ is the water density and τ_{bx} and τ_{by} are the bottom shear stresses in the x and y directions. The shear forces due to turbulence τ_{xx}, τ_{yy}, τ_{xy} are described as follows;

$$\frac{\tau_{xx}}{\rho} = 2\varepsilon\frac{\partial u}{\partial x}, \ \frac{\tau_{yy}}{\rho} = 2\varepsilon\frac{\partial v}{\partial x}, \ \frac{\tau_{xy}}{\rho} = \varepsilon\left(\frac{\partial u}{\partial y} + \frac{\partial v}{\partial x}\right) \tag{3.22}$$

Where ε is eddy viscosity ($\varepsilon = (\kappa u_* h) / 6$), κ is von-Karman's constant, and u_* is friction velocity. The bottom shear stresses are expressed as follows:

$$\tau_{bx} = \rho g n^2 u \, {\sqrt{u^2 + v^2}}\Big/{h^{1/3}} \tag{3.23}$$

$$\tau_{by} = \rho g n^2 v \, {\sqrt{u^2 + v^2}}\Big/{h^{1/3}} \tag{3.24}$$

Where n is the manning's coefficient. The discretization equation of the flow module are solved by using the SIMPLE revised (SIMPLER) scheme, a widely used scheme that utilizes the relationship between velocity and pressure corrections to enforce mass conservation (Patanakar 1980). The scheme is described in detail below.

3.2.2. The SIMPLER method

3.2.2.1 Overview

SIMPLE algorithm is a widely used numerical procedure to solve the Navier-Stokes equations. SIMPLE is an acronym for Semi-Implicit Method for Pressure Linked Equations. Instead of simultaneously solving the momentum and continuity equations to obtain the velocity and pressure fields, we decouple the equations so that the pressure and velocity fields are solved independently. How can this be accomplished? The first step is to assume a pressure field, p^{i-1}, as well as an x and y velocity field, u^{i-1} and v^{i-1} . Using these "known" fields, we solve for the u^* component of the $\vec{u}^*$ velocity field with the help of the x momentum equation and solve for the v^* component of the $\vec{v}^*$ G velocity field with the help of the y momentum equation.

The next step involves computing a pressure correction p'. The equation for p' is derived by implementing a Darcy-like flow assumption on the velocity correction. This gives rise to a pure diffusion equation for the pressure correction, which serves to drive the system toward conserving mass; see continuity equation, eq. This iterative procedure is repeated successively until the entire flow field satisfies continuity. As an additional check for solution convergence, the calculated velocities may only change slightly from a previous iteration to a current one. The commercial CFD tool Fluent, for example, requires that the velocity field change less than 0.1% from one iteration to the next before reporting a converged solution.

3.2.2.2 Implementation

The first step in the SIMPLE method is to solve the following momentum equations (assuming steady-state for simplicity):

$$\text{X-momentum}: 0 = -\int_{cv} \nabla_x p^{i-1} dV - \rho \int_{cv} \vec{u}^{i-1} \cdot (\nabla u^*) dV + \mu \int_{cv} \nabla \cdot (\nabla u^*) dV \tag{3.25}$$

$$\text{Y-momentum}: 0 = -\int_{cv} \nabla_y p^{i-1} dV - \rho \int_{cv} \vec{u}^{i-1} \cdot (\nabla u^*) dV + \mu \int_{cv} \nabla \cdot (\nabla v^*) dV \tag{3.26}$$

As stated above, two fields are provided *a priori*: the pressure field, p^{i-1} and the velocity field, $\vec{u}^{i-1}$, where *i*-1 indicates initial guess or value from previous iteration. On the first iteration, *i* equal 1, so the initial guess, u^0 is given. Equations (1-8) and (1-9) will lead to two independent systems of equations. One system will yield solution u^*; the other will yield v^*. Since the initial guess may be far off from the actual solution, $(u^* \, v^*)$ will likely not equal $(u^{i-1} \, v^{i-1})$. Thus, we devise an equation for the velocity correction, $\vec{u}'$. As documented in (Patankar 1980; Versteeg and Malalasekera 1995), it may be assumed that the velocity correction at a control volume face (boundary) is proportional to the pressure gradient across that same face. The proportionality constant is a conglomerate of fluid viscosity, density, and sizes of neighboring control volumes (see eqs. 6.19-6.23 of (Versteeg and Malalasekera 1995)).

In the SIMPLE method, some of the contributions to the velocity correction from the neighboring cells are ignored (compare eqs. 6.19 and 6.21 of (Versteeg and Malalasekera 1995)). Thus, the velocity correction does not need to be derived rigorously from the governing equations. (Dropping the contributions from the neighbor cells is quite an arbitrary choice). The authors contend that "The omission of terms such as $\sum a_{nb} u'_{nb}$ the derivation does not affect the final solution because the pressure correction and velocity corrections will all be zero in a converged solution…" (pg. 145, (Versteeg and Malalasekera 1995)). Based on this argument, we propose the following form for the velocity correction:

$$\vec{u}' = -\frac{k}{\mu} \nabla p' \tag{3.27}$$

Equation (3.27) is similar in form to Darcy's Law. μ and κ account for the diffusion and convective contributions to the velocity correction, respectively. Whereas μ is always set to the actual value of the fluid viscosity, κ is an adjustable constant needed for improving convergence speed. For example, setting κ to 0.01 accelerates convergence speed by about 20 times (compared to when κ is set to 1). To account for generalized coordinates, (3.27) is written:

$$\binom{u'}{v'} = -\frac{1}{\mu}\begin{pmatrix} \frac{\partial p'}{\partial x} \\ \frac{\partial p'}{\partial y} \end{pmatrix} with \quad \begin{matrix} \frac{\partial p'}{\partial x} = \frac{\partial p'}{\partial \xi}\frac{\partial \xi}{\partial x} + \frac{\partial p'}{\partial \eta}\frac{\partial \eta}{\partial x} = \xi_x \frac{\partial p'}{\partial \xi} + \eta_x \frac{\partial p'}{\partial \eta} \\ \frac{\partial p'}{\partial y} = \frac{\partial p'}{\partial \xi}\frac{\partial \xi}{\partial y} + \frac{\partial p'}{\partial \eta}\frac{\partial \eta}{\partial y} = \xi_y \frac{\partial p'}{\partial \xi} + \eta_y \frac{\partial p'}{\partial \eta} \end{matrix} \tag{3.28}$$

Recall the metrics of transformation:

$$\xi_x = \frac{y_\eta}{|J^{-1}|}; \ \eta_x = -\frac{y_\xi}{|J^{-1}|}; \ \xi_y = -\frac{x_\eta}{|J^{-1}|}; \ \eta_y = -\frac{x_\xi}{|J^{-1}|} \tag{3.29}$$

So that we have:

$$u' = -\frac{1}{\mu|J^{-1}|}\left[y_\eta \frac{\partial p'}{\partial \xi} - y_\xi \frac{\partial p'}{\partial \eta}\right]; \quad v' = -\frac{1}{\mu|J^{-1}|}\left[x_\eta \frac{\partial p'}{\partial \xi} - x_\xi \frac{\partial p'}{\partial \eta}\right] \tag{3.30}$$

From (Linninger 2011) we have that $\frac{\partial p'}{\partial \xi} = \Delta p'_\xi = p'_0 - p'_1$ and $\frac{\partial p'}{\partial \eta} = \Delta p'_\eta = p'_N - p'_S$

This leads to the final form for the velocity correction:

$$u' = -\frac{1}{\mu|J^{-1}|}\left[y_\eta(p'_0 - p'_1) - y_\xi(p'_N - p'_S)\right] \tag{3.31}$$
$$v' = -\frac{1}{\mu|J^{-1}|}\left[x_\eta(p'_0 - p'_1) - x_\xi(p'_N - p'_S)\right] \tag{3.32}$$

The velocity correction, $\vec{u}'$ is the difference between the correct velocity, $\vec{u}$ and the solution variable, $(u^* \ v^*)$:

$$\begin{pmatrix} u' \\ v' \end{pmatrix} = \begin{pmatrix} u \\ v \end{pmatrix} - \begin{pmatrix} u^* \\ v^* \end{pmatrix} \tag{3.33}$$

After rearranging the above expression, eq. (1-12) emerges:

$$\begin{pmatrix} u \\ v \end{pmatrix} = \begin{pmatrix} u^* \\ v^* \end{pmatrix} + \begin{pmatrix} u' \\ v' \end{pmatrix} \tag{3.34}$$

This leads to two equations that represent the correct velocity components, u and v. After substituting eq. (1-11) into eq. (1-12) we have:

$$u = u^* - \frac{1}{\mu|J^{-1}|}\left[y_\eta(p'_0 - p'_1) - y_\xi(p'_N - p'_S)\right] \tag{3.35}$$

$$v = v^* - \frac{1}{\mu|J^{-1}|}\left[x_\eta(p'_0 - p'_1) - x_\xi(p'_N - p'_S)\right] \tag{3.36}$$

If u and v above were the correct velocity, we should expect these velocity components to satisfy continuity for an incompressible fluid:

$$\int_{cv} \nabla \cdot \vec{u} \, dV = 0 \ \Rightarrow \oint_{face} \vec{u} \cdot \hat{\vec{n}} \, dA = 0 \tag{3.37}$$

With the relation, $\oint_{face} dA = \sqrt{x_\eta^2 + y_\eta^2}$, the above can be cast into

$$0 = \sum_{f=1}^{\# \ of \ faces} (u \ \ v) \cdot (-1) \begin{pmatrix} y_\eta \\ -x_\eta \end{pmatrix}\Big|^f \tag{3.38}$$

Therefore, the total mass balance is:

$$q = -\sum_{f=1}^{\#\ of\ faces}(u y_\eta - v x_\eta)\big|^f \tag{3.39}$$

For an undeformable fluid grid with an underlying incompressible fluid, q in eq. (3.39) will be zero. For a given face, we can substitute eq. (3.37) into (3.39) and rewrite continuity as:

$$-1\left[y_n\left\{u^* - \frac{1}{\mu|J^{-1}|}\left[y_\eta(p'_0 - p'_1) - y_\xi(p'_N - p'_S)\right]\right\} - x_\eta\left\{v^* - \frac{1}{\mu|J^{-1}|}\left[-x_\eta(p'_0 - p'_1) - x_\xi(p'_N - p'_S)\right]\right\}\right] \tag{3.40}$$

This simplifies to:

$$-1\left[y_\eta u^* - x_\eta v^* - \frac{(y_\eta^2 + x_\eta^2)}{\mu|J^{-1}|}(p'_0 - p'_1) + \frac{(y_\xi y_\eta + x_\xi x_\eta)}{\mu|J^{-1}|}(p'_N - p'_S)\right] \tag{3.41}$$

Or more simply as:

$$-1\left\{y_n u^* - x_n v^* - \frac{1}{\mu}\left[\frac{q_1}{|J^{-1}|}(p'_0 - p'_1) - \frac{q_2}{|J^{-1}|}(p'_N - p'_S)\right]\right\} \tag{3.42}$$

We can again use the approximation for the diffusion term introduced earlier to rewrite continuity as:

$$-1\left\{y_\eta u^* - x_\eta v^* - \frac{1}{\mu}\left[\frac{(p'_0 - p'_1)}{q_3}|J^{-1}|\right]\right\}, where \quad \begin{matrix} q_3 = x_\xi^2 + y_\xi^2 \\ |J^{-1}| = x_\xi y_\eta - x_\eta y_\xi \end{matrix} \tag{3.43}$$

The complete equation which takes into account the contributions from all faces of a control volume is:

$$\sum_{f=1}^{\#\ of\ faces}\left\{-y_\eta u^* + x_\eta v^* + \frac{1}{\mu}\left[\frac{(p'_0 - p'_1)}{q_3}|J^{-1}|\right]\right\}\bigg|^f = 0 \tag{3.44}$$

This leads to the pressure correction equation for p ' :

$$\sum_{f=1}^{\#\ of\ faces}\underbrace{\frac{1}{\mu}\left[\frac{(p'_0 - p'_1)}{q_3}|J^{-1}|\right]\bigg|^f}_{Deviation\ from\ Continuity} = \sum_{f=1}^{\#\ of\ faces}\underbrace{y_\eta u^* - x_\eta v^*\big|^f}_{Continuity} \tag{3.45}$$

If convergence has not been reached, we apply the relation, $p = p^{i-1} + p'$ to improve the quality of the pressure field. p^{i-1} is the pressure value at the previous iteration—the value used in (3.25) and (3.26). Actually, the improved pressure value will be calculated via under-relaxation:

$$p^{new} = p^{i-1} + \alpha_p p' \quad where\ o < \alpha_p < 1 \tag{3.46}$$

For the second iteration, p^{i-1} will be set equal to p^{new} ; this updated p^{i-1} will be used as the new pressure guess in eqs. (1-8) and (1-9). The velocities are also updated with

under-relaxation ($0\ 1 << \alpha_u$ and $0\ 1 << \alpha_v$); the velocity components that will be used in eqs. (1-8) and (1-9) for the next iteration are:

$$u^{new} = \alpha_u u + (1 - \alpha_u)u^{i-1} \tag{3.47}$$

$$v^{new} = \alpha_v u + (1 - \alpha_v)v^{i-1} \tag{3.48}$$

A flow diagram of the SIMPLE method is given in Figure 3.5. It is easy to extend existing SIMPLE solution to be SIMPLER one. Treating the boundary conditions and numerical methods used in SIMPLER solution is almost the same as in SIMPLE, so I will not repeat myself. The flow diagram of SIMPLER scheme is shown in Figure 3.6.
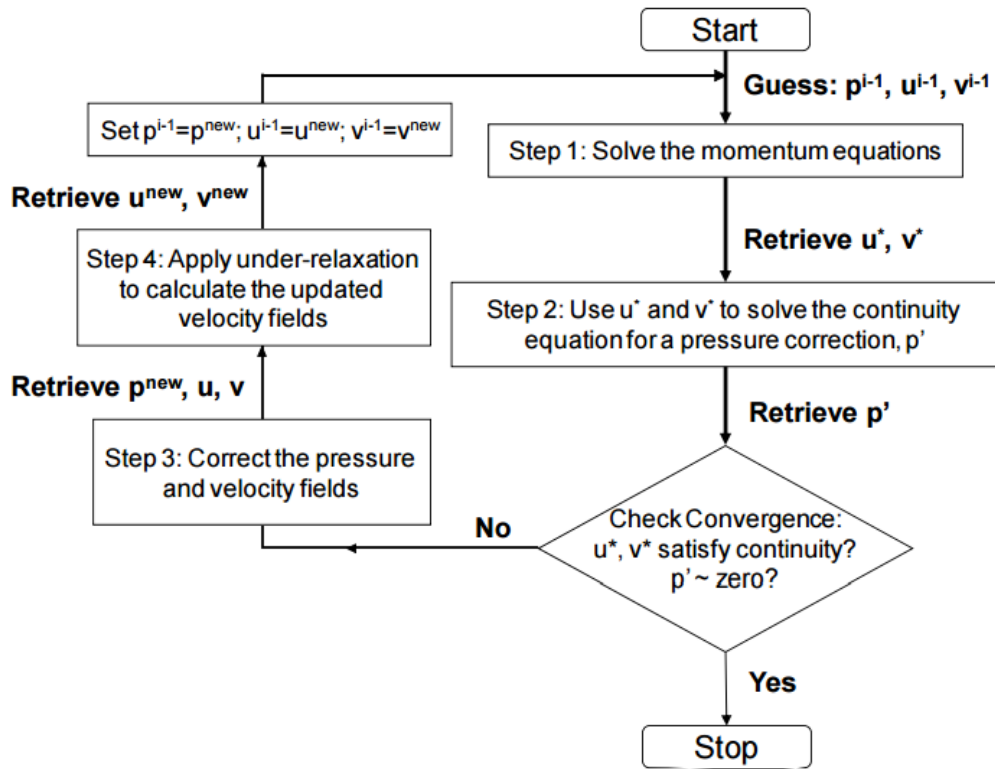
Figure 3.3 Flow diagram of SIMPLE method

Guess
$(U^\wedge)^n$, $(V^\wedge)^n$

Solve Momentum
eq. (without P)
$(U^\wedge)^{n+1}$, $(V^\wedge)^{n+1}$

Solve Poisson eq.
for (P^{n+1}) using
$(U^\wedge)^{n+1}$, $(V^\wedge)^{n+1}$

Solve Poisson eq.
for (P') using
$(U^*)^{n+1}$, $(V^*)^{n+1}$

If not coverged

Solve Momentum
eq. (using P^{n+1})
$(U^*)^{n+1}$, $(V^*)^{n+1}$

$U^{n+1} = (U^*)^n + (U')$
$V^{n+1} = (V^*)^n + (V')$

If coverged

Visualize Results
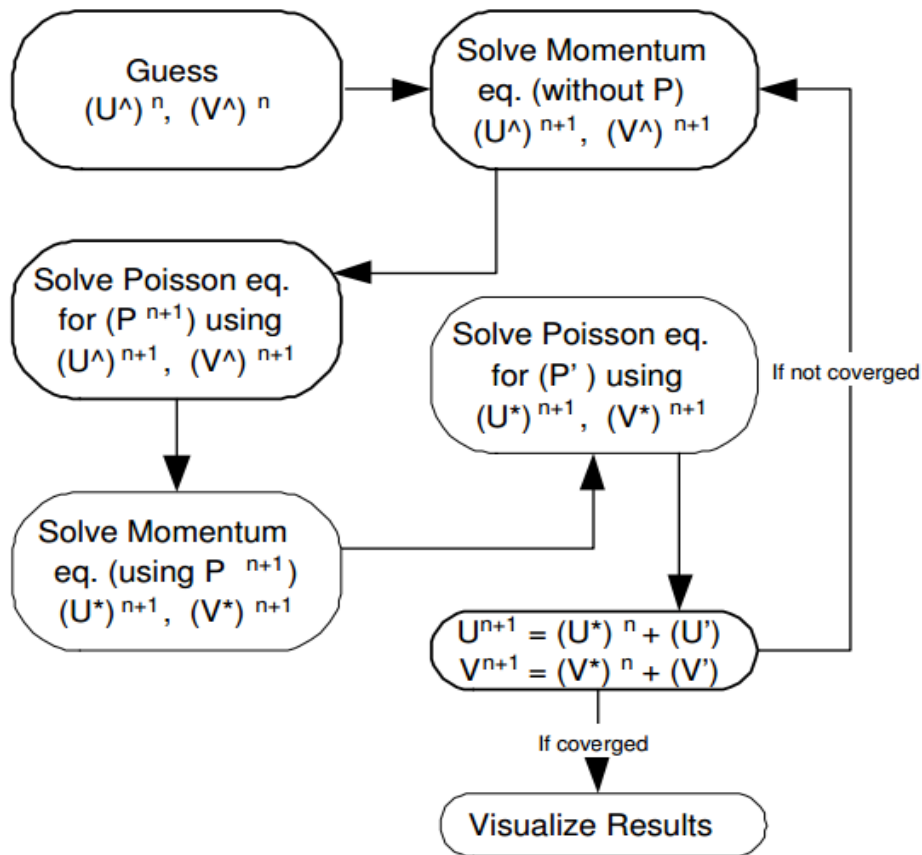
Figure 3.4 Flow chart of SIMPLER Scheme

3.2.2.3 Staggered grid

For discretization of differential equations I am using staggered grid. In the figure staggered grid for rectangular area is sketched. Primitive variables are placed in different places. In points i, j on a grid pressure P values, in points $i + 0.5, j$, ux-velocity components and in points $i, j + 0.5$, vy-velocity components are placed. That simple model of staggered grid gives us possibility to use simple discretization with second order accuracy
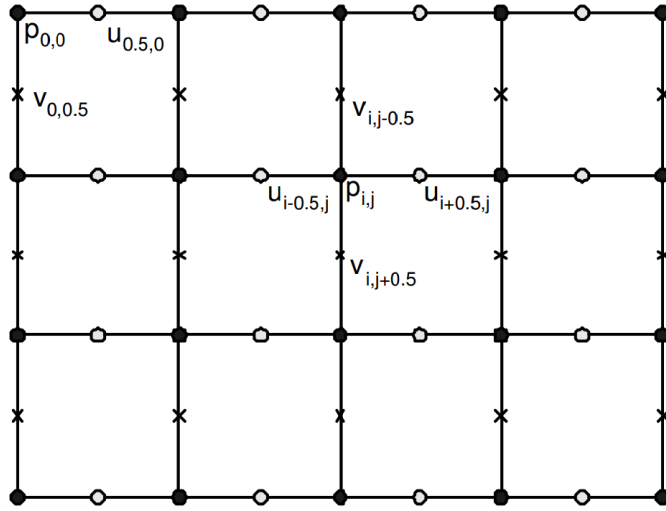
Figure 3.5 Staggered grid: filled circles P, outline circles U x-velocity, cross V y-velocity component

Table 3.1 Discretization used in SIMPLE algorithm

Differential	Discretization	Type
$\dfrac{\partial u}{\partial t}$	$\dfrac{u^{n+1} - u^n}{\Delta t}$	forward, O(h)
$\dfrac{\partial^2 u}{\partial x^2}$	$\dfrac{u_{i+1,j} - 2 * u_{i,j} + u_{i-1,j}}{(\Delta x)^2}$	central, O(h 2)
$\dfrac{\partial u^2}{\partial x}$	$\dfrac{u_{i+1,j}^2 - u_{i-1,j}^2}{2\Delta x}$	central, O(h 2)
$\dfrac{\partial p}{\partial x}$	$\dfrac{p_{i+1,j} - p_{i,j}}{(\Delta x)}$	forward, O(h)
$\dfrac{\partial p}{\partial y}$	$\dfrac{p_{i,j+1} - p_{i,j}}{(\Delta y)}$	forward, O(h)

3.3 Erosion and deposition model

The erodible bed thickness of earthen dam at each calculation time step may be partly saturated and partly unsaturated. Usually top surface close to the flowing water is saturated (Nakagawa et al. 2011). In saturated region, there is no effect of suction in the soil mass. However, in unsaturated region, the suction effects in the erosion of soil. Therefore, the erosion process of dyke is computed by considering both the saturated and unsaturated erosion mechanism (Nakagawa et al. 2011). The erosion velocity equation given by Takahashi et al. (1992) for unsaturated bed without considering suction is described as

$$\frac{i_{bsat}}{\sqrt{gh}} = K_e sin^{3/2}\theta_b \left\{1 - \frac{\sigma-\rho}{\rho}c\left(\frac{tan\phi}{tan\theta_b}-1\right)\right\}^{1/2} \times \left(\frac{tan\phi}{tan\theta_b}-1\right)(c_\infty - c)\frac{h}{d_m} \tag{3.49}$$

where ibsat is the erosion rate without considering suction, K_e (=0.8) is the erosion rate constant, c_∞ is the equilibrium sediment concentration, ϕ is the angle of internal friction, θ_b is the slope of the channel and the value of $tan\theta_b$ in the above equations is used the energy gradient as follows:

$$tan\theta_b = \sqrt{\tau_{bx}^2 + \tau_{by}^2}/(\rho gh) \tag{3.50}$$

The erosion velocity equation for unsaturated bed considering suction is described as (Nakagawa et al. 2011)

$$\frac{i_{bunsat}}{\sqrt{gh}} = K_e sin^{3/2}\theta_b \left\{1 - \frac{\sigma-\rho}{\rho}c\left(\frac{tan\phi}{tan\theta_b}-1\right) - \frac{\Delta\tau_{suc}}{\rho ghsin\theta_b}\right\}^{1/2} \times \left(\frac{tan\phi}{tan\theta_b}-1\right)(c_{\infty suc} - c)\frac{h}{d_m} \tag{3.51}$$

$$\Delta\tau_{suc} = \rho g|\psi|\left(\frac{\theta-\theta_r}{\theta_s-\theta_r}\right)tan\phi \tag{3.52}$$

where i_{bunsat} is the erosion rate considering suction, $\Delta\tau_{suc}$ is the shear stress increment due to the suction and $c_{\infty suc}$ is the equilibrium sediment concentration considering suction, which is expressed as

$$c_{\infty suc} = \frac{\rho tan\theta_b - \frac{\Delta\tau_{suc}}{ghcos\theta_b}}{(\sigma-\rho)(tan\phi - tan\theta_b)} \tag{3.53}$$

The total erosion rate considering both with and without suction effect is expressed as

$$i_b = f \cdot i_{bsat} + (1-f) \cdot i_{bunsat} \tag{3.54}$$

Where f is the variable based on thickness of saturated part of total eroded thickness (0<f<1), and f=0.5 is used as Nakagawa et al. (2011) for the computation.

If sediment concentration in the flow is greater than the equilibrium sediment concentration (c>c_∞), the deposition occurs and the deposition velocity equation is expressed as follows (Takahashi et al. 1992):

$$i_b = \delta_d \frac{c_\infty - c}{c_*}\sqrt{u^2 + v^2} \tag{3.55}$$

Where δ_d (=0.03) is the deposition coefficient.

The variation in the embankment shape is expressed as follows:

$$\frac{\partial z_b}{\partial t} + i = i_{sml} + i_{smr} \tag{3.56}$$

Where, z_b is the erosion or deposition thickness of the bed measured from the original bed surface elevation, i_{sml} and i_{smr} are the mean recessing velocity of the left and right hand side banks of the incised channel respectively.

3.4 Lateral erosion equations

Lateral erosion velocity is assumed as a function of the shear stress on the side wall assigned by the interstitial fluid of the overlying sediment-laden flow τ_{sf}. The value of τ_{sf} is then assumed as the half of the bed shear stressτ_f. One may write the recession velocity of the wetted sidewall under the surface of the flow i_s as

$$\frac{i_s}{\sqrt{gh}} = \left(\frac{1}{2}\right)^{1.5} K_e sin^{3/2}\theta_b \left\{1 - \frac{\sigma-\rho}{\rho}c\left(\frac{tan\phi}{tan\theta_b} - 1\right) - \frac{\Delta\tau_{suc}}{\rho ghsin\theta_b}\right\}^{1/2} \times \left(\frac{tan\emptyset}{tan\theta_b} - 1\right)(c_{\infty suc} - c)\frac{h}{d_m} \tag{3.57}$$

Where Ke is a constant. By recession of the wetted sidewall, the part of the wall upward of the surface of the flow may lose its stability and fall into the flow. If one assumes the recession of the whole sidewall is parallel as shown in Figure 3.3, the mean recession velocity of the side walls would be

$$i_{sml} = \frac{h_l}{l_l+h_l}i_{sl} \;,\;\; i_{smr} = \frac{r}{l_r+h_r}i_{sr} \tag{3.58}$$

The finite difference calculation of the system of equations referred to above on the two dimensional rigid grid system set on the horizontal plane requires a little contrivance, because on such grid the channel can enlarge its width only discretely in spite of the actual continuous widening. To overcome this problem, one may assume that the sediment produced by the recession of banks, e.g. $i_{smr} = (z_{bs} - z_b)\Delta t$ is supplied only to the cell adjacent to the bank, e.g. cell A in Figure 3.6, and it instantaneously raises the elevation of that cell to be eroded by the flow in the channel in the next time step. The channel width is considered not to be changed until the total volume of the sediment supplied, for example, to the cell A becomes equal to the volume of the sediment in the side bank cell at the beginning of the side bank erosion, t_0. At the moment when the two respective volumes of sediment become equal, the channel is considered to be widened by one cell width and the bottom elevation of the new cell adjacent to the new bank is set to be equal to that of the former adjacent cell at time t_0. The formulation of the procedure is as follows:

$$\int_{t_o}^{t} i_{sr}h_r\Delta x dt = (z_{bs} + z_{so} - z_b - z_o)|_{t=t_o}\Delta x\Delta y \xrightarrow{yields} z_b = z_b|_{t=t_o} \tag{3.59}$$
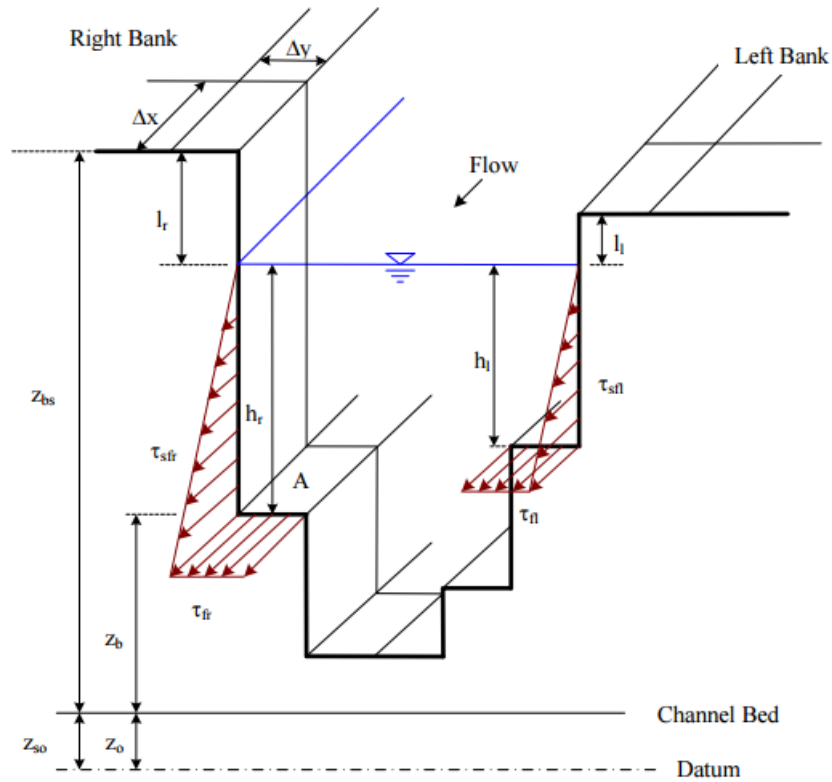
Figure 3.6 A cross-section of the incised channel on a dam

3.5 Summary

In this chapter, the different modules of the integrated model are discussed in details. The two dimensional seepage models based on Richard's equation and its solution procedures, two dimensional depth-averaged flow model and SIMPLER method of its solution, Erosion and deposition model and lateral erosion model are discussed in details.

The novelty of this study is in the combination of these modules to reproduce the complicated embankment failure process. There are many interactions among the modules, and the highlight of the present model is its estimation of the erosion rate by considering that the effect of resisting shear stress due to suction depends on saturation conditions on the embankment surface, which is calculated using the result from the seepage flow module. In order to focus on the improvement in the treatment of the surface erosion process, the developed model was reduced to vertical two-dimensional calculations in seepage and erosion modules; however, the horizontal 2D flow model was introduced to consider the extensibility for our future work.

CHAPTER 4

COMPARISON OF NUMERICAL RESULTS WITH NEW EXPERIMENT CASES

4.1 General

In this section, the results obtained from numerical simulation discussed in chapter 3 are compared with new set of experiments and generate the results. The main goals of this study are to establish a simple model setup for testing pure overtopping failure mode (i.e. no internal erosion or sliding), obtain information such as, the temporal and spatial lateral widening process along the dyke length, resulting water and sediment hydrographs and study the scour pattern for different scenarios of dyke and flood plain. Special attention is paid to the influence of the differences in sediment size and degree of saturation in a river dyke body on the erosion process. Given the overtopping failure mode, the model dyke represents the worst-case scenario and any surface strengthening or sealing may be considered an added safety against dyke breaching.

4.2 Verification of model with experiments

4.2.1 Laboratory experiments

The experimental flume was prepared considering realistic orientation of dyke in relation to river flow i.e. the dyke structure was placed parallel to the river flow with the flow direction towards dyke non-perpendicular. The plan and section view of the flume and the picture of setup without the sand dyke are as shown in Fig. 2 and Fig.3 respectively below. The flume was made with acrylic plastic materials with the total length of 4m, out of which, only middle 1 m was made movable dyke while other portions were made fixed.

The main hydraulic test conditions assumed in the current research include: 1) Trapezoidal shaped River and Dyke, 2) Homogenous non-cohesive sediments, 3) 10% moisture content by weight was added initially to dyke materials and compacted using a similar procedure throughout all the experiments, 4) No core layer or protection was added, 5) Steady inflow with downstream gated weir control, 5) Optical recording by video, high-speed camera and laser equipment for the scour pattern measurement. The intake is equipped with pump connected supply tank with water collector chambers with flow straightener to generate undisturbed flow from the underground tank with a pump that circulates water continuously between upstream and downstream.
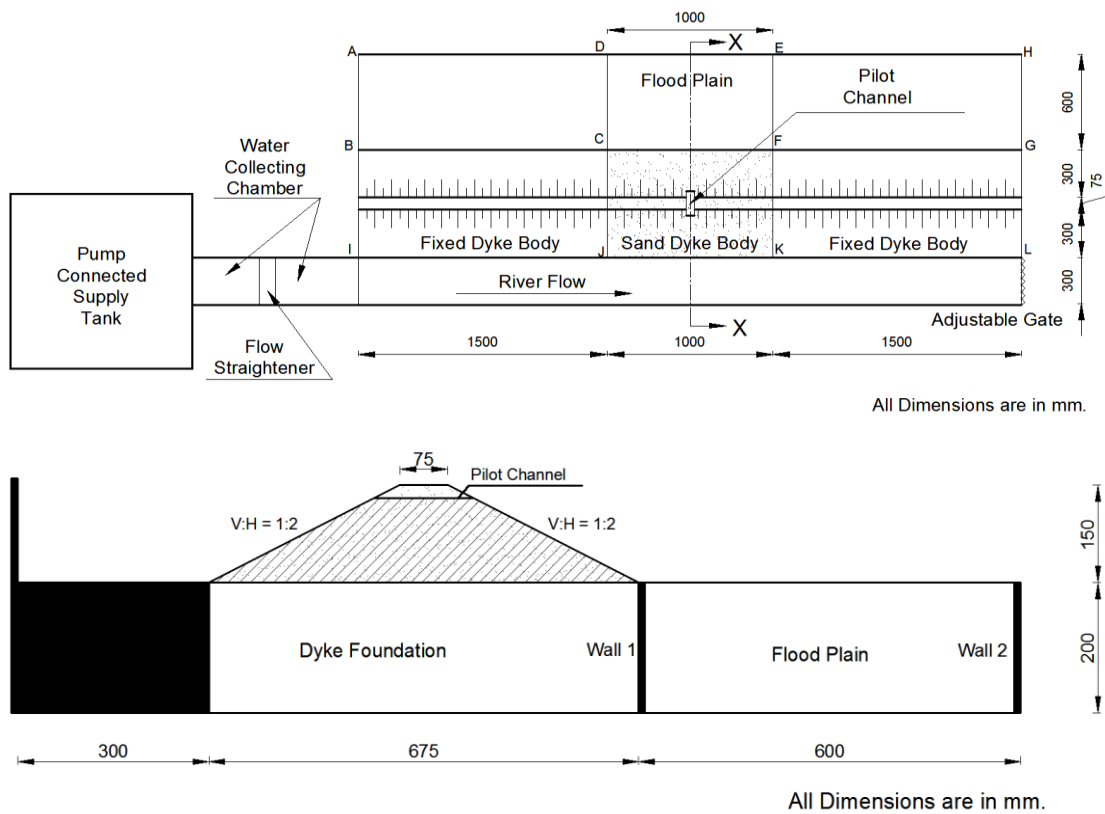
Figure 4.1 Experimental setup
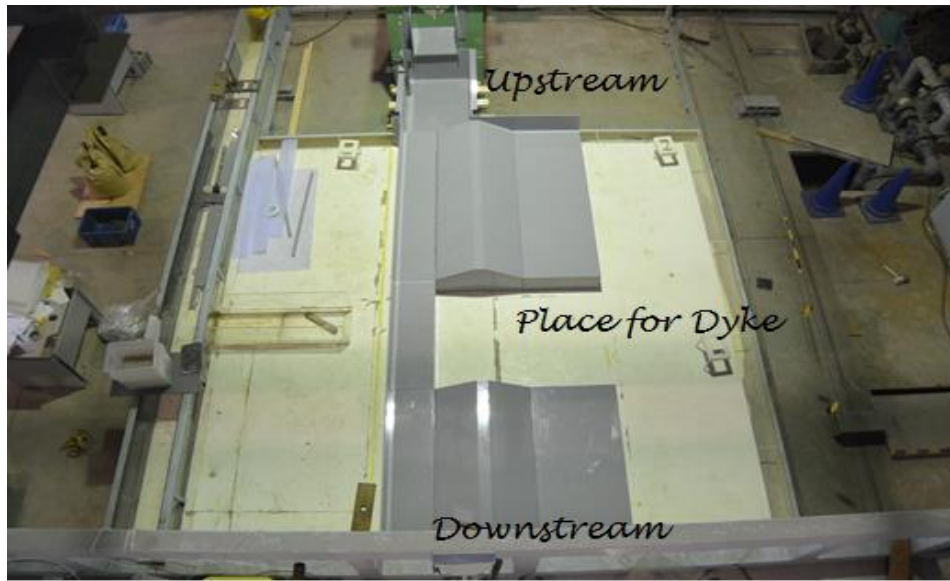
Figure 4.2 Bird's eye view of the experimental setup

Table 4.1 Experimental Plan in detail

Experiment Plan	Experiment Type	Sed. No.	Mean Diameter	No. of Experiments	Remarks
PLAN A	**1. Breach Characteristics**				
	Dynamic Lateral Widening	6	0.066	3	Repeatability OK
	Breach and sediment	7	0.018	3	Repeatability OK
	Hydrograph	8	0.089	3	Repeatability OK
PLAN B	**2. Scour Pattern**				
	a) Scenario 1	6	0.066	2	Repeatability OK
	Movable dyke, foundation	7	0.018	2	Repeatability OK
	and Flood plain	8	0.089	2	Repeatability OK
	b) Scenario2	6	0.066	2	Repeatability OK
	Fixed Dyke and Foundation	7	0.018	2	Repeatability OK
	but Movable Flood Plain	8	0.089	2	Repeatability OK

4.2.2 Experimental procedure

All experiments were conducted using a constant flow discharge in a flume referred to as the inflow. The dyke material was initially provided with 10% moisture content by weight and thoroughly mixed and then compacted with the help of a tamping plate and cylindrical small roller by spraying water layer by layer until about approx.. 90% compaction was achieved. The inflow was added rapidly to attain a steady state before overtopping started. The flow overtopped the dyke from the pilot channel thus resulting in the lateral widening of the breach from that point.

The detail experiment plans with number of experiments are shown in Table 1. For Plan A, a total of 9 experiments and for plan B, 12 (6 each for two scenarios) experiments were conducted for three sediment types. Each experiment was repeated three times for plan A and two times for plan B to observe the effect of repeatability. The sediment properties are already described in chapter 2.

For experiment plan 'Á' case, the wall 1 and wall 2 were placed and the dyke foundation and flood plain portion were made fixed considering only the movable dyke body (See Fig 2(b). The parameters investigated include: Flume discharge Q = 10 liters per sec, dyke height H = 0.15 m, dyke length L = 0.3 m, dyke crest width b = 0.075m (0.5H), and particle size = No.6, No. 7 and No. 8 (See Fig. 3). The upstream and downstream both dyke slopes are 1:2 (V: H) resulting in a total dyke width of B = 2H+0.5H+2H =4.5H. The pilot channel is made at the center of the 5 cm x 2 cm dyke as a point for the initiation of breach at the desired location. Once the overtopping start and the pilot channel starts to widen laterally, the discharge was measured at the end of the dyke point with the help of collecting water by plastic boxes at certain intervals simultaneously. Such boxes were weighed and computed the discharge by knowing the time intervals for collecting water for each boxes by optical measurement. The entire process of lateral widening was filmed by top and frontal video camera. The dynamic widening process were directly derived from the camera records

For Experimental Plan B, two scenarios were studied:

1) Scenario 1: Dyke body, foundation and flood plain all are movable (Representing the areas where the dyke is not strong enough to resist overtopping failure and farm or utility lands in the flood plain)

2) Scenario 2: Dyke body and foundation are fixed but flood plain is made movable (Representing the areas where the dyke is strong enough to overcome failure but the flood plain has populations or farm lands.
For Scenario 1, the wall 1 was removed while wall 2 was placed and the dyke body, foundation and flood plain portions were made movable. Then the breach discharge and the scour pattern after some reference point of time (time when the upstream portion of dyke remained around 10 cm, considering as equilibrium condition) were measured. The pilot channel was still used in this case. The equilibrium bed profile was measured from the Keyence laser profiler.

4.3 Experimental results (Plan A)

4.3.1 Lateral widening process

The overflow rate increased little at the initial overflow stage but begin to increase more when the dyke breakage widened. After the rate peaked, the water level remained almost the same for some time. Since the dyke material is unsaturated, therefore the suction pressure plays a greater role for the stability of almost vertical slopes two sides of pilot channel. Figure 5 shows the observed flow regime for the dyke breach analysis. The figure shows the hydrological regime from the channel strikes the downstream end of dyke in an angle developing stagnant region at upstream region. The dyke is always eroded by the main stream of flow passing through the actual flow width and asymmetrical propagation is observed as dyke breaching progressed. The frontal part (downstream part) is eroded continuously while the upstream part, the erosion stops after some time. The lateral widening pattern is quite different to the results obtained when the dyke was placed perpendicular to the flow (like a dam breach) i.e. the widening pattern followed symmetry (Bhattarai et al. 2014).

For all sediment sizes, the lateral widening process follows following four phases (See Figure 4.3 below):

1) Vertical undermining phase (VUP)

The crown of the dyke and downstream slope (slope towards flood plain) area were eroded slowly after overtopping starts the widening did not proceed but vertical undermining of the pilot channel start till it reached toe of the dyke. This process is named as Initiation of dyke erosion. The breach discharge was slow in this stage. This stage remains long for the finer sediment size (sed 8) while as the sediment sizes became coarser, this stage ceased fast.

2) Initiation of lateral widening Phase (ILWP)

When the vertical undermining reached the toe, the cross-section was eroded rapidly at toe first and then at top of dyke. The dyke widening progressed in both upstream and downstream directions. The middle of the dyke expands less in comparison to top and toe in this stage. Due to skewed flow direction, asymmetrical widening proceeds.

3) Lateral widening acceleration phase (LWAP)

Once the initiation of widening occurred, the erosion rate increased rapidly and the breach discharge also increased accordingly. The downstream part was now severely damaged than the upstream one.

4) Widening Deceleration cum stable phase (WDSP)

Once the most of the dyke portions were eroded and the stream width through the dyke increased, the breach discharge started to decrease and become stable but there was still very slow widening proceeding downstream but surprisingly, the upstream portions seem stable.

However, Figure 4.3 shows the cumulative lateral widening velocity distribution curve at different time steps. The difference between two time step curves shows the erosion rate between those two time steps. The curve clearly shows that the erosion process is asymmetrical with upstream portion erosion speed are always greater than equal to downstream. Also, sediment 6 has higher erosion rate for d/s dyke than sed 7 and sed 8 but, for all sediments, the upstream portion erosion seems more or less similar.

In summary, for all sediment sizes, the nature of the curve remains same except the rate of erosion i.e. erosion of dyke takes little longer time for finer sediment than coarser one. It shows an important impact of sediment size. Finer the sediment size, higher the development of suction pressures due to unsaturated condition which finally develops resistance against failure so the finer sediments reluctant to faster erosion. Hence the times taken to reach similar final condition for various sediment sizes are different; finer having late. The middle part of the dyke acts like a hinge as top and bottom of dyke already eroded in some extent.
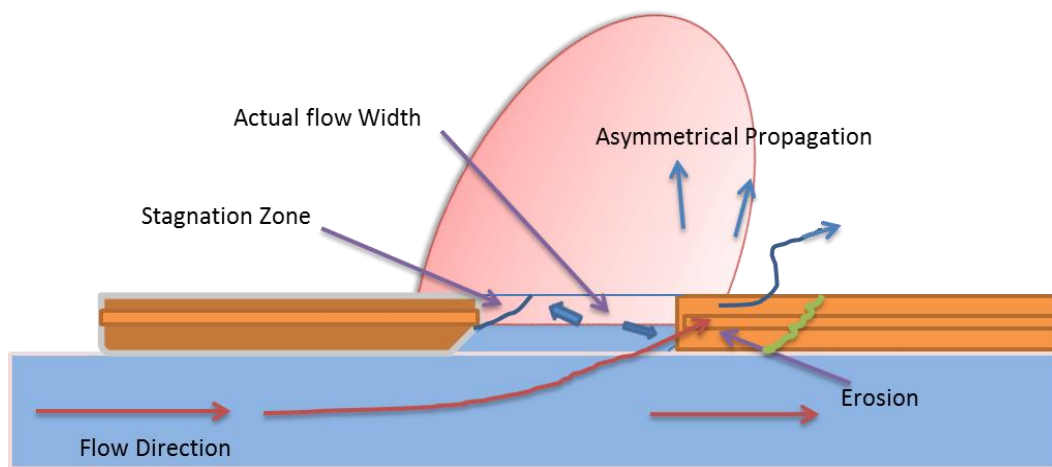
Figure 4.3 Observed flow regime during dyke breaching

Figure 4.4 Four phases of lateral widening process (Top left-1, Top right-2, Bottom left-3 and bottom right-4)
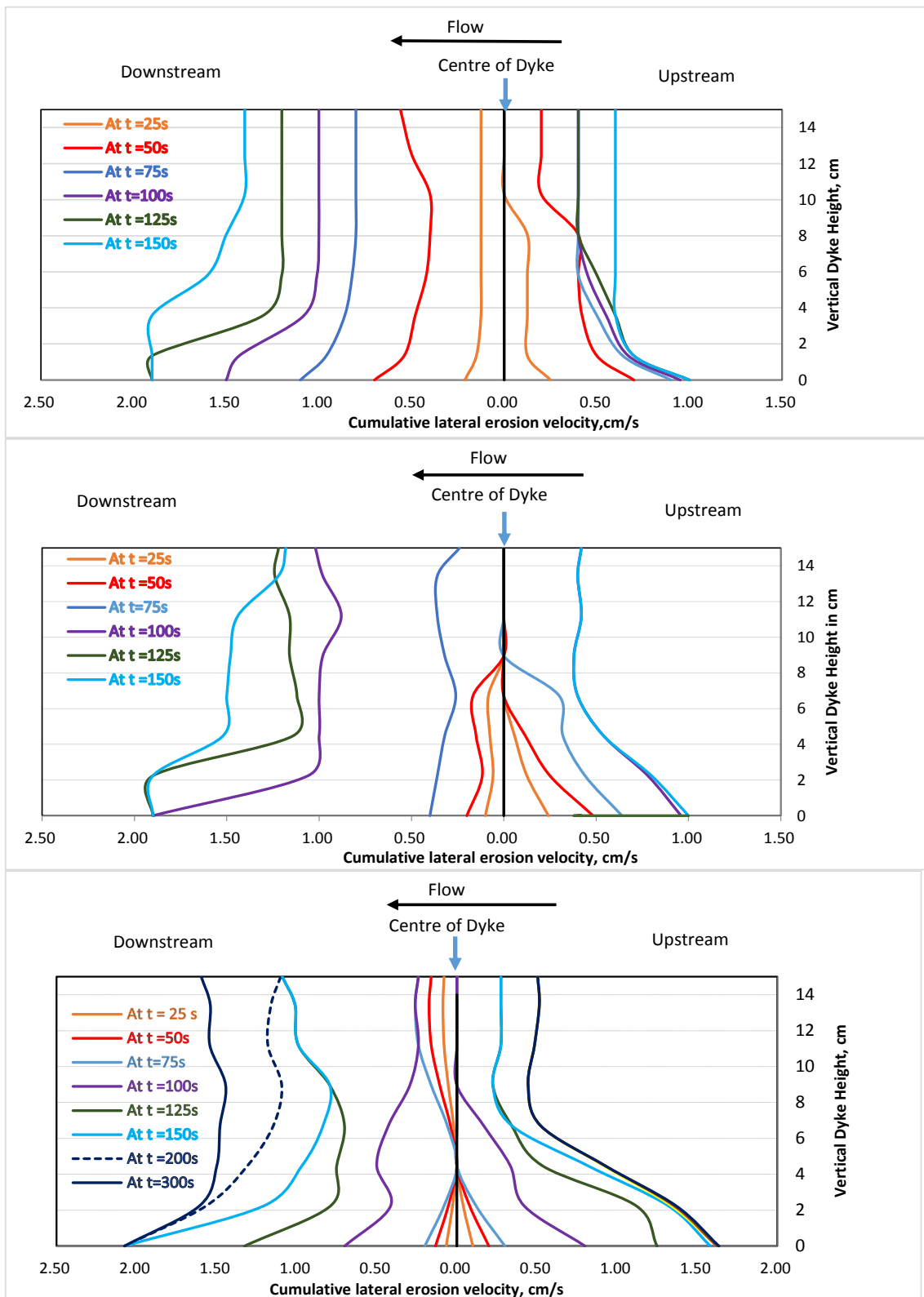
Figure 4.5 Cumulative lateral erosion speed curve for sed 6(top), sed7 (middle) and sed 8(bottom) respectively
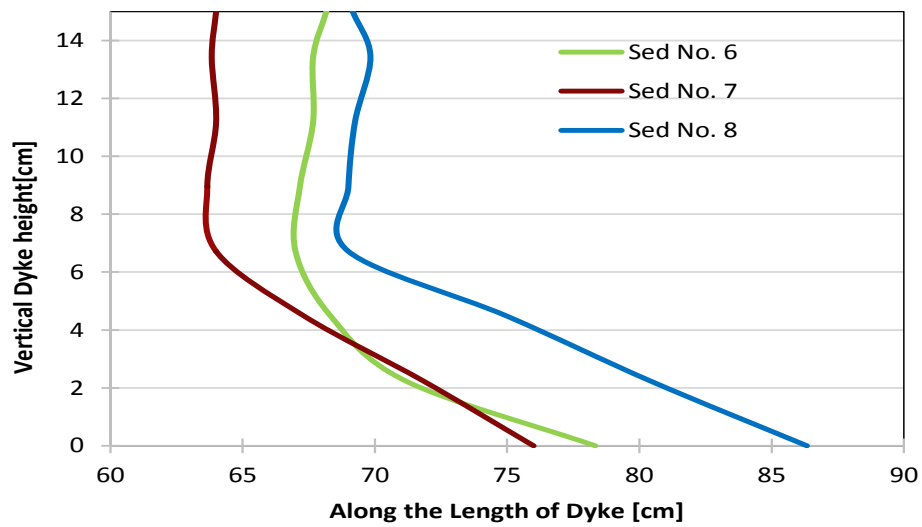
Figure 4.6 Final shapes of u/s portion of dyke for three sediment cases on the vertical plane along length
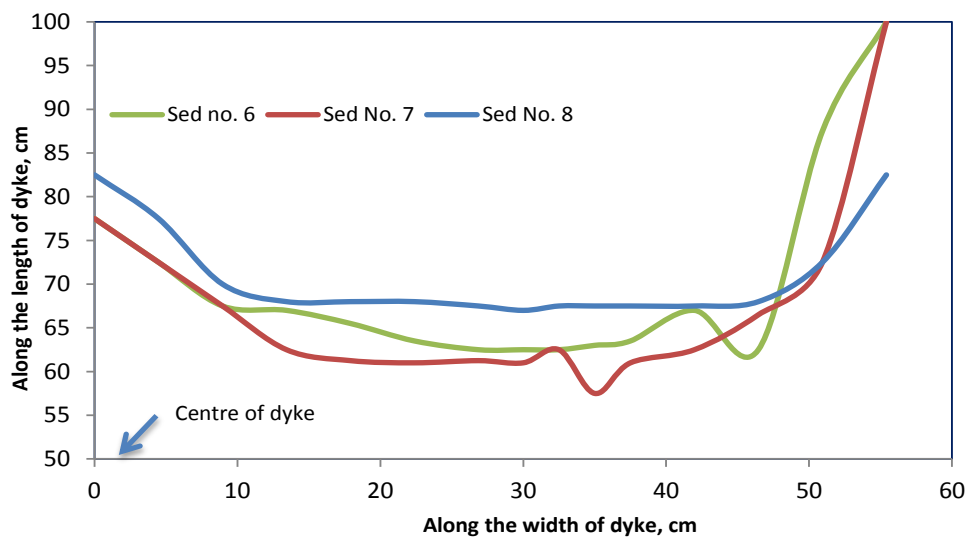
Figure 4.7 Final shapes of u/s portion of dyke for three sediment cases on the horizontal plane (plan view)

4.4 Comparison of numerical and experimental result

4.4.1 Numerical simulation parameters

Numerical simulations and flume experiments were performed to investigate the mechanism of dyke breach and resulting hydrograph due to overtopping and channel breach. Table 4.1 summarizes the geometry of the dams and hydraulic conditions used in different experimental cases.

The meshes used for the calculation of surface flow and seepage belong to structured mesh, and the resolution of the computational mesh was set to dx=1.0 cm in the embankment body region and to dx=2.0 cm in other regions of the entire flume area; to dy=1.0 cm in transverse direction for the calculation of flow; and to dx=1.0 cm and dz=0.5 cm for the calculation of seepage flow inside the embankment. Soil parameters for different sands used in these calculations were determined by laboratory experiments conducted by Nakagawa et al. (2011). The results were analysed to study the model performance.

4.4.2 Breach hydrographs

A numerical simulation of laboratory experiments on embankment erosion was carried out using the developed numerical model. Notch of the width 5cm and depth 2 cm was incised at the crest of the dyke body at the center and the erosion of the surface of the dyke body was observed by optical measurements. The overtopping flow incised a channel on the slope of the dam and that channel increased its cross-sectional area with time caused by the erosion of released water. The breach discharge increases rapidly after the initial overtopping until the maximum value is attained. The graph clearly shows that time lag of peak of the hydrograph increases with increase in sediment number i.e. decreasing mean diameter of sediments.

Figure 4.8-4.10 shows the repeatability test for the breach hydrographs. The figure reveals perfect repeatability and only one case study is taken further for comparison to numerical simulation. The overflowing water depth was very small so the shear stress due to flowing water in the side wall of incised channel was also small. Figure 4.11-4.13 shows breach hydrograph for different sediment sizes.

During breach formation, breach enlargement proceeded rapidly below the water surface in the breach channel. Above the water level there was some apparent cohesion added by water content and adhesion so the side wall was very steep and undermines the slope. The erosion process continues until slope stability was encountered. The slope failure of channel bank around crest of the dam is one of the main causes of higher peak discharge in the experiment compared to simulation. Figure 4.11-4.13 shows the comparison of numerical and experimental results and the results shows relatively well correlated. The peak discharge is underestimated by model due to collapse nature of failure and uncertainty in material properties (degree of compaction, mixing of sediments etc.) of the dyke body.
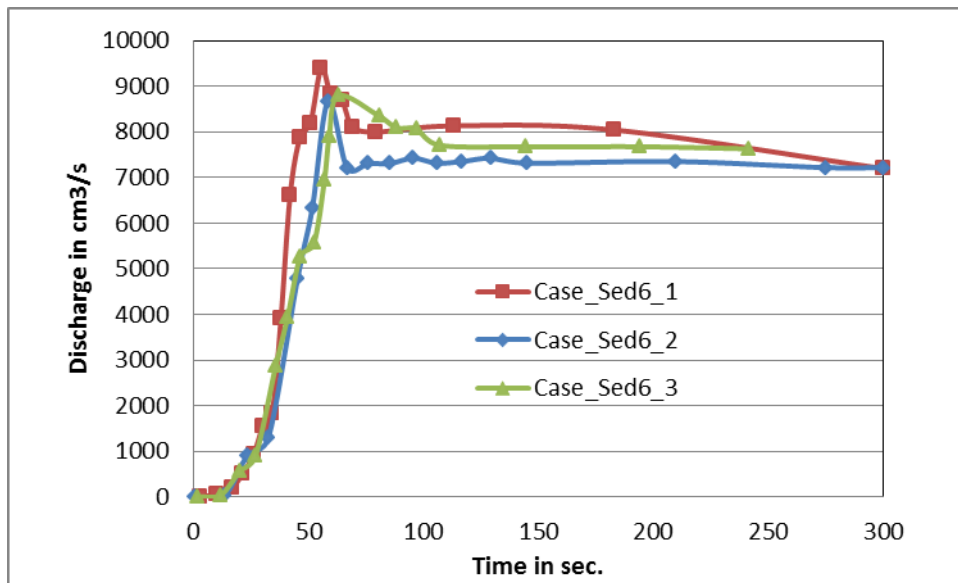
Figure 4.8 Repeatability check for the discharge from experiment (Sediment 6)
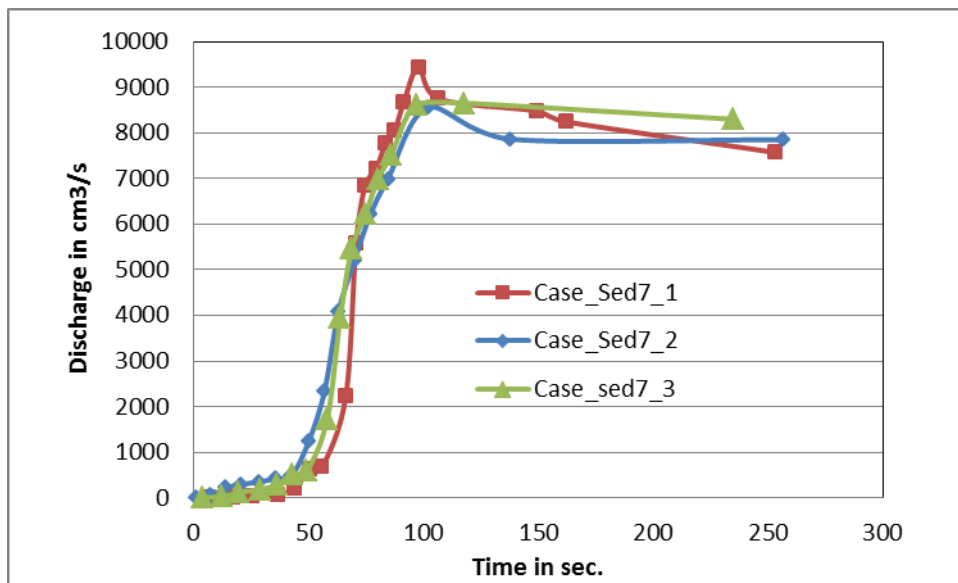
Figure 4.9 Repeatability check for the discharge from experiment (Sediment no. 7)
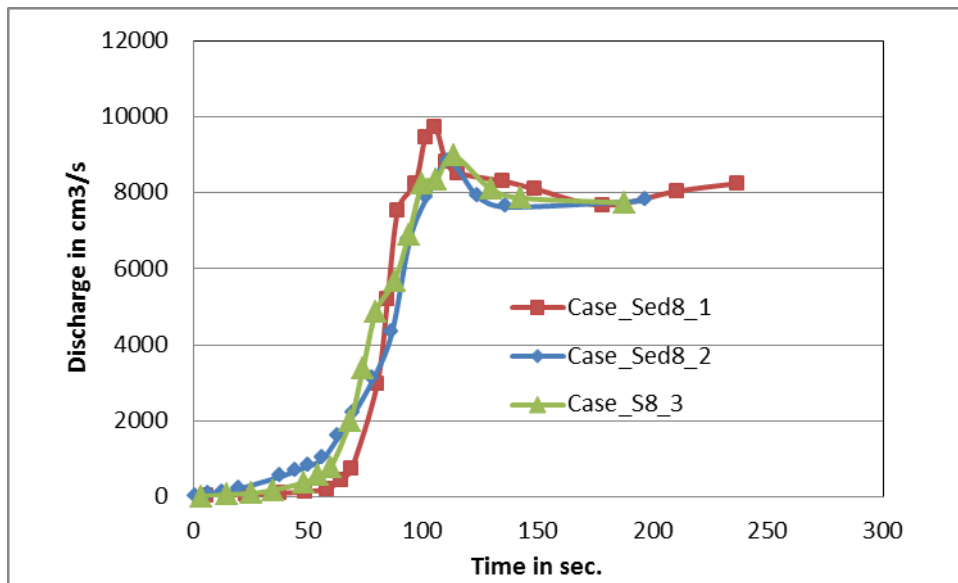
Figure 4.10 Repeatability check for the discharge from experiment (Sediment no. 8)
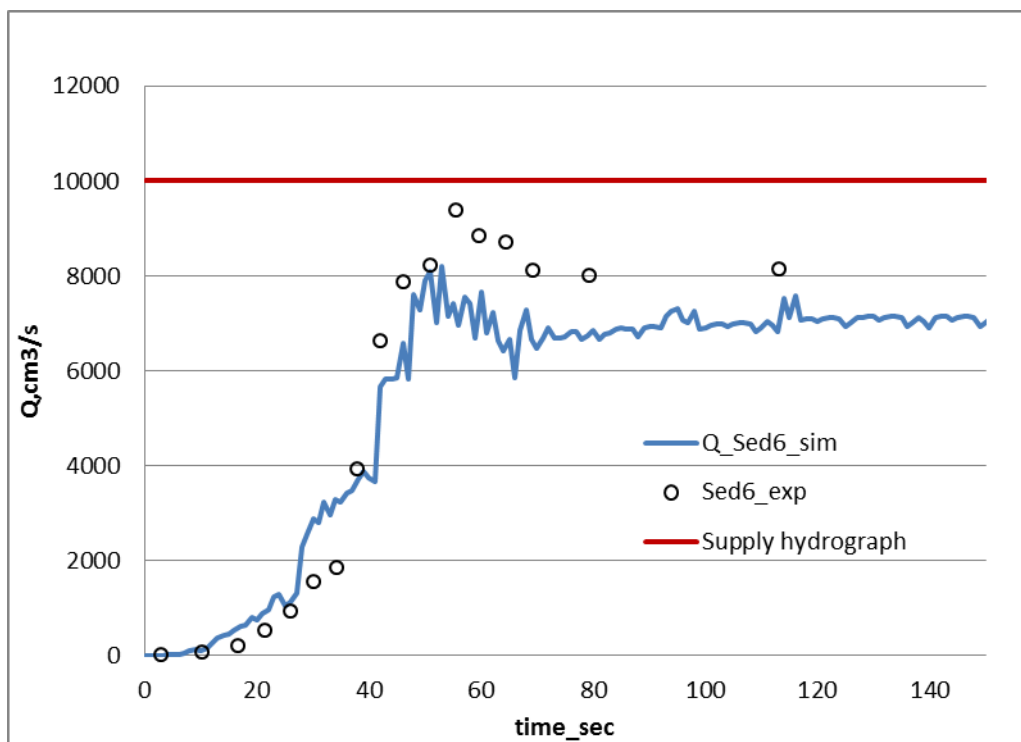
Figure 4.11 Breach Hydrograph (for sediment no.6)
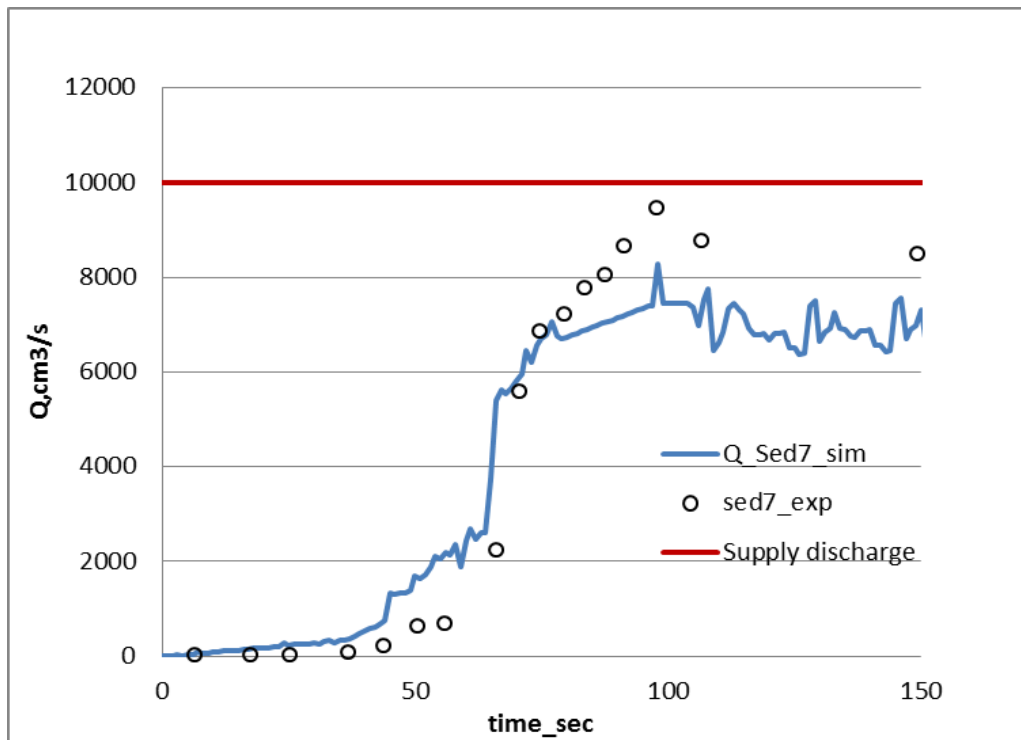
Figure 4.12 Breach Hydrograph (for sediment no.7)
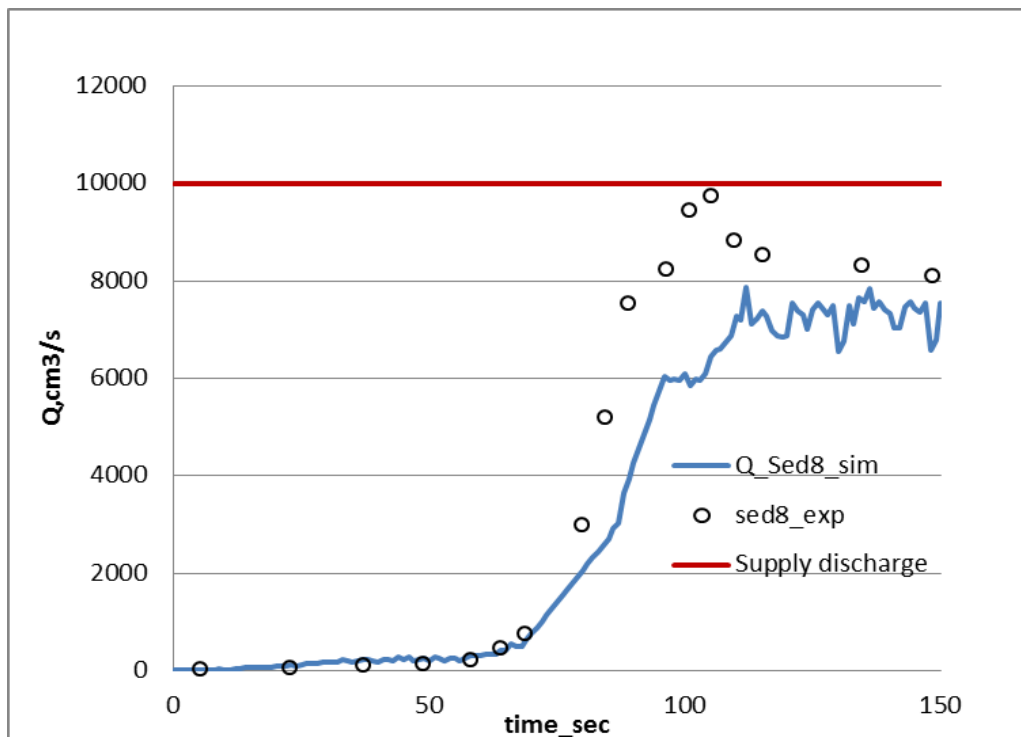
Figure 4.13 Breach Hydrograph (for sediment no.8)

4.4.3 Sediment hydrographs

Figure 4.14-4.16 shows the repeatability test for the sediment hydrographs. The figure reveals perfect repeatability and only one case study is taken further for comparison to numerical simulation. The overflowing water depth was very small so the shear stress due to flowing water in the side wall of incised channel was also small.

Figure 4.17-4.21 shows the sediment discharge for various sediment sizes. During breach formation, breach enlargement proceeded rapidly below the water surface in the breach channel. Above the water level there was some apparent cohesion added by water content and adhesion so the side wall was very steep and undermines the slope. The erosion process continues until slope stability was encountered. The slope failure of channel bank around crest of the dam is one of the main causes of higher peak discharge (sediment discharge) in the experiment compared to simulation.
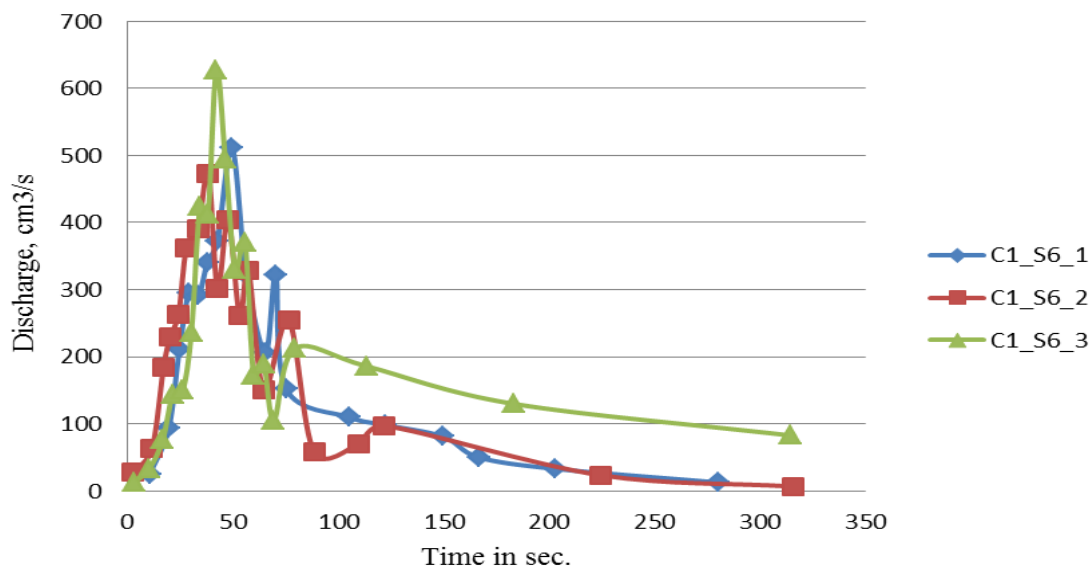
Figure 4.14 Repeatability test for sediment hydrograph (for sediment no.6)
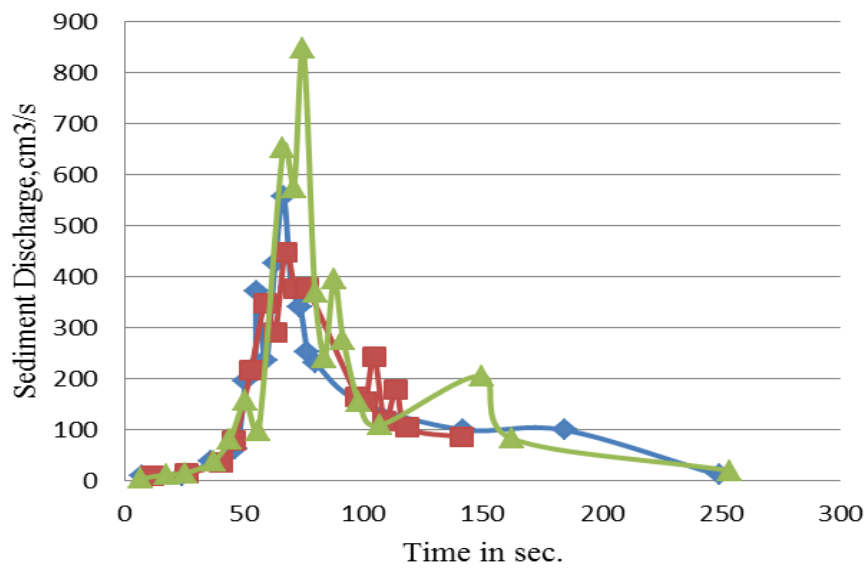
Figure 4.15 Repeatability test for sediment hydrograph (for sediment no. 7)
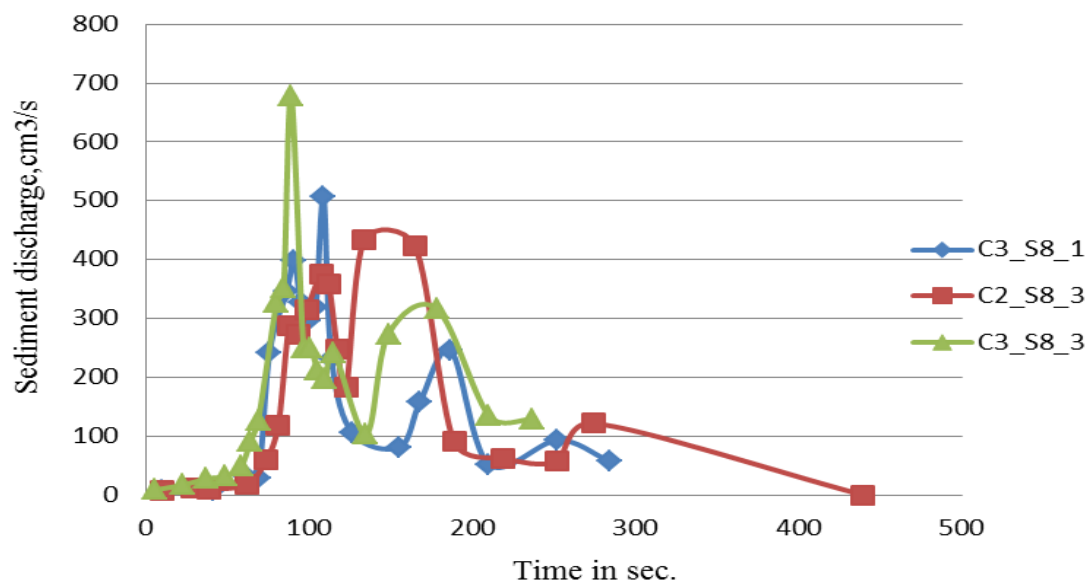
Figure 4.16 Repeatability test for sediment hydrograph (for sediment no 8)
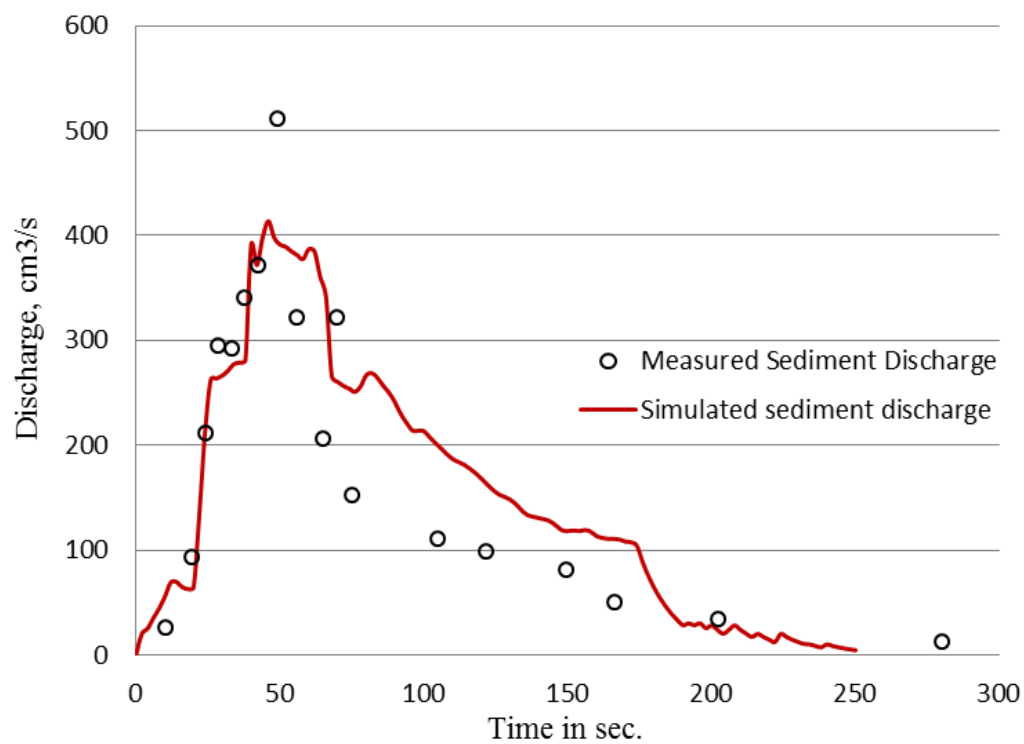
Figure 4.17 Sediment Hydrograph (for sediment no.6)
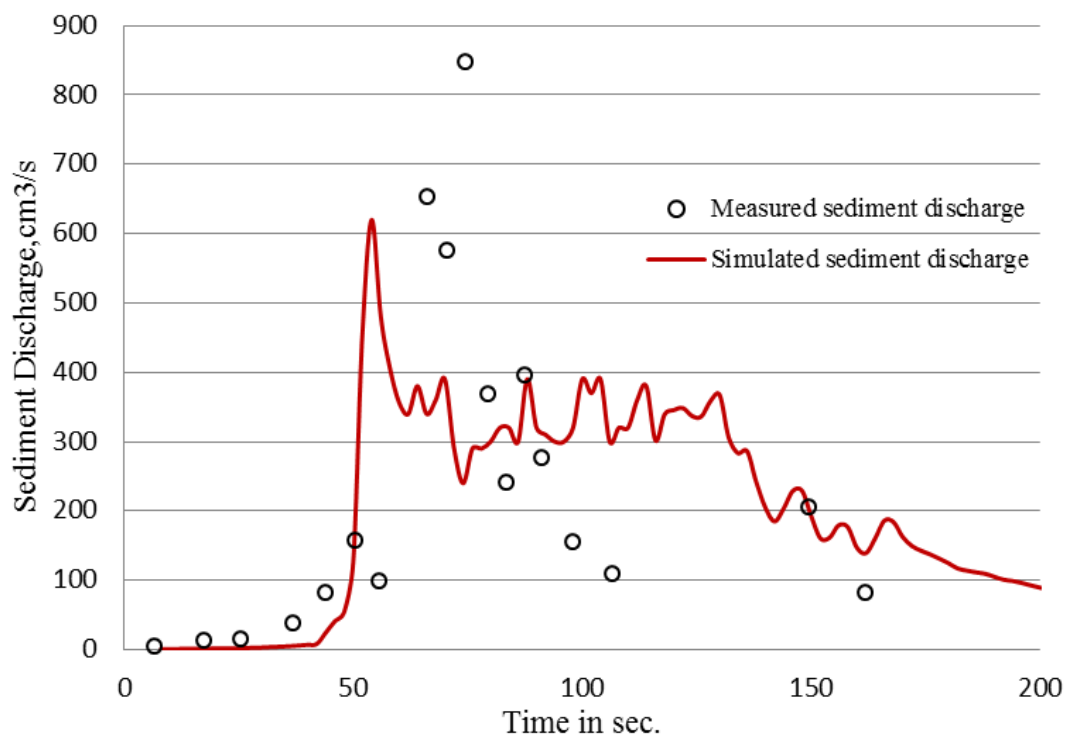
Figure 4.18 Sediment Hydrograph (for sediment no.7)
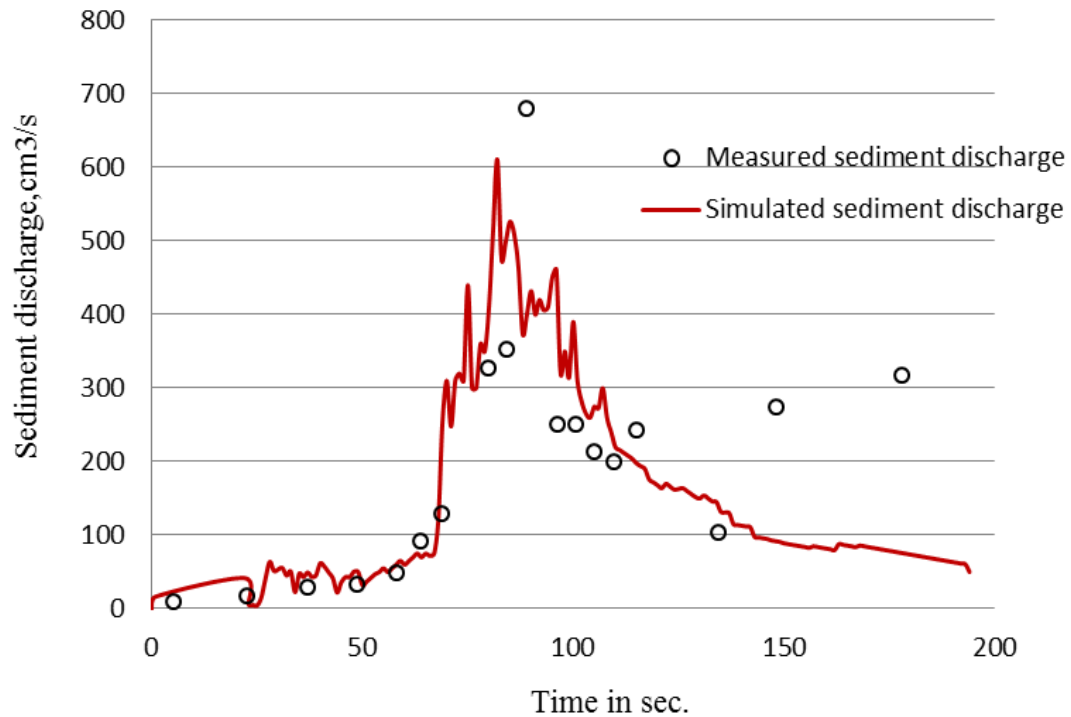
Figure 4.19 Sediment Hydrograph (for sediment no.8)

4.4.4 Lateral widening process

Immediately after over-spilling from the notch, the flow elongated downstream with an almost constant width. On arriving at the toe of the dyke, the flow gradually enlarged its width and by that time the failure of side banks of the channel had started in the neighbourhood of the crest. By the widening of the channel at the crest the overflow discharge increased and it rapidly eroded the channel. The side bank erosion proceeded downstream keeping the width of the channel almost uniform in an early stage, but later the width downstream became wider. As time went by the upstream width widened and finally the channel had nearly the parallel side banks throughout the length on the slope of the dam.

The lateral widening process is simulated to compare with the experimental result. The result shows as the sediment sizes decreases the consistency is little bit distorted. Otherwise, the simulated result shows good agreement. Hence we can conclude that the effect of sediment size is very important and hence some other collapse type mode l needed to be incorporated in current model. Initially when the incise channel eroded till bottom, the agreement is best. The result of the simulation clearly shows the widening and deepening of the channel and a slight deposition around the foot of the dam.

76
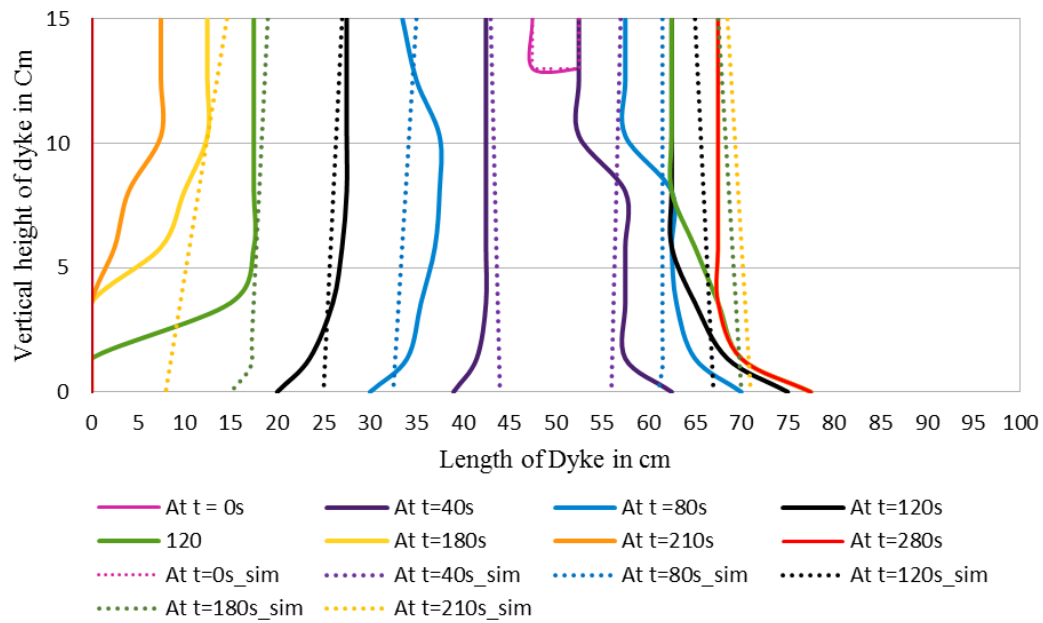
Figure 4.20 Lateral widening process (for sediment no.6)
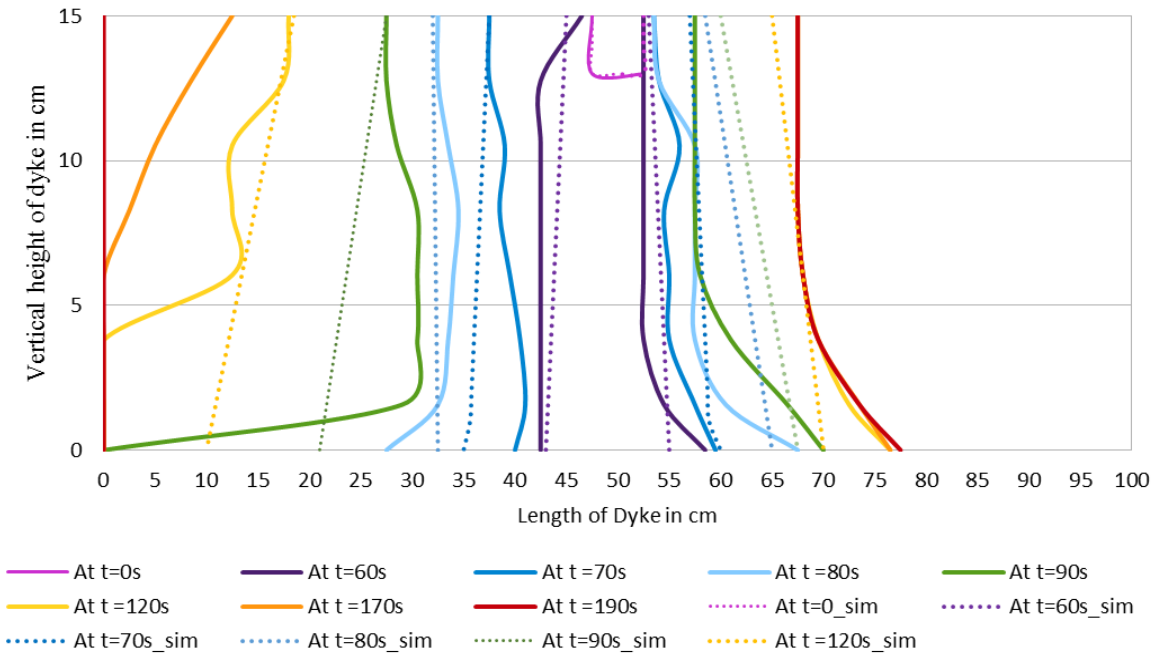
Figure 4.21 Lateral widening process (for sediment no.7)
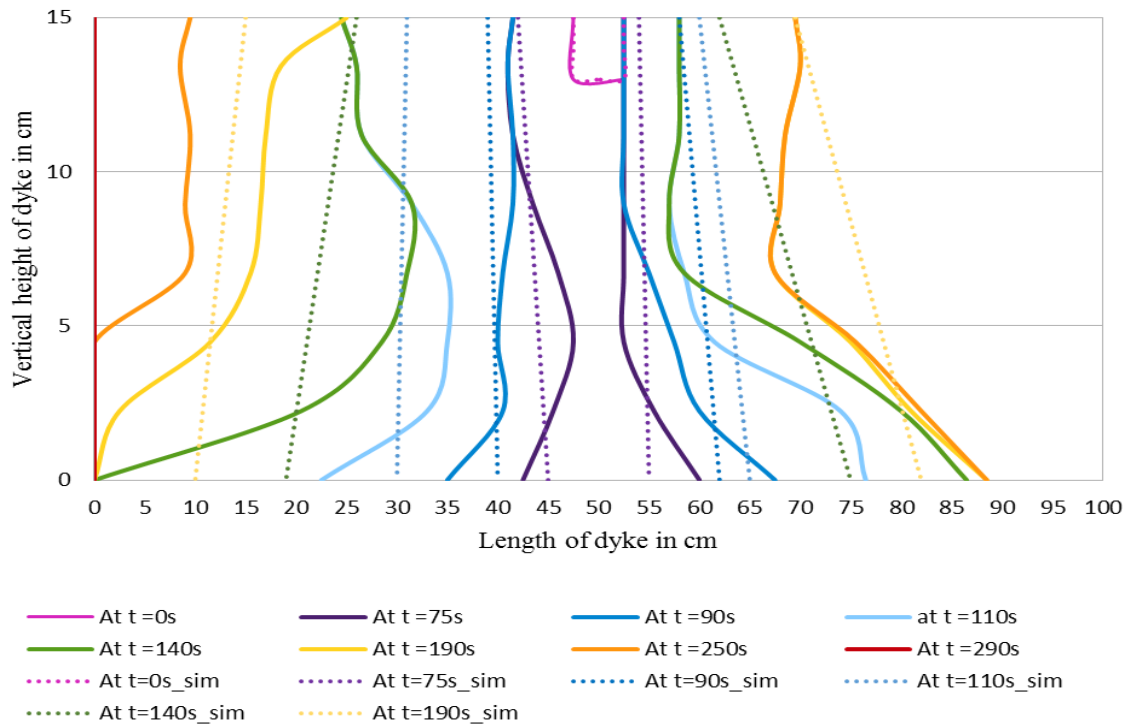
Figure 4.22 Lateral widening process (for sediment no.7)

4.5 Experiment result: Scenario A (Experiment Plan B)

4.5.1 Results and discussion on scour pattern

Scouring may be defined as the removal of material around embankments caused by flow acceleration and turbulence near embankments. Scour has been the major concern for safety of hydraulic structures. A large number of hydraulic structures failed as the local scour progresses which gradually undermines the foundations. It is important to control the local scour depth under foundation and at downstream of hydraulic structures to ensure safety of these structures But, the study of scour pattern and depth is poorly understood if it comes in the case of dyke foundation and downstream.

As dyke breach progressed, the channel bed upstream of the broken part underwent scouring due to shear stress applied by the flow. Figure 4.23 shows the bed shape after the end of flow as determined using laser measurement for scenario 1 in which case dyke body, foundation and flood plain all are movable. The flow velocity vectors were also determined by PIV method to observe the flow regime which was also plotted overlapping with the scour figure. From the figure, it can be inferred that the maximum scour depth occurred in between the center of dyke and toe. As the sediment size became finer, more scour depth was seen to form. The analysis shows that the maximum scour depth follows approximately linear relation with the sediment

size which needs to be verified with more data in near future. The Fig 4.24 shows the linear relation between dimensionless sediment size (ratio between mean diameter of sediment and maximum foundation depth with same materials below the dyke) and dimensionless maximum scour depth (ratio between maximum scour depth and the maximum foundation depth below the dyke). The graph is only representative one; more data will be needed to give a concrete equation for the relation.

The ripples and dunes of various dimensions are observed in the flood plain because of the fine bed materials. The deposition pattern in the flood plain indicates that initially the flow diverted towards right side of the flood plain but later due to exposition to the deposited sediment the flow travels all along the flood plain. The experiments were also performed for the nearly full saturation of foundation material; the results seem no difference than the previous one; only difference found was the time taken to reach the same equilibrium position. The time was short for the saturated case than unsaturated cases.
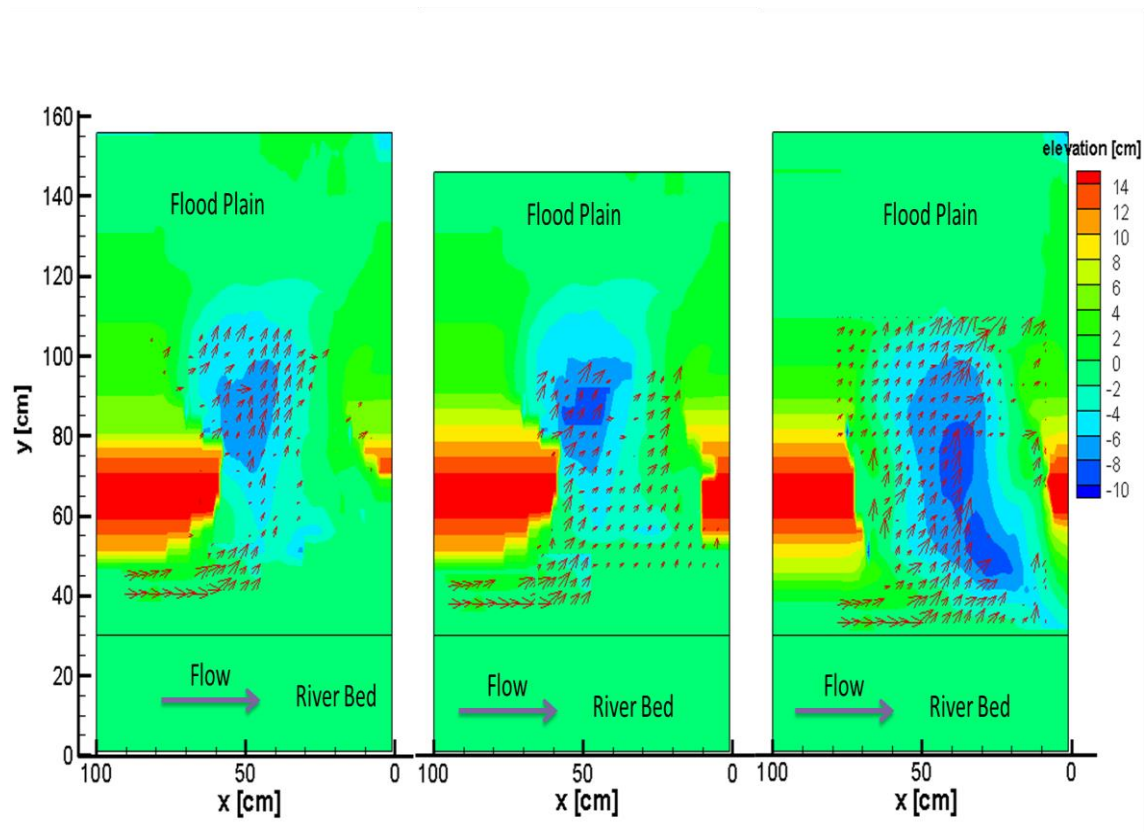
Figure 4.23 Equilibrium Scour Pattern overlapped with flow velocity vectors (by PIV) for Sediment 6, 7 and 8 respectively (Scenario 1)
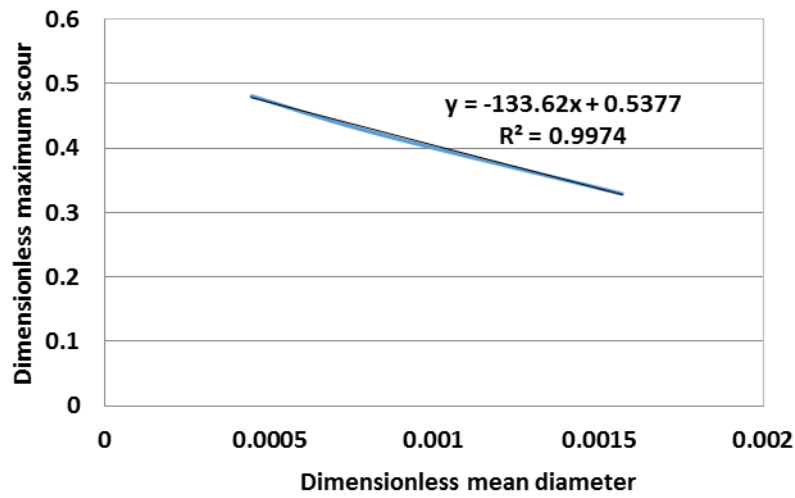
Figure 4.24 Relation between maximum scour depth and sediment size

4.5.2 Results and discussion on breach hydrograph

The discharge was measured a part from the scour measurement to see the effect of breach expansion and figure 4.25-4.27 represents typical result for three sediment sizes.
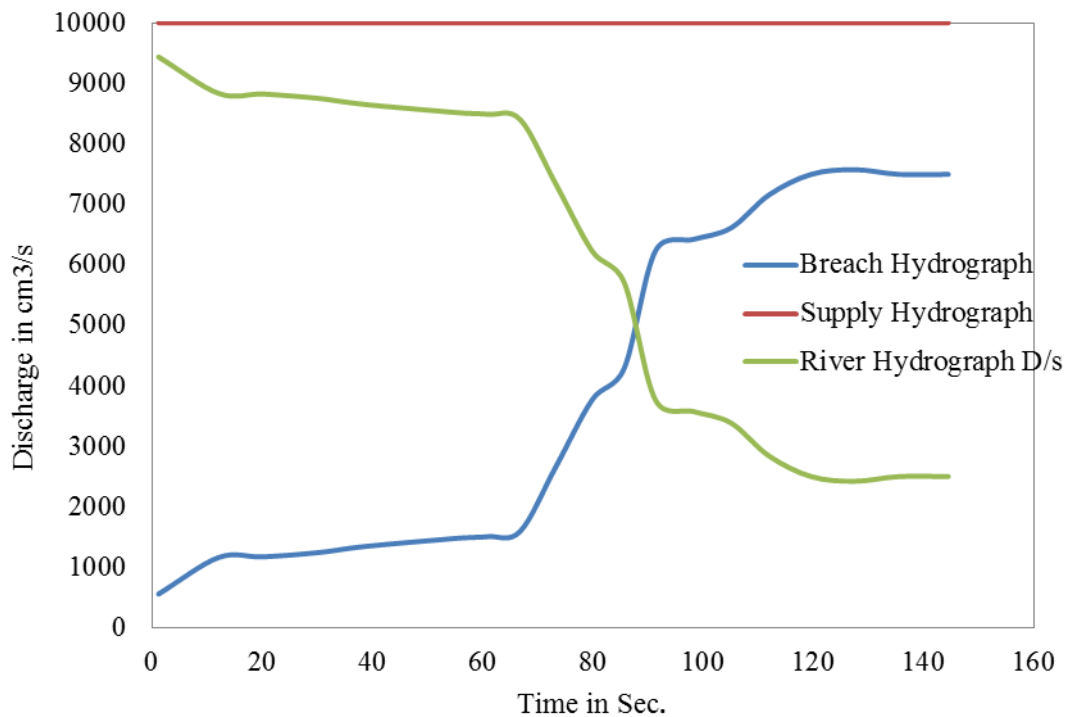
Figure 4.25 River and inundation flow hydrograph on flood plain (sediment No.6)
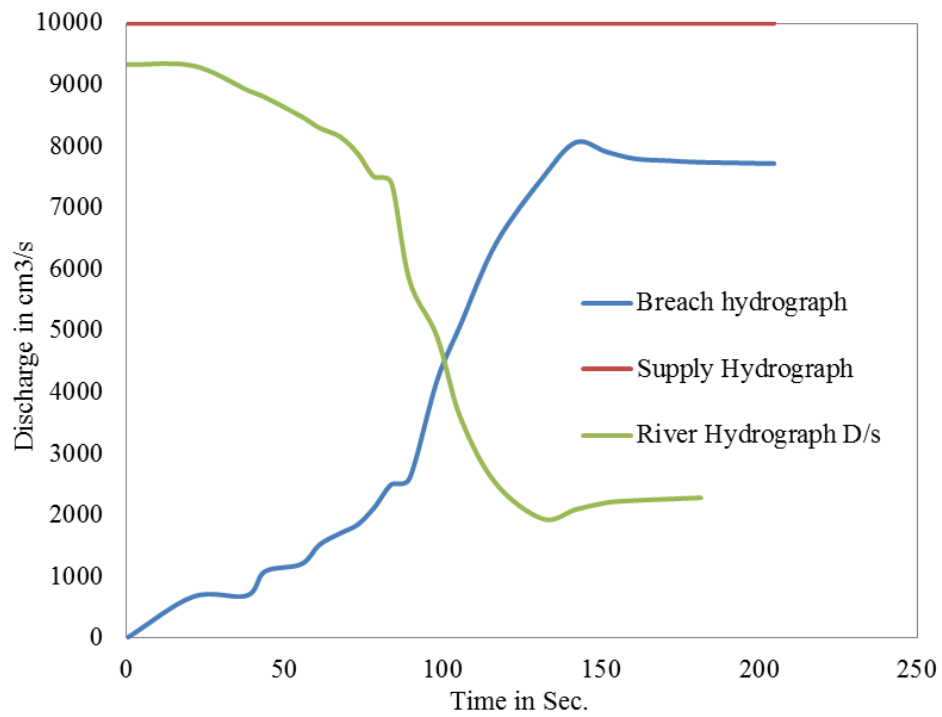
Figure 4.26 River and inundation flow hydrograph on flood plain (sediment No.7)
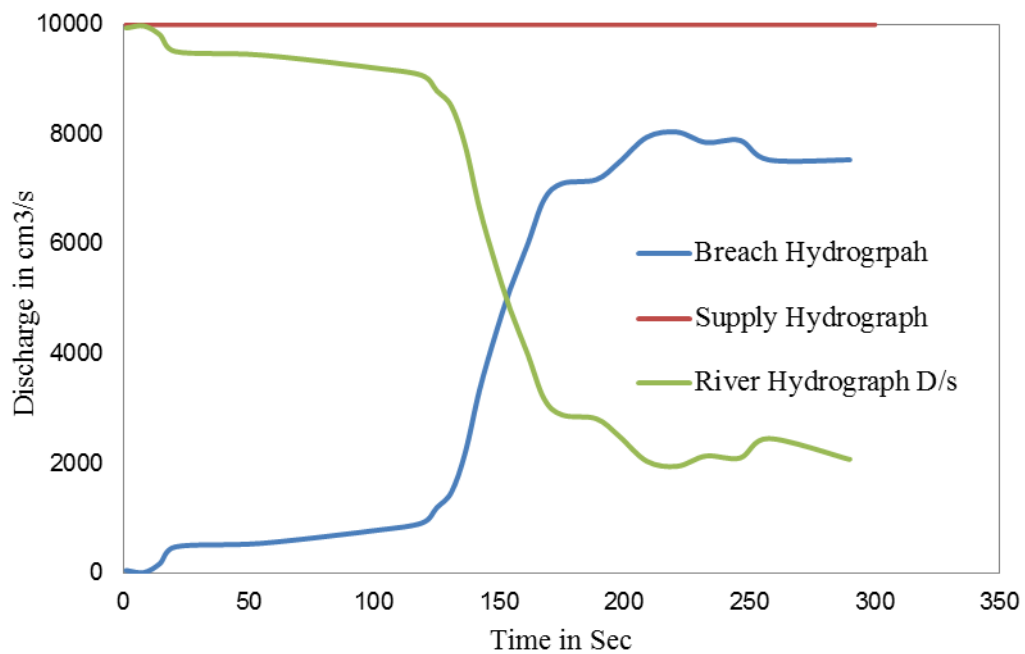
Figure 4.27 River and inundation flow hydrograph on flood plain (sediment No.8)

The hydrograph initially increases slowly then reaches just below the supply level at its peak and drops a little bit and becomes constant. The figure clearly illustrates that the ratio of total supply discharge divides at approximately ratio of 80:20 percent during the process.

4.6 Experimental results: Scenario 2

The scenario 2 experiments were performed by making dyke body and foundation fixed and flood plain only movable. The results are shown in Figure 4.28 in terms of laser measurement of bed morphology after the equilibrium state was reached by the same discharge used in the previous case. In this case there was no pilot channel and the dyke was overtopped from the whole length. The result also shows similar trend like the scenario 1. The finer the sediments, more large the maximum scour depth. The location of maximum scour depth is just near the toe for all the cases and the flood plain has no erosion but little deposition or formation of small ripples and dunes. In this case, the process was similar to the scour developed by spillways and due to scouring at the toe, the foundation was exposed, so that there will be danger of failure of hydraulic structure, even though the dyke is strong enough to resist overtopping flow.
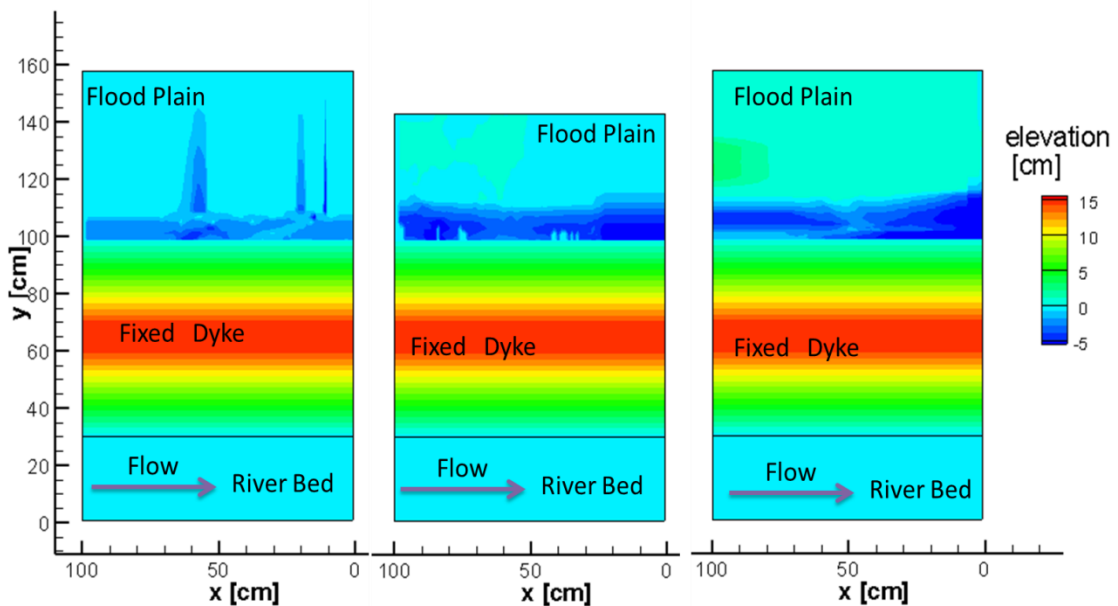
Figure 4.28 Equilibrium Scour Pattern for Sediment 6, 7 and 8 respectively (Scenario 2)
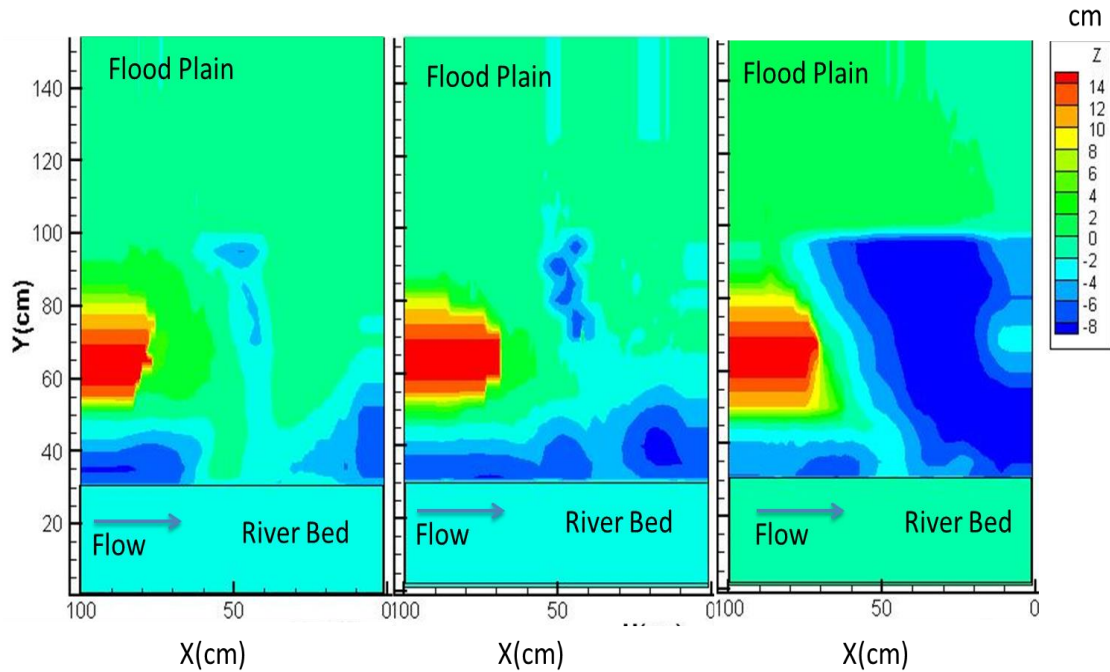
4.5 Summary

The present experimental work investigated the breach characteristics (lateral widening and hydrographs) and scour pattern at the foundation of dyke for various scenarios with the variation of different sediment sizes due to overtopping. A simple but realistic dyke model was used consisting of homogenous uniform materials of various sediment sizes. A steady inflow scenario was tested and all the processes were recorded optically and with laser measurement system. Within the range of test parameters, the dyke breach process was accelerated with the increase in the mean diameter of the particle. For coarser sediments, due to quick saturation of the dyke body, the collapse time decreased. The width of the breach increased at the top and toe section compared to the middle section which acted as a hinge point. In the final stage, middle section also failed leading to the entire dyke collapse. The downstream dyke portion is more vulnerable as due to the flow angle the downstream part always eroded till the equilibrium condition will reach but for upstream part, the equilibrium condition will reach far early than the later one. So, the four phases of the dyke breach phenomena was observed. The breach discharge and sediment discharge showed the time lag and peak according to the sediment sizes.

The numerical simulation was performed which shows quite good agreement in the case of breach hydrograph, sediment hydrograph and lateral widening process.

The scour pattern is also following a trend with regards to materials forming the dyke and the foundation. The finer the materials, more vulnerable to the scouring were observed. The breach discharge measurement during scour experiment shows that 80% of the total supply discharge passes through the breach area and rest passes as river discharge downstream.

After hydraulic and physical mechanism of dyke breach process are understood, this experimental flume can be adapted to account for further parameters affecting the dyke breach such as surface protection, cohesive materials, core layers, compaction or soil moisture content. The current findings have to be expanded in the next stage where the authors are developing simulation model to verify the claim.

CHAPTER 5

CONCLUSIONS AND RECOMMENDATIONS

River Dykes is an important and effective measure to prevent floods. The main consequences on the flood risk due to construction of river embankments or dykes are that, firstly, it increases the flood hazard reducing the lateral flow storage area and hence the flow capacity of peak discharges attenuation and, secondly, the amount of potential damages induced by flooding is dramatically increased, being the surrounding areas often urbanized. Therefore, although the existence of dyke lowers the probability of flooding but the consequences to personal safety and property are much higher should a dyke overtop or fail. Although several researches have been conducted to understand the embankment dam failure, there has been little focus on river dyke breaching processes and scour under the dyke and the flood plain.

As previously described, several numerical simulations have been conducted regarding embankment erosion; however, problems remain regarding the effects of infiltration on erosion due to overtopping flow. The infiltration process on the backside slope is very complex because the surface erosion and the saturation conditions on an embankment surface are continually and simultaneously changing due to the infiltration of overtopping flow. Indeed, solving this problem is not easy; we had no choice but to individually adjust the coefficients simply related to erodibility to fit the results of the experiments to focus on other topics because of a lack of understanding of erosion at different saturation levels.

The present research work investigated the breach characteristics (lateral widening and hydrographs) and scour pattern at the foundation of dyke for various scenarios with the variation of different sediment sizes due to overtopping. A simple but realistic dyke model was used consisting of homogenous uniform materials of various sediment sizes. A steady inflow scenario was tested and all the processes were recorded optically and with laser measurement system. An integrated model consisting of two dimensional depth averaged flow model, Seepage model and erosion and deposition model is developed to simulate the dyke breach characteristics i.e. lateral widening pattern, breach discharge and sediment hydrograph. The simulated results were compared with those obtained from the laboratory experiments. Finally, the scour pattern with various situations is also analyzed experimentally. These conclusions are presented in the following.

The key features of integrated model can be summarized as follows:

- Infiltration process and effect of suction are incorporated in an integrated model although this process is neglected in almost all available models.

- The model can predict both total discharge and sediment discharge hydrograph.

- The model can also predict lateral widening process with variation of sediment sizes.

5.1 Conclusions

The conclusions of this study are summarized as follows.

Breach characteristics in the case of flow perpendicular to the dyke length

In this case, preliminary experiments were performed to analyze breach characteristics considering flow perpendicular to the dyke body but trapezoidal shaped dike kept parallel to the river flow direction.

For sediment no 5, 6, 7 and 8 with all other parameters constant resulting in different breach shapes but the process of the enlargement seems to be followed similar procedure. For all the processes, initially, as the water overtops through pilot channel, the channel is eroded vertically layer by layer until the water surface touches the fixed bed. The reason for that is the vertical layer is saturated quickly with the flow which creates erosion of the channel surface by shear stress. Interestingly, at the both side of the channel there is the formation of vertical slope of the sediment material. The vertical slope seems stable enough due to the matric suction of the soil in unsaturated case. When the vertical undermining reaches the fixed bed, then the erosion starts to expand laterally from the toe of the opposite slope of the dyke. In the meantime, the seepage travels through the vertical slope developed at the both side of the channel. If the vertical slope is saturated enough to be overcome the sectional resistance stress, then those slope fell down at the channel flow at the center. The result shows that the breaching phenomenon was very slow at the beginning at top, middle and toe section. Then as the vertical breaching reaches the fixed bed, the toe section as well as the top section rapidly eroded in comparison with other section causing most of the breaches of the dyke. The middle section acts like a hinge section for both the erosion and finally the middle section collapse suddenly. Thus, finally the collapse of the whole dyke occurs.

In another case, the breach discharge increases fast after initial overtopping until the maximum breach discharge $Q_{max} > Q_{in}$ is attained. After reaching the maximum outflow, the breach discharge decreases slowly to $Q = Q_{in}$ and then remains constant. The maximum discharge obtained is around 1.6 times the discharge in the flume. The sediment graphs has more than one peaks which reveals that the vertical stable wall at the side of channel falls into the Centre of

breach at different time step. The time of failure curve shows that It has a minimum value at $\dfrac{K_s T}{d_{50}}$ = 33.5 which can be considered as the critical dimensionless failure time.

Hence, the breach discharge and sediment discharge shows the time lag and peak according to the sediment size. Finally, the time of failure curve is proposed for the pre determination of occurrence of peak breach discharge based on the pre-disaster parameters

Development of integrated Numerical model to reproduce dyke breach characteristics

A numerical model for predicting erosion due to overtopping flow at a river embankment was developed by combining four modules: surface flow, seepage flow, sediment transport, and slope failure. The novelty of this study is in the combination of these modules to reproduce the complicated embankment failure process. There are many interactions among the modules, and the highlight of the present model is its estimation of the erosion rate by considering that the effect of resisting shear stress due to suction depends on saturation conditions on the embankment surface, which is calculated using the result from the seepage flow module. In order to focus on the improvement in the treatment of the surface erosion process, the developed model was reduced to vertical two-dimensional calculations in seepage and erosion modules; however, the horizontal 2D flow model was introduced to consider the extensibility for our future work.

Experimental observation for breach characteristics for realistic orientation of dyke

The second case of experimental setup is constructed considering the realistic orientation of dyke in relation to river flow i.e. the dyke structure was placed parallel to the river flow with the flow direction towards dyke non-perpendicular. For all sediment sizes, the lateral widening process follows following four phases: Vertical undermining phase (VUP), Initiation of lateral widening Phase (ILWP), lateral widening acceleration phase (LWAP) and Widening Deceleration cum stable phase (WDSP). The erosion process is asymmetrical with upstream portion erosion speed are always greater than equal to downstream. Finer the sediment size, higher the development of suction pressures due to unsaturated condition which finally develops resistance against failure so the finer sediments reluctant to faster erosion. The breach discharge increases rapidly after the initial overtopping until the maximum value is attained. The graph clearly shows that time lag of peak of the hydrograph increases with increase in sediment number i.e. decreasing mean diameter of sediments. The sediment discharges have more than one peak which reveals that the vertical stable wall at the side of the pilot channel falls into the center of the breach intermittently.

Comparison of breach characteristics obtained from realistic experimental case to Numerical simulation

Dyke surface erosion and flow model is developed for simulation of outflow hydrograph due to dyke failure by overtopping. The proposed model is tested for different experimental cases of dyke failure for overtopping over partial pilot channel width. The model is able to reproduce the resulting hydrograph reasonably. The simulated overtopping time and dyke surface erosion at different time steps are also in good agreement with experiments. The incised channel is almost vertical for both simulations and experiments in small inflow discharge. In the case of larger inflow discharge and larger reservoir volume, slumping occurred at irregular time steps. The lateral widening pattern is somehow reproduced well with experimental values. The numerical simulation was performed which shows quite good agreement in the case of breach hydrograph, sediment hydrograph and lateral widening process. The peak discharge of both sediment and breach hydrograph is underestimated from the numerical results.

During breach formation, breach enlargement proceeded rapidly below the water surface in the breach channel. Above the water level there was some apparent cohesion added by water content and adhesion so the side wall was very steep and undermines the slope. The erosion process continues until slope stability was encountered. The slope failure of channel bank around crest of the dam is one of the main causes of higher peak discharge (both flow and sediment discharge) in the experiment compared to simulation. The peak discharge is underestimated by model due to collapse nature of failure and uncertainty in material properties (degree of compaction, mixing of sediments etc.) of the dyke body.

Importance of sediment sizes on the scour formation at the foundation and flood plain

Two cases were tested in this scenario: one with movable flood plain and foundation, other with only movable flood plain case. The linear relation between dimensionless sediment size (ratio between mean diameter of sediment and maximum foundation depth with same materials below the dyke) and dimensionless maximum scour depth (ratio between maximum scour depth and the maximum foundation depth below the dyke) is observed.

The ripples and dunes of various dimensions are observed in the flood plain because of the fine bed materials. The deposition pattern in the flood plain indicates that initially the flow diverted towards right side of the flood plain but later due to exposition to the deposited sediment the flow travels all along the flood plain. The experiments were also performed for the nearly full saturation of foundation material; the results seem no difference than the previous one; only difference found was the time taken to reach the same equilibrium position. The time was short for the saturated case than unsaturated cases.

Discharge ratio in the case of dyke breaching

The hydrograph initially increases slowly then reaches just below the supply level at its peak and drops a little bit and becomes constant. The figure clearly illustrates that the ratio of total supply discharge divides at approximately ratio of 80:20 percent during the process i.e. larger portion towards breached area.

5.2 Recommendations for future studies

Although this study has some difficulties during measurements and numerical analysis, the ultimate target has been achieved very satisfactorily. And, the research findings would be utilized in the field of river engineering as well as disaster risk assessment on the floodplain due to dyke breach. The study is focused on breach of river dyke of homogenous non-cohesive materials. The failure mechanism of river dyke of cohesive material is different, so further study is essential for the application in such a case. The model developed in this study is still in the preliminary stage of concept of integrated model and it has many limitations. Some limitations and recommendations to improve and make fully integrated model to predict failure modes and resulting flood is discussed here.

(a) The river dyke breaching process is very complex process. In my study, two dimensional model is used to understand the behavior but to understand fully the lateral widening behavior of river dyke breach, The authors feel that three dimensional model seems necessary. So, improvement of current model to three dimensional models is recommended.

(b) The current model used debris flow based equations for analyzing the process, the author feel non-equilibrium model should be developed also in this case.

(c) The enlargement of breached channel is modeled as erosion of side wall due to shear stress of flowing water. However slumping of side slope of breached channel occurs at irregular time steps and is depending on condition of flow and material of the dyke body. During breach formation, breach enlargement proceeded rapidly below the water surface in the breach channel. Above the water level there was some apparent cohesion added by water content and adhesion so the side wall is very steep and undermines the slope. So, further improvement of model is necessary to incorporate this phenomenon. Breached channel bank stability model with capability to predict timing and dimensions of bank failure along breach channel is required to couple with integrated model.

(d) In spite of real field survey data, for the time being this research has been conducted on the model floodplain considered with the river channel and dyke, and the idealized flow and sediment parameters were selected with the conformity of the typical field. It would be better and might be realistic understanding of the levee breaching and disaster effect on the floodplain, if in a real-life situation.

(e) In laboratory experiments, the inflow water was supplied without suspended sediment, and the breach is investigated with clear water condition. So, the elaborate laboratory experiments are recommended considering the inflow supplied with sediment.

(f) The developed models are deterministic. There are many uncertainties in soil properties of dyke materials such as hydraulic conductivity, angle of friction, cohesion etc. So, probabilistic approach is necessary to take into account different uncertainties.

(g) The predicted flood hydrograph can be used as a boundary condition for downstream flood routing. 1D or 2D flood routing model with the capability to model sediment transport can be used to predict downstream hazard and its mitigation. Proper location of refuges and

evacuation routes can be shown in the hazard map to evacuate local residents in a safe and proper manner in the event of dyke failure.

(h) In current study, only the variation in sediment sizes is considered. There may be possibility to carry out experiment considering other variables like river bed elevation, dyke height, inflow discharge, movable river bed etc.

References

Assouline, S., Tessier, D. and Bruand, A.: A conceptual model of the soil water retention curve, Water Resour. Res., Vol. 34, pp223–231, 1998.

Aureli F. and Mignosa P. (2001). Comparison between Experimental and Numerical Results of 2D flows due to Levee breaking, *XXIX IAHR Congress Proceedings*, Theme C, September 16-21, Beijing, China.

Awal, R., Nakagawa, H., Baba, Y. and Sharma, R. H.: Numerical and experimental study on landslide dam failure by sliding, Annual Journal of Hydraulic Engineering, JSCE, Vol.51, pp.7-12, 2007

Awal, R., Nakagawa, H., Kawaike, K., Baba, Y. and Zhang, H.: An integrated approach to predict outflow hydrograph due to landslide dam failure by overtopping and sliding, Annual Journal of Hydraulic Engineering, JSCE, Vol. 52, pp.151-156, 2008

Bhattarai, P.K., Nakagawa, H., Kawaike K. and Zhang H. (2014). Experimental study on river dyke breach characteristics due to overtopping flow. *Journal of Japanese Society of Natural Disaster Science*, Vol.33, 65-74.

Broich, K.: Mathematical modeling of dambreak erosion caused by overtopping, Proceedings of the 2nd CADAM Workshop, Munich, October 1998.

Casagrande, A. (1961). Control of seepage through foundations and abutment dams. *Géotechnique* 11(3), 161-182.

Chinnarasri, C., Tingsanchali, T., Weesakul, S., Wongwises, S. (2003). Flow patterns and damage of dike overtopping. *International Journal of Sediment Research* 18(4), 301-309.

Chinnarasri, C., Jirakitlerd, S., Wongwises, S. (2004). Embankment dam breach and its outflow characteristics. *Civil Engineering and Environmental Systems* 21(4), 247- 264
.
Coleman, S.E., Andrews, D.P. and Webby, M.G.: Overtopping breaching of noncohesive homogeneous embankments, Journal of Hydraulic Engineering, Vol. 128(9), pp.829-838, 2002.

David C. Froehlich: Peak Outflow from Breached Embankment Dam, J. Water Resour. Plng. and Mgmt., Vol 121(1), pp. 90-97, 1995.

De Looff, H., Steetzel, H.J. and Kraak, A.W.: Breach growth: experiments and modeling, Proc. 25th Int. Conf. Coastal Engineering, Orlando, USA, pp.2746-2755, 1997.

Dupont, E., Dewals, B.J., Archambeau, P., Erpicum, S., Pirotton, M. (2007). Experimental and numerical study of the breaching of embankment dam. Proc. 32nd *Congress of IAHR* Venice 1(178), 1-10, IAHR, Madrid.

Evans, S. G.: The maximum discharge of outburst floods caused by the breaching of man-made and natural dams, Can. Geotech. J., Vol.23(4), pp.385–387, 1986.

Fread, D.L.: The NWS DAMBRK: The NWS dam-break flood forecasting model, Office of Hydrology, National Weather Service, Silver Spring, Maryland, USA, 1984.

Fread, D.L.: The NWS DAMBRK model: theoretical and background/user documentation, National Weather Service (NWS) Report, NOAA, Silver Spring, Maryland, USA, 1988a.

Fread, D.L.: BREACH: an erosion model for earthen dam failures, National Weather Service (NWS) Report, NOAA, Silver Spring, Maryland, USA, 1988b.

Froehlich, D. C.: Peak outflow from breached embankment dam, J. Water Resour. Plan. Manage. Div., Am. Soc. Civ. Eng., Vol. 121(1), pp. 90–97, 1995.

Fujita Y., Muramoto Y. and Tamura, T. (1987). On the inflow of river water and sediment due to levee breach. *Annual of Disaster Prevention Research Institute, Kyoto University.* 30 (2), 527-549 (in Japanese).

Fujita Y. and Tamura, T. (1987). Enlargement of breaches in flood levee on alluvial plains. *J. of Natural Disaster Science* 9 (1), 37-60.

Hagen, V. K.: Discussion: Peak outflow from breached embankment dam, Journal of Water Resources Planning and Management, Vol.122, pp.314-316, 1996.

Hahn, W., Hanson, G.J. and Cook, K.R.: Breach morphology observations of embankment overtopping tests, Proc. 2000 Joint Conf. Water Resources Engineering and Water Resources Planning and Management, Minneapolis, USA, 2000. (CD-ROM)

Hager, W.H., Unger, J. (2006). Dike Erosion - A preliminary outlook. Proc. Intl. Conf. *River Flow*, R.M.L. Ferreira, E.C.T.L Alves, J.G.A.B Leal, A.H. Cardoso, eds., Lisbon, Portugal, 1511-1519.

Höeg K., Lövoll, A. and Vaskinn K.A.: Stability and breaching of embankment dams: field tests on 6 m high dams, International Journal on Hydropower and Dams, Vol.11(1), pp.88-92, 2004.

Islam M. Z., Okubo K., Muramoto Y. and Morikawa H. (1994). Experimental study on sedimentation over the flood plain due to river embankment failure. *Annual of Disaster Prevention Research Institute, Kyoto University.* 44 (2), 69-92

Ito, N.: Study on river embankment failure caused by overtopping, Master's Thesis, Department of Civil and Earth Resources Engineering, Kyoto University, 2007.

Lecointe, G.D. (1998). Breaching mechanisms of embankments: An overview of previous studies and the models produced. MSc *Project*. The University of Birmingham, School of Civil Engineering, Birmingham UK.

Morris M. W., Hassan M., Kortenhaus A. and Visser P.J.(2009). Breaching Processes, A State of the Art Review.*Floodsite Report* T06-06-03.

Morris, M.W., Hassan, M.A.A.M., Vaskinn, K.A. (2007). Breach formation: Field test and laboratory experiments. Journal of Hydraulic Research 45(Extra Issue), 9-17.

Tsujimoto T., Mizoguchi A. and Maeda A. (2006). Levee Breach process of river by overflow erosion, *Int. conference of Fluvial Hydraulics*, Portugal 6-8 September

Morris, M.W., Hassan, M.A.A.M., Samuels, P.G., Ghataora, G.S. (2008). Development of the HR BREACH model for predicting breach growth through flood embankments and embankment dams. Proc. Intl. Conf. River Flow, M.S. Altinakar, M.A. Kokpinar, I. Aydin, S. Cokgor and S. Kirkgoz, eds.), Çeşme, Izmir, Turkey, 679- 687.

Kakinuma T., Tobita D., Yokoyama H. and Takeda A. (2013). Levee Breach Observation at Chiyoda Experimental Flume..*Advances in River Sediment Research*, Taylor and Francis Group. Pg. No. 105

Nakagawa H., Mizutani H., Kawaike K., Zhang H., Yoden Y., Shrestha B. (2013).Numerical Modelling of Erosion of Unsaturated River Embankment due to Overtopping Flow. *Advances in River Sediment Research*,.Taylor and Francis Group, London. P113

Peviani, M.A.: Simulation of earth-dams breaking processes by means of a morphological numerical model, Proc. CADAM (EU Concerted Action on Dam Break Modelling) Zaragoza meeting, Zaragoza, Spain, pp.381-397, 1999.

Pickert, G., Jirka, G.H., Bieberstein, A., Brauns, J. (2004). Soil/water interaction during the breaching process of overtopped embankments. Proc. Intl. Conf. *River Flow*, M. Greco, A. Carravetta, and R. Della Morte, eds., Naples, Italy, 903-910.

Pickert, G., Weitbrecht, V., Bieberstein, A. (2011). Breaching of overtopped river embankments controlled by apparent cohesion. *Journal of Hydraulic Research* 49(2), 143-156.
Pontillo, M., Schmocker, L., Greco, M., Hager, W.H. (2010). Two-dimensional numerical modelling of dike erosion due to overtopping. *Journal of Hydraulic Research* 48(5), 573-582.

Powledge, G.R., Ralston, D.C., Miller, P., Chen, Y.H., Cloppner, P.E., Temple, D.M. (1989a). Mechanics of overflow erosion on embankments I: Research activities. *Journal of Hydraulic Engineering* 115(8), 1040-1055.

Powledge, G.R., Ralston, D.C., Miller, P., Chen, Y.H., Cloppner, P.E., Temple, D.M. (1989b). Mechanics of overflow erosion on embankments II: Hydraulic and design considerations. *Journal of Hydraulic Engineering* 115(8), 1056-1075.

Schmocker L., Hager W.H. (2009).Dike breaching due to overtopping. 33rd IAHR Congress: Water Engineering for a Sustainable Environment.

Schmocker, L., Hager, W.H. (2009). Modelling dike breaching due to overtopping. *Journal of Hydraulic Research* 47(5), 585-597.

Schmocker, L., Hager, W.H. (2010). Overtopping and breaching of dikes - Breach profile and breach flow. Proc. Intl. Conf. *River Flow*, A. Dittrich, K. Koll, J. Aberle & P. Geisenhainer, eds., Braunschweig, Germany, 515-522.

Singh, V.P. (1996). *Dam breach modelling technology*. Kluwer, Dordrecht NL.

Spinewine, B., Delobbe, A., Elslander, L., Zech, Y. (2004). Experimental investigation of the breach growth process in sand dikes. Proc. Intl. Conf. *River Flow*, M. Greco, A. Carravetta, R. Della Morte, eds., Naples, Italy, 903-910.

Takahashi, T. and Kuang, S.F.: Hydrograph prediction of debris flow due to failure of landslide dam, Annuals, Disas. Prev. Res. Inst., Kyoto Univ., No.31 B-2, pp.601-615, 1988. (In Japanese with English abstract)

Takahashi T. and Nakagawa, H.: Flood/debris flow hydrograph due to collapse of a natural dam by overtopping, Journal of Hydroscience and Hydraulic Engineering, JSCE, Vol.12, No.2, pp.41-49, 1994.

Takahashi, T., Chigira, M., Nakagawa, H., Onda, Y., Maki, N., Aguirre-Pe, J. and Jáuregui, E.: Flood and sediment disasters caused by the 1999 heavy rainfall in Venezuela, Research Report of Natural Disasters, pp.1-141, 2001.

TAW (1991). *Guidelines on design of river dikes*. Technical Advisory Committee for Flood Defence (TAW), Published by the Centre for Civil Engineering Research and Codes (CUR), Gouda NL.

USACE (2000a). *Design and construction of levees*. Engineer Manual Engineering Design, US Army Corps of Engineers, Washington DC.

Visser, P.J., Zhu, Y., Vrijling, J.K. (2006). Breaching of dikes. 30th Int. Conf. *Coastal Engineering*, San Diego CA, 2893-2905.

Wahl, T.L. (1997). Predicting embankment dam breach parameters - A needs assessment. Proc. 27th *Congress of IAHR* San Francisco, 48-53, IAHR, Madrid.

Wahl, T.L. (2004). Uncertainty of prediction of embankment dam breach parameters. *Journal of Hydraulic Engineering* 130(5), 389-397.

Walder, J. S., and O'Connor, J. E.: Methods for predicting peak discharge of floods caused by failure of natural and constructed earth dams, Water Resour. Res., Vol.33(10), pp.12, 1997.

Zhu, Y.H., Visser, P.J., Vrijling, J.K. (2004). Review on Embankment Dam Breach Modeling. *New Developments in Dam Engineering*, M. Wieland, Q. Ren, and J.S.Y. Tan, eds., Taylor & Francis, London, UK, 1189-1196.

Zhu, Y. (2006). Breach growth in clay dikes. *PhD Thesis*. TU Delft, Delft NL.

List of Figures

List of Tables

Curriculum Vitae

Name   BHATTARAI Pawan Kumar

Citizenship   Republic of Nepal

Date of Birth   June 24, 1979

E-mail   Nepal.pawan@gmail.com

Key Qualification

Ph.D. Student (2012 ~ 2015)
Department of Civil and Earth Resources Engineering
Kyoto University, Kyoto, Japan

M. Sc. (2006~2008)
M.Sc. in Hydropower Development
Department of Hydraulics and Environment Engineering Norwegian University of Science and Technology (NTNU); Major Specialization: Hydropower Hydraulics

B.E. (1998~2002)
Bachelor Degree in Civil Engineering
Institute of Engineering (IOE), Pulchowk Campus, Tribhuwan University (TU), Nepal

Key Employment Record

From September   2002   to 2012
Employer: Pulchowk Campus Institute of Engineering, Tribhuwan University
Position Held: Assistant Professor in Water Resources Engineering

From January 2009: To September 2010 (Part time)
Employer: Shah Consult International (P) Ltd., Kathmandu, financed by Patel Engineering Private Limited, Mumbai, India
Position Held: Hydraulic Design Engineer

Papers Based on the Thesis

Bhattarai, P., Nakagawa, H., Kawaike, K., and Zhang, H.: Study of Breach characteristics and scour pattern for overtopping induced river dyke breach, Proceedings of 36th IAHR congress-The Hague, The Netherlands, June 2015. (Accepted)

Bhattarai, P.,Nakagawa, H., Kawaike, K. and Zhang, H.: Analysis of Breach Characteristics and Equilibrium Scour Pattern for Overtopping-induced River Dyke Breach. Annuals of the Disaster Prevention Research Institute, Kyoto University, No.58B, June 2015. (to be published)

Bhattarai, P.,Nakagawa, H., Kawaike and Zhang, H.: Experimental Evidence of Impact of Flow Direction on Dyke Breach Characteristics due to Flow Overtopping, Proceedings of the Eighth NEAJ Seminar on "Current and Future Technologies", 25 January 2015 (in CD ROM and Web portal).

Bhattarai, P., Nakagawa, H., Kawaike K. and Zhang H.   (2014). Experimental study on river dyke breach characteristics due to overtopping flow. *Journal of Japanese Society of Natural Disaster Science*, Vol.33, 65-74.

Bhattarai, P.,Nakagawa, H., Kawaike, K. and Zhang, H.: Experimental Study on Effect of Sediment Size on River Dyke breach Characteristics Due to Overtopping, Annuals of the Disaster Prevention Research Institute, Kyoto University, No.57B, June 2014.